Order Number 9119669

A theory of cochlear input impedance and middle ear parameter estimation

Puria, Sunil, Ph.D.

City University of New York, 1991

U·M·I
300 N. Zeeb Rd.
Ann Arbor, MI 48106

A THEORY OF COCHLEAR INPUT IMPEDANCE AND MIDDLE EAR PARAMETER ESTIMATION

BY

SUNIL PURIA

A dissertation submitted to the Graduate Faculty in Engineering in partial fulfillment of the requirements for the degree of Doctor of Philosophy, The City University of New York.

1991

This manuscript has been read and accepted for the Graduate Faculty in Engineering in satisfaction of the dissertation requirement for the degree of Doctor of Philosophy.

1/30/91
Date

Professor Nenad M. Marinovic
(Chair of Examining Committee)

1/30/91

Dean Gerald G. Lowen
(Executive Officer)

1/29/91

Dr. Jont B. Allen
(AT&T Bell Laboratories)

Prof. Louis Weinberg - Electrical Engineering Department

Prof. Leonid Roytman - Electrical Engineering Department

Prof. Harry Levitt - Speech and Hearing Department

Dr. Duck O. Kim - University of Connecticut

Supervisory Commitee

The City University of New York

Abstract

A THEORY OF COCHLEAR INPUT IMPEDANCE AND MIDDLE EAR PARAMETER ESTIMATION

by

SUNIL PURIA

Advisers: Professor Nenad M. Marinovic and Dr. Jont B. Allen

In this thesis it is hypothesized that the geometry of the cat cochlea has evolved to maximize sound transmission from the eardrum to the cochlea. This hypothesis is shown to be tenable by modeling the cochlear input impedance and the middle-ear. It is also hypothesized that the geometric configuration of the middle-ear cavities plays an important role in its acoustic properties.

Various aspects of the cat cochlear input impedance $Z_c(\omega)$ are implemented using a transmission line model having perilymph viscosity and a varying cross-sectional scalae area. These model results are then compared to the experimental results of Lynch *et al.* [JASA **72**, (1982) pp. 108-130]. From the model, the following observations are made about $Z_c(\omega)$: (a) The use of anatomically measured scalae cross-sectional areas improves the fits to the magnitude of the experimental data. (b) Improved agreement between model and experimental phase for frequencies below approximately 150 Hz is obtained when perilymph viscosity and tapering are included in the cochlear model. (c) When model scalae tapering and perilymph viscosity are chosen to match physiological conditions, the effect of the helicotrema impedance on $Z_c(\omega)$ is insignificant.

To quantify the effect of $Z_c(\omega)$ on the eardrum impedance, a cat middle-ear model is presented. The parameters of the model were evaluated by modeling the eardrum impedance, measured [J.B. Allen, (1986) in *Peripheral Auditory Mechanisms*, eds. J.B. Allen, *et al.*, Springer-Verlag] at each step of various "surgical modifications" to the cochlea and middle-ear. The model indicates that as much as 80% of the incident wave in the ear canal is absorbed by the cochlea in the mid-frequency region and as a result inaccurate representations of $Z_c(\omega)$ will result in inaccurate representations of the middle-ear.

A physical model for the middle-ear cavities is presented. The model explicitly takes into account effects of non-planar wave propagation due to area discontinuities and visco-thermal effects at the walls. This model is experimentally verified by making impedance measurements on several cylindrical cavities with area discontinuities in its acoustic path.

The models for the ossicular path and middle-ear cavities are combined to obtain a comprehensive model for the "intact" cat eardrum impedance.

To

my parents

Nathmull and Gayatri Puria

Acknowledgements

I was in the course "Physiology of Hearing" being taught by Prof. Juergen Tonndorf at the Speech and Hearing Department of the CUNY Graduate School. It was that very semester that Prof. Tonndorf became ill and Dr. Jont B. Allen was asked to teach the course in his place. Subsequently, Jont brought me into the Acoustics Research Department at AT&T Bell Laboratories. During my almost four years of association with Jont he has been a mentor, a colleague, and a friend. He has taught me many of the subtleties of cochlear and middle-ear mechanics. He has also taught me the many tools necessary for good research that will be of vital importance in my future career. I thank Jont for believing in me and giving me so much of his time.

The hearing group of the Acoustics Research Department at Bell Laboratories consisted of Jont B. Allen, Joe L. Hall, Odet Ghitza, David A. Berkley, Patricia S. Jeng, and Brent S. Townshend. In the half-monthly meetings, I had the opportunity to learn various aspects of hearing which has contributed significantly to broaden my understanding of hearing. I thank everyone in that group.

With his tremendous patience Mohan M. Sondhi has been a role model as a researcher and as a teacher. We have had many discussions that extended my understanding and appreciation of acoustics.

I thank my adviser Prof. Nenad M. Marinovic for giving me the freedom and encouragement to pursue my interests in hearing research.

It was in Prof. Aurel A. Lazar's course on Speech and Hearing at Columbia University that cochlear mechanics captured my imagination. I thank him for introducing me to the field.

I thank the Information Principles Research Laboratory at AT&T Bell Laboratories for providing financial support and use of its facilities. The list of the many wonderful people that I met there is much too long for me to replicate here. They collectively made Bell Laboratories not only intellectually rewarding but also a fun place to be.

My friend and office-mate Patricia S. Jeng provided much moral support which I can never forget. I will also never forget the many wonderful evenings spent at Pat and Jont's house.

I wish to thank my family who have supported me many ways. By working hard himself, my father taught me the importance of hard work. The help of my sister Sunita and my brother-in-law Krishan Bansal during the early stages of Graduate School is greatly appreciated. Finally, I wish to thank all my friends for all the fun we have had together.

Contents

List of Tables

List of Figures

Chapter 1

Introduction

The mammalian auditory system is a highly complex one, consisting of peripheral auditory mechanisms and central auditory mechanisms. The role of the peripheral auditory mechanisms, collectively called the ear, is to convert the acoustic sound energy in the external environment to neural information which is further processed by central auditory mechanisms. In this study we will concentrate on the peripheral auditory mechanisms.

The ear can be, anatomically and functionally, divided into three distinct sub-systems called the external ear, middle ear, and the inner-ear. Figure 1.1 shows the anatomy of the human ear. The external ear is made up of the pinna and the ear canal. The middle ear is made up of the tympanic membrane (TM), often reffered to as the eardrum, and three of the smallest bones in the human body, known as the ossicles; they are named the malleus, the incus, and the stapes. The inner ear is commonly referred to as the cochlea. The middle ear is a mechanical coupler that couples sound energy from the air-filled ear canal to the fluid-filled cochlea. Thus sound pressure in the ear canal results in motion of the eardrum, and this results in motion of the stapes. The cochlea is the organ that transduces (or converts) the mechanical motion of the stapes to neural information present in the auditory nerve.

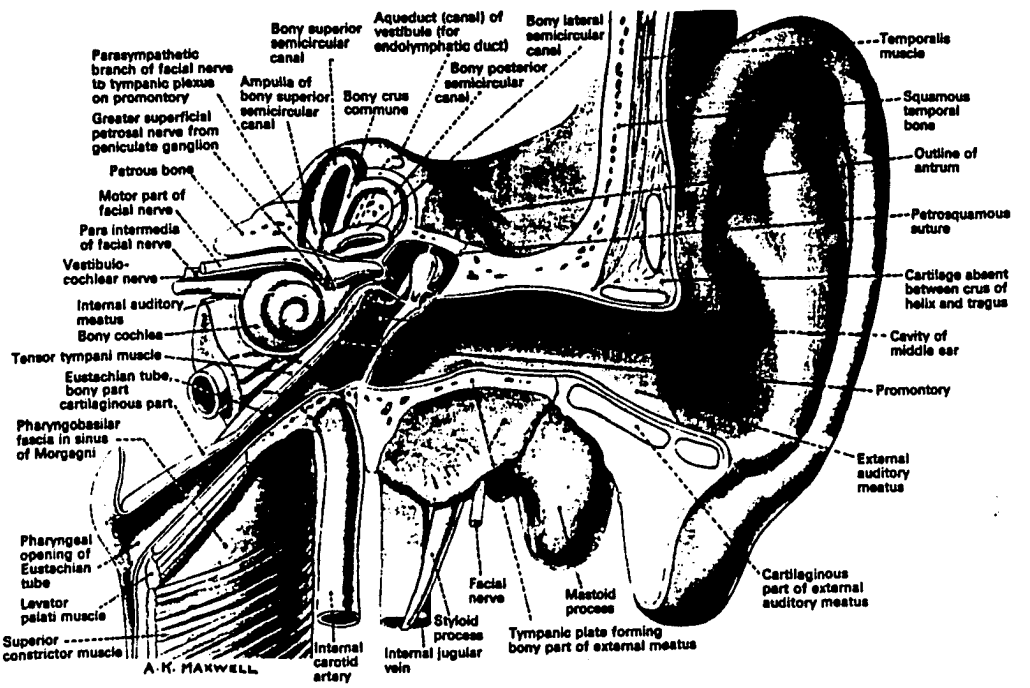

Figure 1.1: *Anatomy of the human auditory periphery:* The ear can be, anatomically and functionally, sub-divided into three sub-systems called the external ear, middle ear, and the inner ear. The external ear consists of the pinna, and the external auditory meatus (earcanal). The middle ear consists of the tympanic membrane, also known as the eardrum, and the three ossicles named: malleus, incus, and stapes. The spiral-shaped cochlea, is the fluid filled organ that transduces mechanical motion of the stapes to neural information present at the cochlear nerve.

Progress has been made in the past to understand and characterize each of the three subsystems of the ear by both direct experimental observations and models. Given the location – deep in the temporal bone – and the size of the cochlea and middle ear anatomy, it is a difficult task to accurately measure motions of the various components directly. Since models depend on measured data, it is important to have accurate measurements. Accurate measurements of the cochlear input impedance and the driving point impedance of the eardrum are available in the literature for the cat. In broad terms, the tack taken here is to first model the impedance data of the inner ear and then to model the impedance data of the eardrum. In addition, a model for the external auditory meatus is proposed.

The cochlea, a distributed parameter system consisting of many physically moving components, is the most complex organ of the auditory periphery. The net effect of all these moving parts, on the middle ear, can be described by a single measure called the cochlear input impedance $Z_c(\omega)$. Thus $Z_c(\omega)$ is the "load" seen by the middle ear. A large portion of the energy that appears in the ear canal is dissipated by the cochlea, indicating that the effect of the cochlear input impedance on the middle ear is quite significant. Theoretical models of $|Z_c|$ for the cat are below the measured data by as much as 20 dB for frequencies below 1-2 kHz. One of the assumptions of past theoretical cochlear models has been that the geometry of cochlea does not play a role in the transduction process. As a result, the fluid filled vestibule of the cochlea was typically represented by a constant cross-sectional area model. This dogma is reexamined in this thesis by modeling the measured cochlear input impedance. Effects of other cochlear model parameters such as the cochlear map, fluid viscosity, and the helicotrema boundary condition are also reexamined. Computations of the cochlear input impedance for man, chinchilla, and guinea pig are compared to those of the cat.

The middle ear consists of two distinct acoustic pathways. First, there is the *ossicular* pathway

due to the eardrum, ossicles, and the cochlea. Second, is the acoustic path due to the middle ear cavities. The ossicular path consists of many components that are mechanically connected. The impedance measured at the eardrum is a function of the parameters of its various components. To understand the role of each component, in the transduction process, it is helpful to have eardrum impedance measurements for the normal condition and eardrum impedance measurements with various "surgical modifications" along the ossicular pathway. Eardrum impedance measured with different "surgical modifications" help to constrain the estimated parameters of the middle ear. A specific procedure is outlined to estimate the parameters of the middle ear based on eardrum impedance measurements as such.

The acoustic path of the middle ear cavities is not very well understood. It is believed that the acoustic path due to the middle ear cavities is more species dependent than the ossicular path. The cat middle ear cavity is divided into two cavities by a bony septum. In the past, the middle ear cavities have been modeled as lumped parameter circuit models representing the volumes of the cavities. To analyze the middle ear cavities, a general model for representing a cavity with a varying cross-sectional area is formulated. This model includes effects due to non-planer wave propagation near an area discontinuity, effects due to visco-thermal losses at the cavity walls, and, effects due to finite wall impedances. The chain-matrix model for cavities is used to analyze what possible role the middle ear cavities might play on properties of the eardrum impedance.

Having developed a model for both the ossicular path and the middle ear cavities, the question: how does one combine the two models, arises. The assumption that the two models can be added in series is presently reexamined.

The chain-matrix model for a cavity with a varying cross-sectional area is verified by making impedance measurements on several cylindrical cavities with sudden jumps and constriction in

their cross-sectional area.

In summary, the gross anatomy of the cochlea and the middle ear cavities have been ignored in the past. This thesis endeavors to explore this and other considerations in much greater detail. Additionally, a method for constraining the estimated parameters of the ossicular path based on eardrum impedance measurements is presented.

Chapter 2

The tapered cochlea model *

2.1 Introduction

Many aspects of cochlear models are known to fail at low frequencies (i.e. below 1-2 kHz). These problems become worse as the frequency decreases. As the traveling wave approaches the end of the cochlea, the apical boundary condition becomes important. An improper boundary condition leads to apical reflections of the traveling wave. These model failures are most easily seen by studying the cochlear input impedance $Z_c(\omega)$ where many of the model pathologies manifest themselves. While cochlear input impedance for animals shows no indication of apical reflections at low frequencies, model cochlear input impedance data show the presence of high Q (f_0/bandwidth) cochlear resonances or cochlear standing waves for frequencies below 500 Hz (Matthews, 1980). A presence of these standing waves in nonlinear cochlear models would likely result in other serious artifacts that could confound further interesting results. To our knowledge there does not exist any study in the cochlear modeling literature on how to eliminate these resonances. Most previous one-dimensional cochlear models (Peterson and Bogert, 1950; Zwislocki, 1950), two-dimensional cochlear models (Lesser and Berkley, 1972;

*Portions of this Chapter and Chapter 3 have been accepted for publication in *J. Acoust. Soc. Am.*, 1991, 89(1), pp 287-309.

Sondhi, 1978), non-linear cochlear models (Hall, 1974), active models (Neely and Kim, 1986), and non-linear active models (Diependaal, 1988) have assumed a cochlea map of the form $f_{CF}(x) = A[10^{-\frac{a}{x_L}(x-x_L)}]$. A cochlear map of this form will be referred to as a straight cochlear map. Standing waves exist under the condition of large reflection coefficients at the stapes end and at the apical end of the cochlea. In this study we shall show how standing waves as seen in Z_c, are related to the cochlear map, scalae tapering, viscosity, and the helicotrema impedance.

A second problem concerns the magnitude and phase of the cochlear input impedance at low frequencies. Previous cochlear models indicate that the cochlear input impedance significantly decreases in magnitude for frequencies below 1-2 kHz. For the cat, models and experimental magnitude data of Lynch *et al.* (1982) are in disagreement by as much as 16 dB at 50 Hz. In the real cochlea, the scalae are tapered, with a decreased area at the apex. Also, in the real cochlea, the scalae fluids are viscous. These scalae-area changes and viscous-losses play an important role at low frequencies (Koshigoe *et al.*, 1983). Only by including scalae tapering and viscosity, can we hope to overcome the nonrealistic standing waves, and hope to accurately model the cochlear input impedance at low frequencies.

In summary, there is a poor general understanding of low frequency phenomena in the cochlea. In this study we investigate low frequency cochlear phenomena by modeling the cochlear input impedance.

There are other reasons besides low frequency modeling questions that motivate us to study the cochlear input impedance. *First,* the mechanical "load" on the middle ear is the input impedance of the cochlea $Z_c(\omega)$. Inaccurate representations of Z_c will result in middle-ear model parameters that are not representative of the physical system. A good model for Z_c is necessary to estimate the middle ear parameters accurately (Moller, 1965).

Second, accurate knowledge of Z_c is crucial for energy flow considerations in the forward and reverse directions. The acoustic energy in the ear canal normally propagates towards the cochlea. There have been many observations made in the ear canal indicative of non-linear, and perhaps active, acoustic emissions originating in the cochlea. These emissions result from a reverse energy flow from the cochlea to the ear canal. Examples include the cubic difference tones resulting from non-linearities within the cochlea (Wilson, 1980; Kim *et al.*, 1980; Fahey and Allen, 1985), as well as spontaneous and evoked otoacoustic emissions observed by Kemp (1978;1979), Zurek (1981), and others. The impedance mismatch at the cochlea-stapes boundary reflects back some of the acoustic emissions generated in the organ of Corti (Kemp, 1980). The rest of the energy passes through the middle ear and appears in the ear canal. To estimate the reflection and transmission of energy at the cochlea-stapes interface, it is necessary to have a good model of the middle ear and of the cochlear input impedance.

This Chapter is organized as follows: In Section 2.2 we review previous models and measurements of cochlear input impedance. In Section 2.3 the the model equations are formulated. A summary of this Chapter can be found in Section 2.4. In the Chapter that follows we use the model to analyze some of issues outlined in the introduction.

2.2 Previous work

Figure 2.1 shows the Lynch *et al.* (1982) lumped network representation of the cochlear input impedance, which encompasses many previous models. It is an electrical analog of the mechanical system under consideration with voltage corresponding to pressure and current to volume-velocity. In Table 2.1 we summarize the results of numerous research vis-à-vis the model of Fig. 2.1. Lynch *et al.* (1982) estimated parameters for the network of Fig. 2.1 based on averaged experimental

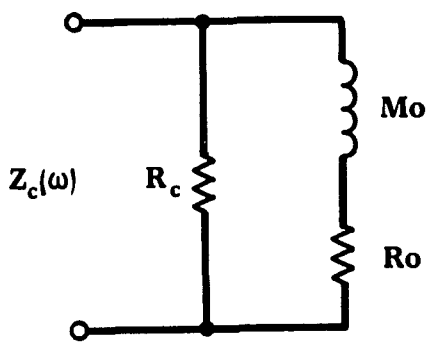

Figure 2.1: Many previous models of Z_c can be generalized by this lumped parameter circuit. The values for R_c, R_o, M_o and the mechanisms corresponding to them are listed in Table 2.1.

input impedance data. We start from the Lynch *et al.* model because the experimental data, on which that model is based, is the most comprehensive. This makes their network model a good reference point for comparisons. R_c in Fig. 2.1 represents the cochlear impedance at high frequencies. At low frequencies, Z_c is given by the parallel combination of R_c and R_o. A transition region exists, which is between 10 Hz and 200 Hz, where the mass M_o has an effect.

Based on modeling considerations, Zwislocki (1965) estimated $Z_c(\omega)$ to be real and of value $R_c = \sqrt{2\rho K_o/\beta_o S_o}$, as shown in Table 2.1.

Tonndorf *et al.* (1966) measured $|Z_c|$ for the cat and showed it to be frequency dependent. They found a 6 dB/oct slope for frequencies below 400 Hz. Near 400 Hz, $|Z_c|$ was approximately 8 $M\Omega$ (10^6 $dyn-sec/cm^5$). Above 400 Hz $|Z_c|$ decreased, and at approximately 1 kHz tended to fluctuate between 2-5 $M\Omega$. The maximum error they reported was a factor of 3 ($\pm$9.5 dB). Dancer and Franke (1980) on the other hand did not find a low frequency slope in their measurements of the guinea pig cochlear input impedance magnitude.

Table 2.1: *Comparison of Z_c by various researchers:*

Figure 2.1 is a companion figure to this table. The model of Z_c by Zwislocki, based on mathematical considerations, is a pure resistor R_c. Dallos' model, builds on Zwislocki's model by adding the series combination of mass of the helicotrema M_o and damping of the helicotrema R_o in parallel with R_c. Allen derived a model for Z_c based on the WKB approximation to the one-dimensional formulation of the cochlea. Allen's model is also the one of Fig. 2.1, but with R_o=0. Since R_o=0 in Allen's model, $\lim_{f\to 0} |Z_c| \to 0$ and $\lim_{f\to 0} \angle Z_c \to \frac{\pi}{2}$. Figure 2.1 is also the Lynch *et al.* model, based on measured data. In that model $\lim_{f\to 0} |Z_c| \to R_c \| R_o$, and $\lim_{f\to 0} \angle Z_c \to 0$, due to the presence of R_o. Thus there is a low frequency discrepancy in the theoretical models of Z_c and the measured data. This discrepancy is most significant for frequencies below 1 kHz, and is as large as 20 dB at 10 Hz. Based on approximate solutions to a one-dimensional formulation of the cochlea, Koshigoe *et al.* conjectured that this low frequency discrepancy in Z_c is due to the effects of viscosity. In addition to not providing a good fit to the measured data, the Koshigoe *et al.* model does not attribute any physical mechanism(s) to R_o. However, they first argued that it is important to incorporate tapered scalae area in model calculations.

Table 2.1: Comparison of Z_c by various researchers.

Reference	Model	Parameter $R : dyn - sec/cm^5$ $M : g/cm^4$	Physical or Physiological Basis
Zwislocki (1965)	Fig. 2.1	$R_c = \sqrt{\frac{2\rho K_o}{\beta_o S_o}}$ $R_o = M_o = \infty$	BM compliance and scala area at base
Tonndorf *et al.* (1966)			measured $\lvert Z_c \rvert$ data for the cat
Dallos (1970)	Fig. 2.1	R_c: as per Zwislocki R_o, M_o species dependent [see Eq. (2.11)]	R_o, M_o due to helicotrema
Sondhi (1978)	Numerical calculation	similar to WKB [see Fig. 3.4]	from one- and two-dimensional cochlear models
Allen (1979)	Fig. 2.1	$R_c = \frac{2\rho c_0}{S_0} = \sqrt{\frac{2\rho H K_o}{S_o^2}}$ $R_o = 0, M_o = \frac{8\rho}{S_o k_1}$	derived from WKB
Dancer and Franke (1980)			measured $\lvert Z_c \rvert$ data for the guinea pig
Lynch *et al.* (1982)	Fig. 2.1	$R_c = 1.2 \times 10^6$, $R_o = 0.28 \times 10^6$, $M_o = 2250$	phenomenological: based on measured data for the cat
Koshigoe *et al.* (1983)	$R + sM$	$R = R_o(\omega), M = M_o(\omega)$	Z_{BM}, viscosity and constant cross-sectional area
Koshigoe *et al.* (1983)	Numerical calculation	see Fig. 3.9	Z_{BM}, viscosity and tapered cochlea

Dallos' (1970) model closely resembles the Lynch *et al.* (1982) model. The physical basis for R_o and M_o, as hypothesized by Dallos, is the viscosity and mass of a short tube representing the helicotrema, with the transition region being between 100 Hz and 1 kHz. In cochlear modeling, the helicotrema boundary condition has always been a point of conjecture. We shall show that when we assume physiologically reasonable parameters, this boundary condition has a negligible effect.

Allen's (1979) derivation of Z_c is based on the Wentzel-Kramer-Brillouin (WKB) approximation to the wave-equation formulated for a cochlea model with constant scalae area, zero perilymph viscosity, no reflections, and no helicotrema. The WKB solution assumes that the wavelength along the cochlea varies slowly and thus there are no reflections. Under such circumstances the forward-traveling wave-equation can be approximately solved by expressing the solution as an asymptotic series. Based on this approach Allen's Z_c is different from the Lynch *et al.* model to the extent that $R_o = 0$. It is the inclusion of R_o in the Lynch *et al.* model that gives rise to the behavior of Z_c below 200 Hz. From Table 2.1 we see that the WKB R_c is given by $2\rho c_0/S_0$, where c_0 is the speed of the traveling wave on the basilar membrane at the stapes and the area at the base is $S_0 = S(0)$. By substituting the value for c_0 it is easy to show that the WKB R_c is equivalent to Zwislocki's radiation resistance R_c. At low frequencies the WKB input impedance is dominated by the mass given by $M_o = 8\rho/(S_0 k_1)$, which depends on the rate of change parameter k_1 of the BM stiffness at the stapes. In this model, the cochlear input impedance depends only on the physical parameters of the cochlea in the neighborhood of the stapes.

Sondhi's (1978) numerical calculations of Z_c from one-dimensional and two-dimensional cochlear models are qualitatively similar to the WKB solutions for Z_c.

It is natural to consider what physical mechanisms give rise to R_o in Fig. 2.1 . Can R_o be

accounted for by including scalae tapering and viscosity? Given that R_o affects the very low frequency region, it is reasonable that perhaps the source of its effect is in scalae viscous losses.

Koshigoe *et al.* (1983) provide a mathematical framework that addresses this issue. Their derivation of Z_c, in a cochlear model with viscosity and constant scalae area, consists of frequency dependent parameters R_o and M_o. However since their results do not provide a reasonable fit to the measured input impedance data, and their expressions fail to give insight into the mechanisms that dominate at frequencies below 500 Hz, further analysis is in order. Koshigoe *et al.* also calculated Z_c for a tapered scalae area model, with and without viscosity. At frequencies below 500 Hz their inviscid calculations indicate $|Z_c|$ to be four to five times *smaller* than those which include viscosity. We will show that this result is inconsistent with our own numerical calculations. However, they were the first to argue the importance of the tapered scalae in model calculations.

In Chapter 3 we have made extensive use of the impedance model and data of Lynch *et al.* (1982). To qualitatively isolate the parameters that have the greatest influence on the cochlear input impedance, we initially use the averaged measured data and model results of Lynch *et al.*. We then use their individual data in an attempt to understand the individual differences.

2.3 The chain-matrix formulation for cochlear mechanics

The cochlea, in most animals, is a spiral-shaped structure. It consists of three fluid-filed chambers called the scala vestibule, scala media, and the scala tympani. In this study we assume that the effect of the spiral-shape on the acoustical properties of the cochlea are insignificant (von Békésy, 1960, p. 407; Viergever, 1978). Figure 2.2a shows a simplified sketch of the cochlea when it is uncoiled from its spiral-shape. In Fig. 2.2a it is further assumed that the scala media is treated as part of the scalae vestibule. The two resulting chambers are separated by the organ of Corti.

which is assumed to have a width $\beta(x)$. The scala vestibule area $S_V(x)$ and scala tympani area $S_T(x)$ are assumed to vary along the cochlear length. The distance x is measured from the stapes end. The basal end of the cochlea corresponds to $x = 0\ cm$ and the apical end of the cochlea corresponds to $x = x_L\ cm$, where x_L is the total length of the cochlea. The scalae are divided into n_p cylindrical segments, each of length $\Delta\ cm$. Under the assumptions of conservation of fluid mass and momentum, we obtain long-wave expressions for the pressure and volume-velocity.

2.3.1 Some definitions

In the formulation of our model equations, several different types of impedances and admittances are required. There are two basic types of velocities in acoustics, particle velocity and volume-velocity. The volume-velocity is given as surface integral over the particle velocity. Frequently an equivalent uniform distribution of velocity is assumed, in which case, the volume velocity is defined as the area times the effective particle velocity. The two different types of velocity lead to two different types of impedance which are called *specific impedance*, and *acoustic impedance*. The specific impedance is given as the ratio of the pressure difference divided by the particle velocity, and has units $dyn - sec/cm^3$. The acoustic impedance is defined as the pressure difference divided by the volume velocity, which has units $dyn - sec/cm^5$. The cochlear input impedance Z_c, the helicotrema impedance Z_h, the characteristic impedance of a tube Z_o, and the series and shunt impedance of a "T" network Z_a and Z_b are all acoustic impedances. We must also define the series acoustic impedance Z and the shunt acoustic admittance Y for the lossy transmission line on a per unit length basis in units of $dyn - sec/cm^6$ and $cm^4 \cdot dyn^{-1} \cdot sec^{-1}$. These and other symbols used in this Chapter and Chapter 3 are listed in Appendix A.

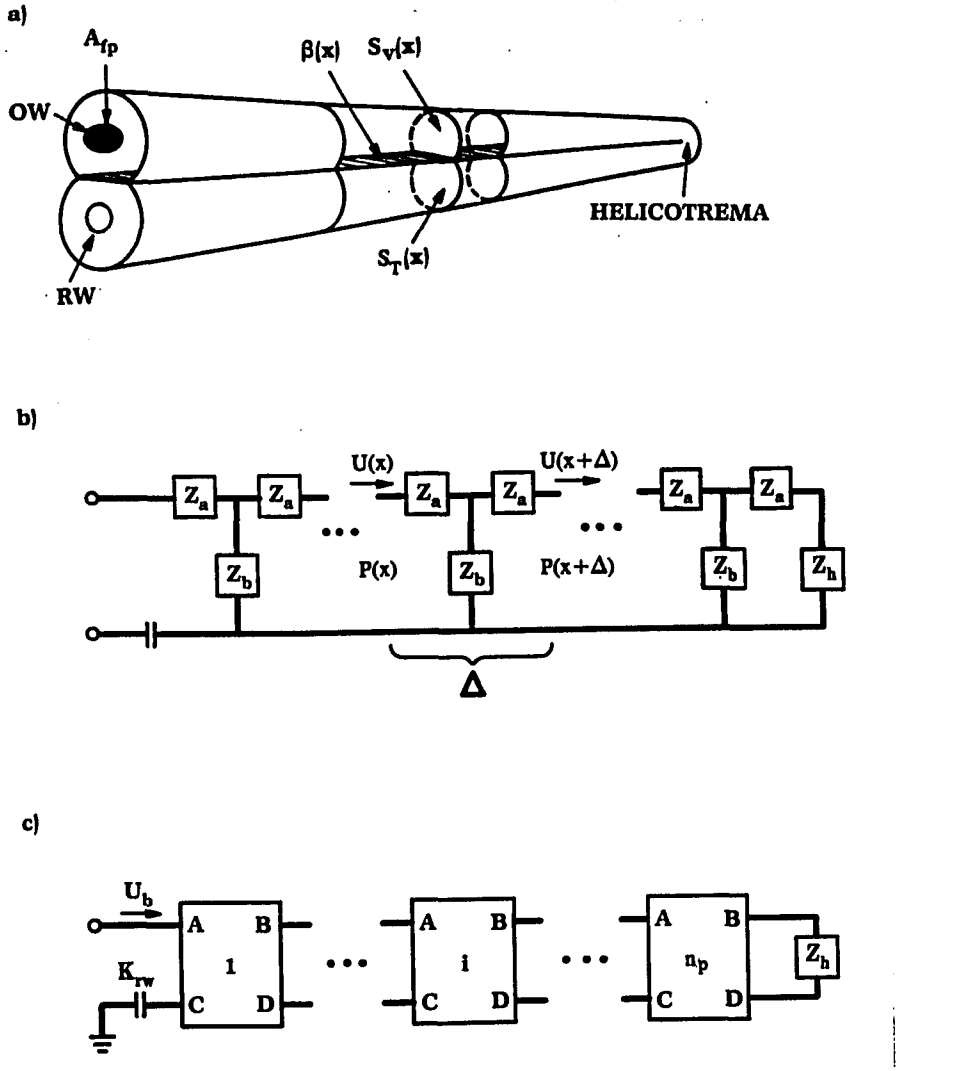

Figure 2.2: (a) *Approximate physical representation of the Cochlea:* $S_V(x)$ and $S_T(x)$ are the scala vestibule and scala tympani area functions, $\beta(x)$ is the basilar membrane (BM) width, RW is the round window, and OW is the oval window. The footplate, with area A_{fp}, is at the basal end of the cochlea and the helicotrema is at the apical end of the cochlea. Not shown here is the stapes which would have been attached to the footplate at the oval window. (b) *Equivalent model in terms of "T" sections:* the elements $Z_a(x,\omega)$ and $Z_b(x,\omega)$ are functions of both position along the length of the cochlea and stimulus frequency. The cochlea is divided into n_p sections of length Δ *cm.* (c) *Chain-matrix formulation of the physical model of (a):* The matrices are formulated to include changes in scalae area, effects due to perilymph viscosity, and variations in the organ of Corti. U_b is the volume velocity at the base, K_{rw} is the round window stiffness, and Z_h is the impedance of the helicotrema.

2.3.2 General approach

Starting from the basilar membrane impedance $Z_{BM}(x,\omega)$, the series impedance $Z(x,\omega)$, and shunt admittance $Y(x,\omega)$ from lossy transmission line theory, we would like to formulate the chain matrix elements, $A(x_i,\omega)$, $B(x_i,\omega)$, $C(x_i,\omega)$, $D(x_i,\omega)$ (as shown in Fig. 2.2c). The basilar membrane impedance $Z_{BM}(x_i,\omega)$ is given in terms of the physical variables relevant to the cochlea as described in Appendix C. From Z_{BM}, the BM width $\beta(x)$, the scalae area $S(x)$, we may find the shunt admittance per unit length of the basilar membrane $Y'_{BM}(x_i,\omega)$. The lossy transmission line impedance Z and shunt admittance Y are described in Appendix B. We then find Z' and Y', which are the cochlear two chamber series impedance per unit length, and shunt admittance per unit length. These allow us to find Γ and Z_0, the propagation constant and characteristic impedance, for the lossy cochlear transmission line. Next we find the "T" elements Z_a and Z_b (see Fig. 2.2b), and finally the chain matrix elements, A, B, C, and D, which can be expressed in terms of the "T" elements.

2.3.3 Lossy BM series impedance

The equation for the series impedance $Z(x,\omega)$ [Eq. (B.1)] is for a single vestibule. Anatomical measurements of scala vestibule cross-sectional area $S_V(x)$ and scala tympani cross-sectional area $S_T(x)$ on humans indicate the areas of the two vestibule to be approximately equal for distances greater than 0.3 cm from the round window (Wever, 1949, pp. 276-278). To our knowledge measurements of the cat scala tympani cross-sectional area are not available in the literature. Thus we will assume $S(x) = S_V(x) = S_T(x)$. The series impedance for a two chamber model then is

$$Z'(x,\omega) = 2Z(x,\omega). \tag{2.1}$$

The two impedances Z and Z' are given as per unit length series acoustic impedances ($dyn - sec/cm^6$) along the vestibule.

2.3.4 Lossy BM shunt admittance

To find the lossy transmission line shunt admittance for the cochlea, we must modify Y of Appendix B to include the shunt admittance due to the basilar membrane. The basilar impedance impedance $Z_{BM}(x,\omega)$is a specific impedance ($dyn - sec/cm^3$). From a macromechanical point of view, Z_{BM} consists of BM stiffness $K_b(x)$, damping, and mass. $Z_{BM}(x)$ is a physically motivated, micromechanical model of BM specific impedance that incorporates a resonant tectorial membrane (Allen, 1980) and which leads to a fourth order equation for partition dynamics. These parameters depend on the cochlear map as shown in Appendix C.

The shunt admittance due to viscous losses Y and the shunt admittance due to the basilar membrane Y'_{BM} are in per unit length acoustic admittances ($cm^4 \cdot dyn^{-1} \cdot sec^{-1}$). The BM impedance $Z_{BM}(x,\omega)$, when transformed † to basilar membrane acoustic admittance per unit length is,

$$Y'_{BM}(x,\omega) = \frac{S_0}{H\ Z_{BM}(x,\omega)} \tag{2.2}$$

Thus, the total lossy transmission line acoustic admittance per unit length is found by adding the two admittances together

$$Y'(x,\omega) = 2Y(x,\omega) + Y'_{BM}(x,\omega). \tag{2.3}$$

The factor of 2 accounts for the admittance due to the two chambers.

† $Z_{BM}(x)$ was formulated for the rectangular coordinate system with height H cm. The present model is formulated in the cylindrical coordinate system. The impedance transformation was necessary for the results of the two formulations to be equivalent (Viergever, 1980, p. 69).

Equation (2.2) is the BM acoustic admittance per unit length. Model parameters and physical measurements of the BM are often given in terms of BM specific impedance. For our model we use

$$Z'_{BM}(x,\omega) = \beta(x)/Y'_{BM}(x,\omega) \tag{2.4}$$

In this equation the transformed BM stiffness is $K'(x)$. The basilar membrane stiffness at the base is defined as $K'_0 = K'(x = 0)$.

2.3.5 Effect of fluid compression

For most fluids, including perilymph, the ratio of specific heats $\gamma \simeq 1$, and thus $G(x,\omega)$ of Eq. (B.5) is zero; consequently $Y(x,\omega)$ in Eq. (2.3) reduces to $sC(x)$.

The compliance $C(x) = S(x)/\rho c^2$ is a measure of compressibility of the fluid. Near the base, $2C(x)$ is less than 6% of the basilar membrane admittance, and in the apical region, $2C(x)$ is at least three orders of magnitude smaller than Y'_{BM}. Although not shown here, the effect of including $s2C(x)$ in Eq. (2.3) on $|Z_c|$, was found to be less than 0.5 dB near 20 kHz. No differences were observed in $\angle Z_c$. This shows that the incompressibility assumption of the cochlear fluids is valid and that the shunt admittance can be approximated as,

$$Y'(x,\omega) \approx Y'_{BM}(x,\omega) \tag{2.5}$$

for all further calculations. In the above formulation, the cells of the organ of Corti are assumed to be incompressible.

2.3.6 Transmission line parameters

Given Z' and Y' one may calculate the characteristic impedance Z_0 and the propagation constant Γ for the lossy cochlear transmission line

$$Z_0(x,\omega) = \left(\frac{Z'}{Y'}\right)^{1/2}, \tag{2.6a}$$

$$\Gamma(x,\omega) = (Z'Y')^{1/2}. \tag{2.6b}$$

Transformation to the equivalent cochlear T network of Fig. 2.2 b is defined in terms of Z_a and Z_b as follows: (Flanagan, 1983, chap. 3):

$$Z_a(x,\omega) = Z_0 \tanh\left(\frac{\Gamma\Delta}{2}\right), \tag{2.7a}$$

$$Z_b(x,\omega) = Z_0 \mathrm{csch}(\Gamma\Delta). \tag{2.7b}$$

2.3.7 Chain-matrix form

The relationship for the pressure and volume velocity of each section of length Δ can now be put in $chain - matrix$ form (Weinberg, 1962; Pierce, 1989)

$$\begin{bmatrix} P(x) \\ U(x) \end{bmatrix} = \begin{bmatrix} A & B \\ C & D \end{bmatrix} \begin{bmatrix} P(x+\Delta) \\ U(x+\Delta) \end{bmatrix}, \tag{2.8}$$

where elements of the ABCD chain-matrix are

$$A = 1 + \frac{Z_a}{Z_b}, \tag{2.9a}$$

$$B = Z_a\left(2 + \frac{Z_a}{Z_b}\right), \tag{2.9b}$$

$$C = \frac{1}{Z_b}, \tag{2.9c}$$

$$D = A. \tag{2.9d}$$

Equation (2.8) relates the pressure difference and volume velocity of a cylindrical section at x given the pressure difference and volume velocity of a section at $x + \Delta$. Inherent in the formulation of Eq. (2.8) is a *forward and backward traveling-wave.*

Referring to Fig. 2.2c, the chain is started at the helicotrema end by assuming $U(x_L) = 1$. The unit volume-velocity results in a pressure drop $P(x_L)$ across $Z_h(\omega)$, the acoustic impedance of the helicotrema. Equation (2.8) is then recursively calculated with the space index decreasing from $x = x_L$ at the helicotrema end to $x = 0$ at the base, for n_p segments. $P(x)$ and $U(x)$ are finally normalized so that the calculated volume-velocity at the base $U(0) = u_b S_0$, to satisfy the boundary condition in the base of the cochlea.

We used the chain-matrix method to do all the calculations for each of the n_p segments. The number of sections n_p was successively increased by a factor of two until no further change in the results were observed; this occurred at $n_p = 1024$. The computations were carried out on an Alliant FX/80 computer. To verify our chain-matrix method we made comparisons of Z_c and the BM velocity calculated by solving Laplace's equation for the constant scalae height and zero viscosity case, using the difference equation [‡] method (Allen, 1977). In making these comparisons, we discovered a helicotrema boundary condition problem at low frequency. This will be further discussed in section 2.3.10. With this exception, calculations of the cochlear input impedance and BM volume-velocity were identical for the two methods.

2.3.8 Cochlear input impedance

The volume-velocity that enters the stapes is $u_{st} A_{fp}$. By conservation of mass, this volume velocity is equal to the volume velocity entering the scala vestibule in the base $u_b S_0$. The cochlear

[‡]The model of (Allen, 1977) was formulated for a two-dimensional cochlear model (4^{th} order system of equations in the notation of that paper). The formulation was sufficiently general enough so as to allow an one-dimensional formulation (2^{nd} order system of equations), as is appropriate for the present case.

acoustic input impedance is then calculated from

$$Z_c(\omega) = \frac{P(0)}{u_{st} A_{fp}}. \tag{2.10}$$

Measurements of pressure in the cat scala vestibule and scala tympani, as a function of the tympanic membrane sound pressure level, and over a wide range of frequencies, have been found to be linear (Nedzelnitsky, 1980). With the tensor tympani muscle cut from the stapes, the mammalian middle ear act as a linear system for sound pressure levels of up to 130 dB-SPL (Guinan and Peake, 1967). Therefore, we assume Eq. (2.10) to hold at all levels of input. The linearity assumption is not necessarily valid for all animals. For example Rosowski *et al.* (1984) have found the acoustic input admittance at the alligator lizard tympanic membrane to be ear canal pressure dependent for stimulus levels greater than 70 dB SPL.

2.3.9 The helicotrema boundary condition

When formulating a cochlear model one may assume different properties for the helicotrema. The two most common boundary conditions are the open circuit $Z_h = \infty$ and the short circuit $Z_h = 0$. A third choice is the (Dallos, 1970) helicotrema model using a short-tube impedance (TI). In this paper we have limited ourselves to either the short-tube or short-circuit impedance boundary condition. The open-circuit assumption is nonphysiological since it does not allow for any flow between the two scalae.

The acoustic impedance of a tube of radius a_h and length l_h given by (Beranek, 1954, p. 135)

$$Z_h(\omega) = \frac{8\eta l_h}{\pi a_h^4} + j\frac{4}{3}\frac{\rho l_h}{\pi a_h^2}\omega. \tag{2.11}$$

This approximate formula is valid for $a_h(\text{cm}) < 0.2/\sqrt{f}$. Dallos (1970) used Eq. (2.11) for his calculations of Z_c. Mulroy (Lynch *et al.*, 1982, note 11) measured the helicotrema radius of the

cat by scanning electron microscope techniques and found it to be $0.0125 \pm 0.0005\ cm$. Using this radius Eq. (2.11) is valid for $f < 256$ Hz. If we assume the helicotrema to be a bent circular tube of radius a_h as above, then the length of the helicotrema $l_h = \pi a_h \approx 0.04\ cm$. The short-circuit condition will be referred to as $Z_h = SC$, and the tube impedance condition will be referred to as $Z_h = TI$ throughout the text.

2.3.10 The BM response

Although this is not explicitly a study of BM mechanics, an intermediate result is the BM volume-velocity at any place along the length of the cochlea

$$U_{BM}(x,\omega) = \frac{P(x+\Delta) + Z_a U(x+\Delta)}{Z_b}, \tag{2.12}$$

where the terms of Eq. (2.12) are identified in Figure 2.2b. The BM center-line particle-velocity, assuming a half-sine shaped velocity distribution over the BM width, is

$$\tilde{U}_{BM}(x,\omega) = \frac{\pi U_{BM}(x)}{2\Delta\beta(x)}. \tag{2.13}$$

By conservation of fluid mass the sum of the complex BM volume-velocity $U_{BM}(x)$ along the length of the cochlea and through the helicotrema *must* be equal to the volume-velocity that enters the base of the cochlea $u_b S_0$, at any given stimulus frequency. This is more formally expressed as the volume-sum

$$u_b S_0 = U(x_L) + \sum_{i=1}^{n_p} U_{BM}(x_i). \tag{2.14}$$

Where $U(x_L)$ is the volume-velocity through the helicotrema and $x_i = \Delta i$. Note that $u_b S_0$ is a real quantity and thus the sum of the imaginary part of Eq. (2.14) must be zero. In the difference equation formulation of Allen (1977), Eq. (2.14) was found to be violated for low frequencies

(below 200-300 Hz). This was true independent of the cochlear map used. We attribute this to an improper volume-velocity at the helicotrema boundary $U(x_L)$ in that model.

2.4 Summary

To this point we have formulated a one-dimensional cochlear model which includes scalae area variations, viscous losses due to perilymph, organ of Corti impedance variations etc., using the chain-matrix formalism. In the following Chapter we analyze the effects of variations in the cochlear map, scalae geometry, perilymph viscosity, and the helicotrema boundary conditions. The transmission line model was chosen so that each of these effects can be analyzed independently. Following Sondhi's observation that the cochlear input impedance for two-dimensional models is indistinguishable from that of one-dimensional models, we have assumed that the one-dimensional formulation will be adequate for this purpose.

Chapter 3

The cochlear input impedance

Having developed the chain-matrix cochlear model in Chapter 2 we now use that model to analyze various low frequency effects discussed in that chapter, as well as high frequency effects that have previously not been analyzed.

This chapter is organized as follows: Section 3.1 shows the effects of various cochlear maps on Z_c. In Sections 3.2 and 3.3, the effects of viscosity and the helicotrema on Z_c are analyzed, assuming a constant scalae area. Sections 3.4 and 3.5 show the effects of scalae tapering on Z_c, and the interactions of tapering with viscosity and the helicotrema. Section 3.6 compares measured data and the model with tapering and viscosity. Resulting comparisons to the Lynch *et al.* (1982) experimental data are also shown in Sections 3.6 for several choices of parameter variations. Inter-animal variations are discussed in Section 3.7. Computations of $Z_c(\omega)$ for man, guinea pig, and the chinchilla are shown in Section 3.8. An inter-species comparison is made in Section 3.9. A discussion of the results can be found in Section 3.10, followed by a summary in Section 3.11. A list some of the symbols used in this chapter can be found in Appendix A.

3.1 Apical reflections and the cochlear map

As discussed in Appendix C, an important parameter for the computation of the basilar membrane impedance $Z_{BM}(x)$ is the cochlear map. The cochlear map defines the BM peak velocity location along the length of the cochlea, as a function of the input frequency. The effect of three different *cat* cochlear maps on $Z_c(\omega)$ are compared in this section:

1. Most existing cochlear models use a "straight" cochlear map of the form

$$f_{CF}^{cs}(x) = 456\left[10^{\frac{2.1}{x_L}(x_L - x)}\right], \tag{3.1}$$

where x is the distance in cm from the stapes, the length of the cochlea is x_L, and CF stands for characteristic frequency. The "c" and "s" in the superscript stand for cat and straight cochlear map.

2. Liberman's (1982) cochlear map derived from single neuron labeling experiments is

$$f_{CF}^{cl}(x) = 456\left[10^{\frac{2.1}{x_L}(x_L - x)} - 0.8\right]. \tag{3.2}$$

3. Greenwood's (1961) cochlear map is derived from human psychophysical critical band experiments. It is then scaled from the human cochlea to the cat cochlea. The Greenwood cochlear map, with some modifications (Greenwood, 1990) to his original parameters, is

$$f_{CF}^{cg}(x) = 456\left[10^{\frac{2.1}{x_L}(x_L - x)} - 1\right]. \tag{3.3}$$

It should be noted that the Greenwood cochlear map for the cat used here contains the original subtractive constant 1, whereas he now uses the constant 0.8 found by Liberman to provide the best fit to neural data (Greenwood, 1990). We have used a subtractive term of 1 simply to illustrate the effect of such a cochlear map on apical reflections.

These three cochlear maps are shown for comparison in Fig. 3.1. Once the cochlear map is chosen, our specification of $Z_{BM}(x,\omega)$ is complete (see Appendix C).

Figure 3.2 shows $Z_c(\omega)$ corresponding to the three cochlear maps with an untapered cochlear model, zero viscosity, and a short-circuit helicotrema boundary condition. Figure 3.2a shows the magnitude of $Z_c(\omega)$ and Fig. 3.2 b shows the phase of $Z_c(\omega)$. All succeeding figures illustrating cochlear input impedance calculations will follow this format. The use of a straight cochlear map results in large oscillations in Z_c for input frequencies below $\approx$ 500 Hz, indicative of apical reflections. Liberman's cochlear map reduces the apical reflections, and Greenwood's cochlear map virtually eliminates them.

To the best of our knowledge all previous cochlear models that have used the straight cochlear map have apical reflections, and therefore standing waves, for frequencies below 500 Hz. Published examples include the oscillations in the BM frequency response (Hubbard and Geisler, 1972; Matthews, 1980) as well as the presence of large oscillations in Z_c (Matthews, 1980), as show in Fig. 3.2 . Understanding and eliminating these artifacts is particularly important in time-domain implementations of non-linear cochlear models.

Apical reflections are directly related to the low frequency limit $f_{CF}(x_L)$ of the cochlear map. For example, close examination of Fig. 3.1 reveals that for f_{CF}^{cs}, frequencies below 456 Hz are not defined. Consequently, for input frequencies below this critical frequency, the traveling wave launched at the stapes will reach the apical end and be reflected back towards the stapes. This results in standing waves along the length of the cochlea. For frequencies below 91 Hz, f_{CF}^{cl} is not defined correspondingly there are apical reflections below 91 Hz. Note that the apical reflections actually begin at a frequency slightly above the low frequency end of the cochlea because of the finite slope of the traveling wave apical to the CF.

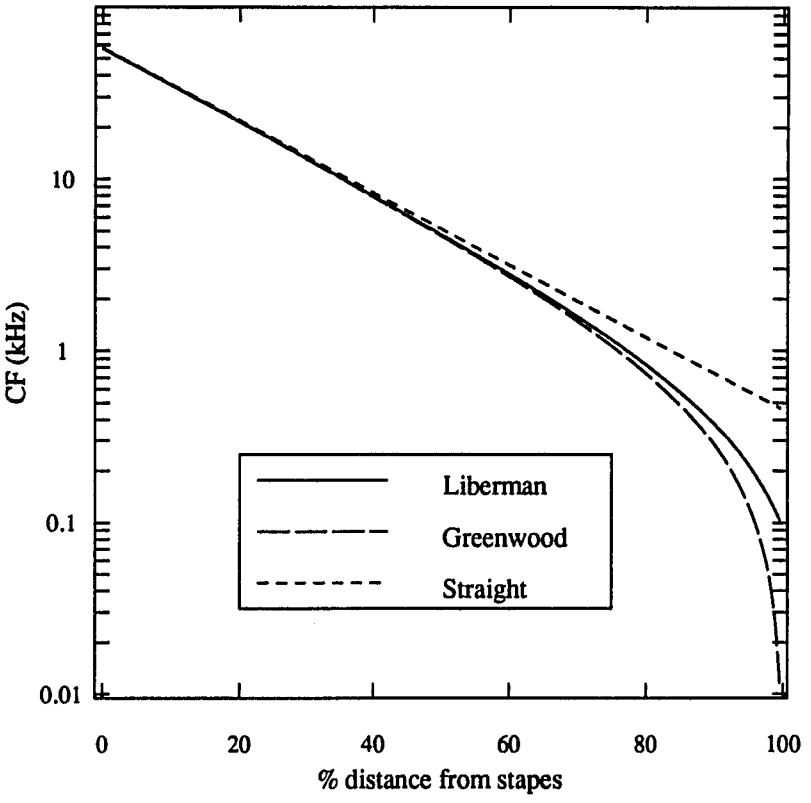

Figure 3.1: *Cochlear map functions for the cat anatomy pertaining to Eqs. (3.1), (3.2), and (3.3) normalized to percent distance from the stapes:* The difference between the three cochlear maps lies mostly in the frequency region below 1 kHz. The cochlear map is used in calculating the basilar membrane specific impedance $Z_{BM}(x,\omega)$. Liberman's cat cochlear map $f_{CF}^{cl}(x)$, based on single auditory-nerve fiber labeling experiments, will be used for all *cat* $Z_c(\omega)$ calculations in this study.

Figure 3.2:

Magnitude and phase of $Z_c(\omega)$ for each of the three cat cochlear maps of Fig. 3.1: The model parameters are: constant scalae area [$S(x) = 0.02\ cm^2$], no viscosity (NV,$\eta = 0$), and an acoustic short circuit (SC) helicotrema boundary condition. The low frequency limit of the straight cochlear map, $f_{CF}^{cs}(x_L)$ is 456 Hz. Stimuli below this frequency result in large amplitude oscillation in Z_c indicating the presence of standing waves. The low frequency limit of Liberman's cochlear map $f_{CF}^{cl}(x_L)$ is 91 Hz. In this case the amplitude of the apical reflections are significantly reduced, but nevertheless present for frequencies below $f_{CF}^{cl}(x_L)$. In Greenwood's cochlear map $\lim_{x \to x_L} f_{CF}^{cg}(x) \to 0$. In this case all frequencies are represented on the basilar membrane and thus the stimulus energy is dissipated by the motion of the BM before it reaches the apical end of the cochlea. Thus there are no apical reflections due to the end of the cochlear map when Greenwood's cat cochlear map is used. Standing waves exist when there are reflections at both the apical end and at the stapes end of the cochlea. One way to eliminate the standing waves is to eliminate the apical reflections. Since the standing waves are eliminated by using Greenwood's cochlear map, we conclude that apical reflections are directly related to the low frequency limit of the cochlear map $f_{CF}(x_L)$.

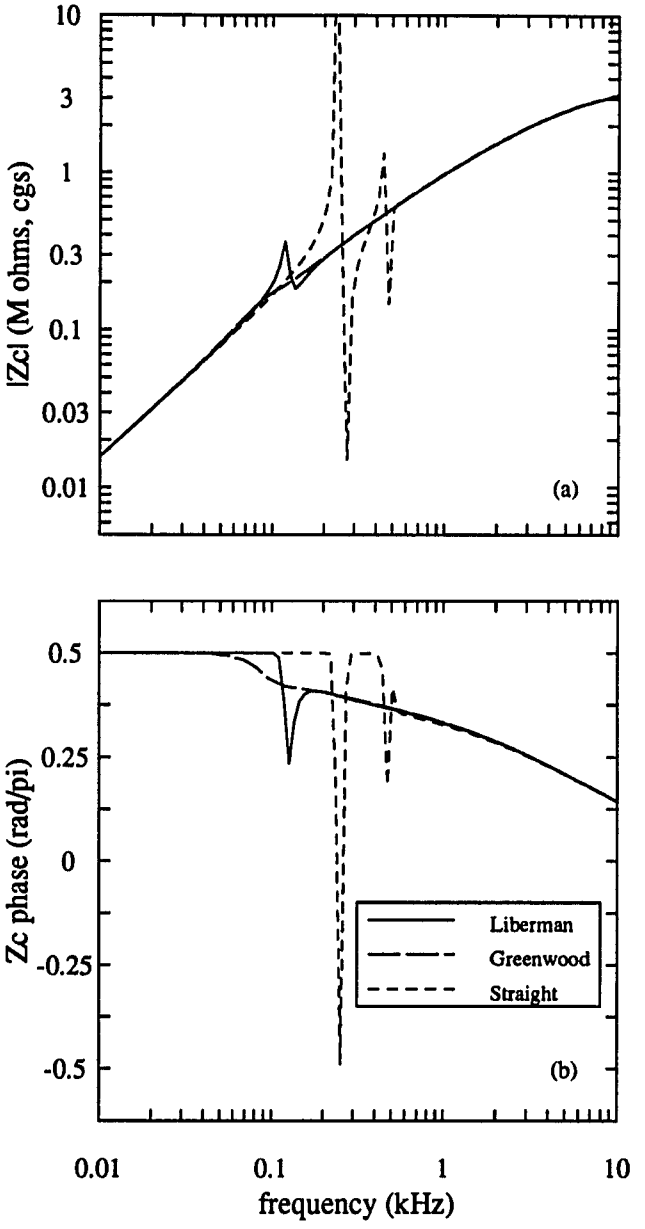

Fig. 3.2: Magnitude and phase of $Z_c(\omega)$ for the three cat cochlear maps

In f_{CF}^{cg}, all frequencies of interest are represented and therefore there are no apical reflections. Only in the later case is the energy completely dissipated by the BM before the wave reaches the helicotrema. Viergever (1988) has argued that minute reflections exist everywhere in the cochlea due to the stiffness gradient in the BM impedance; however, if they exist these reflections have little effect on Z_c and may usually be ignored.

According to Greenwood, f_{CF}^{cg} was obtained by scaling the human function to the cat. Greenwood used a human-to-cat cochlea length ratio of 35:22 respectively. Cabezudò (1978) found the averaged cat cochlea length to be $2.36 \pm 0.1\ cm$. Liberman found that the average cat cochlea length to be about 2.5 cm. Given this length, Liberman found the slope of the cochlear map to be the same as Greenwood's but the end points of the cochlear map differed. Liberman derived a new cochlear map using the Greenwood formula, but with constants determined from his own data. Liberman's cochlear map f_{CF}^{cl} is based on intracellular labeling of single auditory-nerve fibers of known characteristic frequency, and is thus derived from a physical correlation between characteristic frequency and place. Unless otherwise stated, we will use f_{CF}^{cl} in all further calculations of the cat $Z_c(\omega)$.

3.2 Constant scalae area

Figure 3.3 shows the effects of viscosity and the helicotrema on $Z_c(\omega)$ for a constant scalae cross-sectional area cochlear model. The addition of viscosity has very little effect on Z_c except at frequencies below 50 Hz. Without perilymph viscosity (NV), a tube impedance (TI) helicotrema boundary condition slightly reduces the amplitude of apical reflections. The largest difference occurs near 25 Hz where $|Z_c|$ is reduced approximately by a factor of 2.5 (7.6 dB) and $\angle Z_c$ by approximately $-3\pi/4$. When perilymph viscosity (WV) is added to the TI case, $|Z_c|$ increases by

approximately a factor of 1.6 (4.1 dB) near 25 Hz, and the phase changes by less than $\pi/18(10°)$ from the (NV,TI) case. Also shown in Fig. 3.3 is the average of cochlear input impedance measurements made on four cats by Lynch *et al.* (1982). The animal impedance measurements were made with the round window intact. Since the model computations were made without the round window, comparisons between data and model results are meaningful only for frequencies above ≈70 Hz. More will be said regarding the effects of the round window on cochlear input impedance in section 3.5. Figure 3.3 indicates that the animal input impedance magnitude is higher that the magnitude of all four model cases for frequencies below about 1-2 kHz. The phase for all four model cases is significantly higher than the averaged phase data for all frequencies. *We conclude from Fig. 3.3 that in a constant scalae area model, neither the viscosity, or a realistic helicotrema, or the combination of the two, model the experimental data, which shows a significant increase in the cochlear input impedance magnitude below about 1-2 kHz.*

Dallos (1970) hypothesized a helicotrema consisting of a mass and damper in parallel with the cochlear structures, which is represented here as the TI boundary condition. Figure 3.3 shows that for the constant scalae area model, Z_c is mass-like in the 50 Hz $< f <$ 2 kHz region, independent of the helicotrema boundary condition. This conclusion seems to be in direct conflict with Dallos' hypothesis regarding the effect of the helicotrema on the cochlear input impedance.

3.3 Comparison of constant scalae area cochlear models

Some of the input impedance models from Table 2.1 that have constant scalae area and inviscid perilymph are plotted in Fig. 3.4. Not explicitly shown is Zwislocki's (1965, p. 37) theoretical consideration of the specific input impedance (Z_{cs})

$$Z_{cs}(\omega) = \left(\frac{2\rho S_0 K_o}{\beta_o}\right)^{\frac{1}{2}} \left[1 - j\left(\omega R_m C + \frac{R}{\omega\rho}\right)\right]^{-\frac{1}{2}}. \qquad (3.4)$$

Figure 3.3:

The effects of the helicotrema and perilymph viscosity in a cochlear model with constant scalae area [$S(x) = 0.02\ cm^2$]: The "Av cat data" is the average cochlear input impedance of four cats by Lynch *et al.* (1982). The impedance measurements were made with the round window intact. The model calculations are without the round window. Model impedance calculations with perilymph viscosity (WV, $\eta = 0.02$) are not significantly different from the no viscosity (NV, $\eta = 0$) case. For a tube impedance (TI) helicotrema boundary condition, the magnitude of the cochlear input impedance tends to vary in the 25 Hz region, but it does not increase the impedance magnitude over a wide range of frequencies as is seen in the Lynch *et al.* data. The impedance magnitude does not increase when both a TI at the helicotrema and perilymph viscosity are included in the model. Thus the helicotrema, in terms of its effect on the magnitude of Z_c, is not as significant as that hypothesized by Dallos (1970). It is clear from this figure that the magnitude of model results and measured data diverge for frequencies below 1 kHz, and the model phase is substantially higher (more mass-like) than the phase of the averaged data.

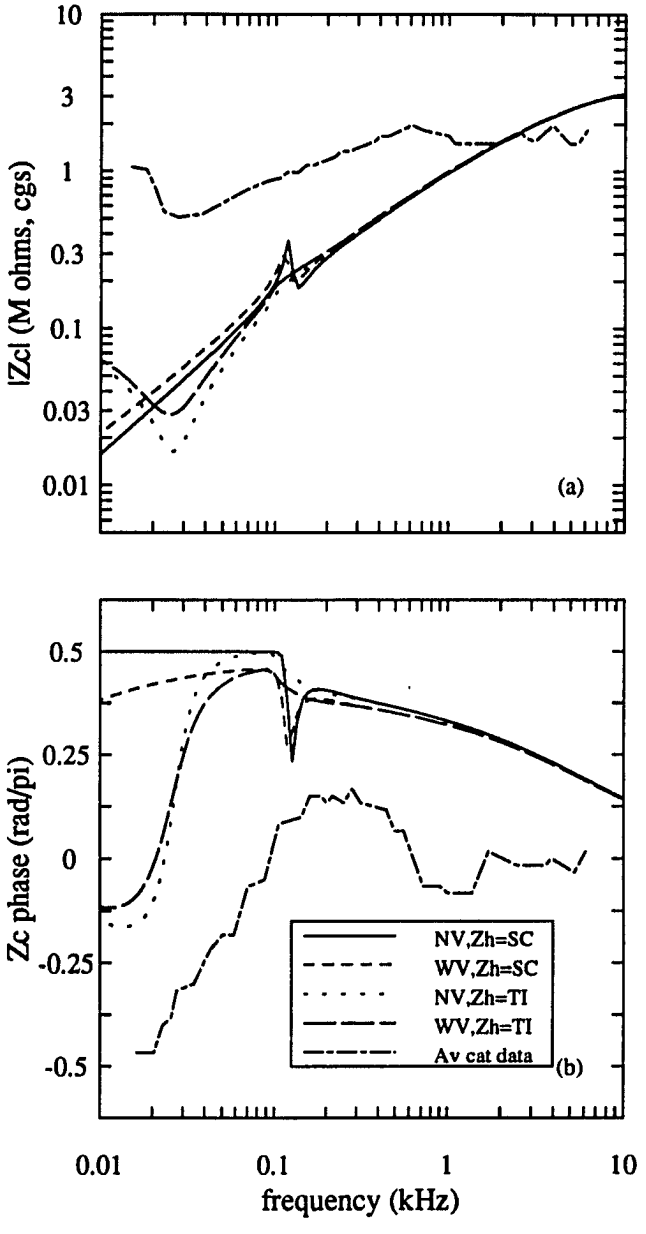

Fig. 3.3: The effects of the helicotrema and perilymph viscosity in a cochlear model with constant scalae area

By assuming the square bracketed quantity of Eq. (3.4) to be approximately equal to 1, Zwislocki concludes that "the specific input impedance of the cochlea is independent of frequency and is real". Note that the left-hand term of Eq. (3.4), when divided by S_0, is equivalent to the radiation resistance R_c derived from the WKB solution (Allen, 1979) which is equal to $2\rho c_0/S_0$, where c_0 is the velocity of the traveling-wave on the BM.

Dallos (1973, Fig. 4.15) calculated Eq. (3.4) exactly and showed that Z_{cs} is resistive at frequencies above $\approx$ 30 Hz – for a given set of parameters. In Dallos' helicotrema model of Z_c, the impedance due to the cochlea Z_{cs} is taken to be independent of frequency, i.e. $Z_{cs} = R_c$.

The solutions for Z_c by the WKB method and Koshigoe *et al.*'s [1983; Eq. (62) without K_{rw}] are also shown in Fig. 3.4. As a result of approximations in their formulation, Koshigoe *et al.*'s constant scalae area results are valid only in the 30 Hz – 1 kHz frequency region (Koshigoe *et al.*, 1983, p. 489). Both Koshigoe *et al.* and the WKB results are derived under the assumption that there is only a forward traveling wave. Since the chain-matrix method for a constant scalae area yields a result similar to that of Koshigoe *et al.*, we might reasonably conclude that: a) the two results give the same answer over most of the frequency range, and b) reflections along the cochlea can be ignored above $f_{CF}(x_L)$, which for Liberman's cochlear map is 91 Hz.

Figure 3.4 shows that in the Koshigoe *et al.*, WKB, and chain-matrix constant scalae area model results are not in agreement with the Lynch *et al.* model based on averaged data. For example, at 70 Hz $|Z_c|$ of the theoretical models are below Lynch *et al.*'s model by a factor of more than 6 (15.6 dB). The model phase is $\pi/3$ larger than the experimental data (in Koshigoe *et al.*'s calculations, the discrepancy in phase is somewhat less).

All models considered thus far have been one-dimensional models, and the possibility remains that in two-dimensional, or even three-dimensional models, the theory and experimental results

Figure 3.4:

Comparison of previous models of Z_c having constant scalae area and inviscid perilymph (see also Table 2.1): As a verification of the chain-matrix calculations, a one-dimensional transmission line model of the cochlea was computed by the difference equation (DE) method using the same set of parameters; the two curves are indistinguishable from each other. The Lynch *et al.* phenomenological model indicates that Z_c is resistive at frequencies above $\approx$ 400 Hz. The theoretical models indicate a mass like behavior at these frequencies. Dallos' model resembles the Lynch *et al.* model but the physiological mechanisms attributed to Dallos' helicotrema model of $Z_c(\omega)$ is not consistent with our results (see Fig. 3.3). Also shown are the constant scalae area closed form expressions of Z_c by Koshigoe *et al.* (1983), valid for frequencies below approximately 1 kHz, and the WKB solution (Allen, 1979), valid for frequencies above approximately 1 kHz. This figure shows that the constant scalae area model calculations using the chain-matrix can be approximated by Koshigoe *et al.*'s (1983) constant scalae area model for frequencies below approximately 4 kHz and by the WKB solutions (Allen, 1979) for frequencies above approximately 4 kHz.

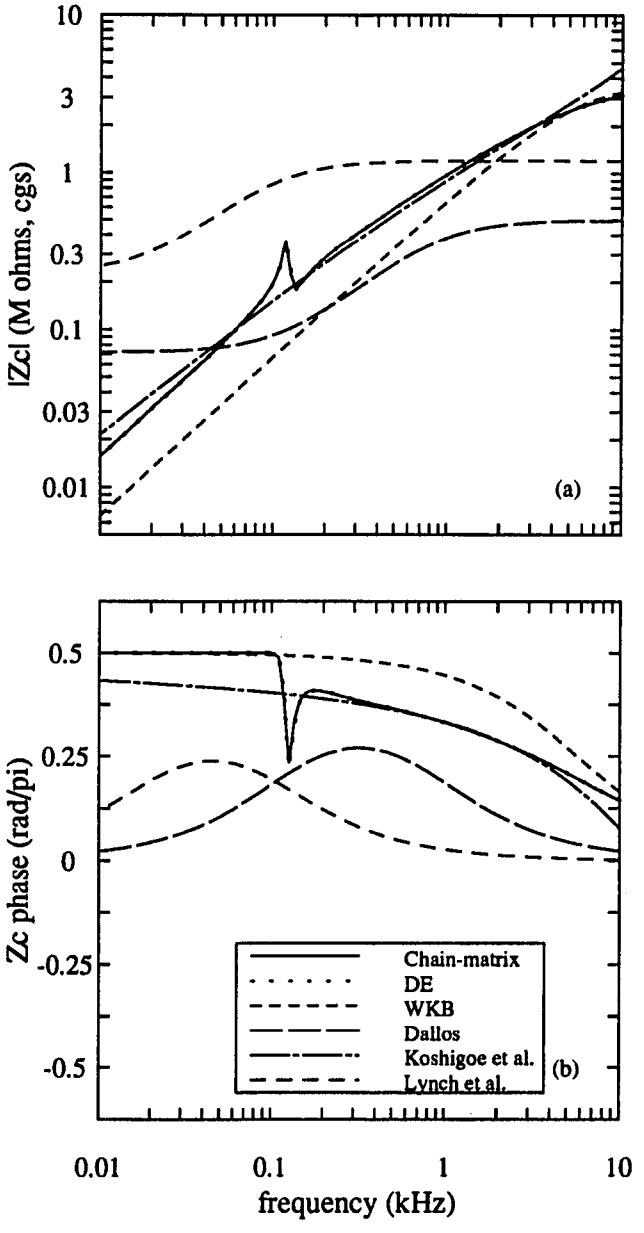

Fig. 3.4: Comparison of previous models of Z_c having constant scalae area and inviscid perilymph

would agree. Higher dimensional models might be expected to effect the results at higher frequencies where the wavelength is shorter. Sondhi (1978) has shown that, for specific model parameters and with constant scalae area and zero viscosity, the acoustic input impedance of a two-dimensional and a one-dimensional model are identical. Therefore a higher-dimensional model does not appear to help. Finally, experimental observations indicate that pressure in the scala vestibule, near the base, is relatively independent of depth of the measurement probe into the vestibule in the frequency range below 10 kHz (Nedzelnitsky, 1980).

In summary, for constant scalae area and no viscosity, the best approximation to the exact calculations by our chain-matrix methods is Koshigoe et al.*'s for 30 Hz < f < 4 kHz and WKB for f > 4 kHz. The parameters considered thus far, namely viscosity, helicotrema, cochlear map, and dimensionality of the model, do not appear to close the gap between theory and measurements.*

3.4 Effects of tapered scalae area

The geometry of the scalae is not that of a constant cross-sectional scalae area as has been assumed thus far. Wever (1949) and Dallos (1970) have made anatomical measurements of the scalae cross-sectional area. To a first order approximation Dallos found the scala vestibule area to be exponentially decreasing along the length of the cochlea [i.e. $S(x) = S_0 exp(-s_1 x)$]. Here S_0 is the area at the base and $s_1 \geq 0$ is the rate of change parameter of the area. In this section we consider the effects of the parameters S_0 and s_1 on $Z_c(\omega)$. In addition, we also analyze the interaction of these parameters with viscosity and the helicotrema boundary condition.

3.4.1 Inviscid perilymph

Figure 3.5 shows $Z_c(\omega)$ in a cochlea without perilymph viscosity ($\eta = 0$) and Liberman's cochlear map, as a function of the taper parameter s_1. The following observations are made:

a. There is an overall increase in $|Z_c|$ as tapering increases. For frequencies above $f_{CF}^{cl}(x_L)$, the $\angle Z_c$ decreases as tapering increases, which means that tapering makes the cochlea more resistive. Eq. (B.1) shows that the series impedance increases as the area decreases. Thus for a fixed S_0 as the tapering parameter increases so does the series impedance. Shera and Zweig (1991b) have recently hypothesized that the increasingly resistive behavior of Z_c, with an increase in tapering parameter s_1, is due to an increase in cancellation of the mass dominated series impedance $Z'(x,\omega)$ and the compliance dominated shunt admittance $Y'(x,\omega)$, basal to the characteristic place.

b. As tapering increases, the amplitude of the standing waves seen in Z_c increase dramatically for frequencies below $\approx f_{CF}^{cl}$. As mentioned above as s_1 increases so does the series impedance and this results in a larger reflection coefficient at the apical end of the cochlea, leading to an increase in the standing wave amplitude.

c. For frequencies below $f_{CF}^{cl}(x_L)$, Fig. 3.5b indicates that Z_c is largely mass dominated.

3.4.2 Viscous perilymph

Figure 3.6 shows the same parameter range for s_1 as Fig. 3.5, but with the perilymph viscosity set to the normal value of $\eta = 0.02$. By comparison with Fig. 3.5 we make the following conclusions:

a. For frequencies greater than 150 Hz, $|Z_c|$ increases as s_1 increases and is within 1 dB of $|Z_c|$ for the no viscosity case, with the corresponding $\angle Z_c$ being within 0.05 π (9°) of the no viscosity case. Thus viscosity has only a small effect on the impedance for frequencies greater than 150 Hz.

b. For frequencies greater than 150 Hz, Z_c becomes increasingly real as tapering parameter (s_1) increases.

Figure 3.5:

The effect of tapering in a cochlear model with inviscid perilymph ($S_0 = 0.02\ cm^2$, $Z_h = SC$): This figure shows that Z_c is strongly dependent on the change in the scalae area. For stimulus frequencies greater than $f_{CF}^{el}(x_L)$, as the tapering parameter $s_1\ (cm^{-1})$ increases, $|Z_c|$ increases and $\angle Z_c$ decreases. This indicates that above this frequency, the real part of Z_c increases as tapering increases. In addition, as tapering increases, the amplitude of the apical reflection also increase for stimulus frequencies below $f_{CF}^{el}(x_L)$. This is due to an increase in impedance mismatch between the helicotrema and the scalae, at the end of the cochlea.

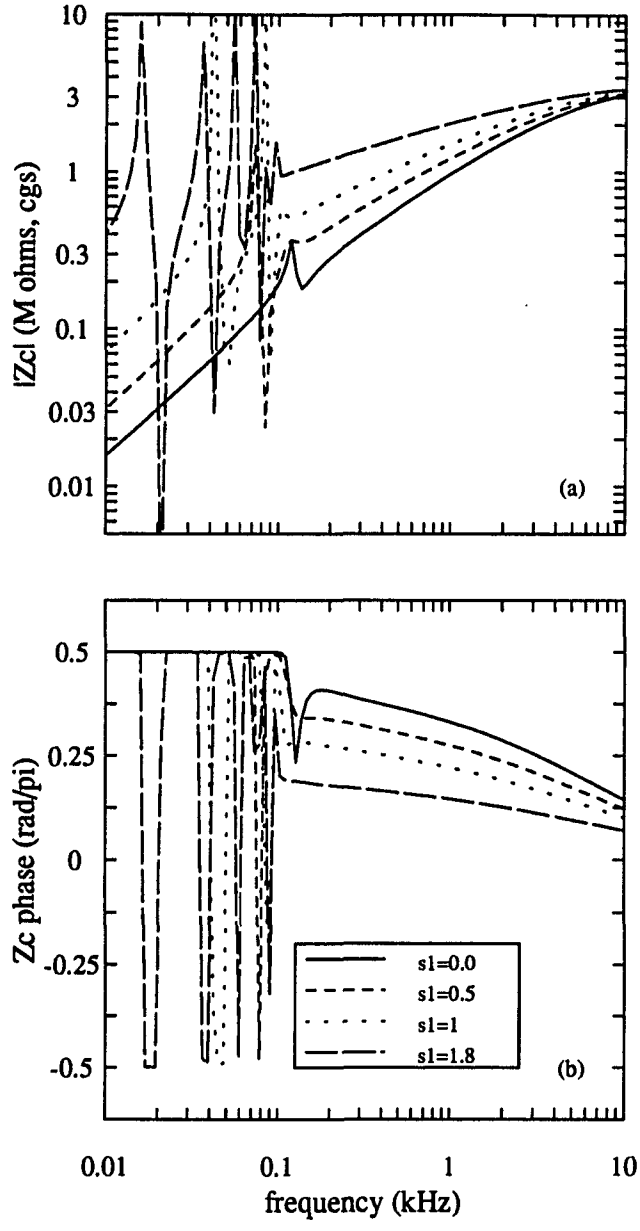

Fig. 3.5: The effect of tapering in a cochlear model with inviscid perilymph

c. For frequencies below 150 Hz Z_c becomes more resistive as tapering parameter s_1 increases only for the viscous perilymph case. Therefore viscosity becomes increasingly important as the scalae radius in the apical region becomes comparable to the viscous boundary layer thickness [see Eq. (B.3)].

d. As tapering is increasing, oscillations in Z_c due to the end of the cochlear map $f_{CF}^{cl}(x_L)$ are diminishing for the viscous case; in fact there are no oscillations in Z_c for $s_1 = 1.8$. Therefore the viscous boundary layer dissipates the apical reflections.

e. If tapering is increased beyond a certain point for the viscous case, then phase of Z_c may become negative, indicating a compliant behavior. For example, for $s_1 = 1.8$ (arbitrarily chosen), the phase is negative for frequencies below 60 Hz. Our interpretation of this observation is that the increase in tapering results in the scalae impedance being greater than the BM impedance. Thus it is easier for the perilymph to flow "into" the BM than to flow down the scala vestibule.

In the above discussions of Figs. 3.5 and 3.6 there are two important frequencies. First, apical reflections occur due to the cochlear map limit. This frequency will be referred to as $f_{CF}(x_L)$. Second, viscous effects become important when the viscous boundary layer becomes comparable to scalae radius. The frequency where this occurs depends on the scalae radius in the apical region. For a fixed S_0 (as in Figs. 3.5 and 3.6) the scalae radius depends on the tapering parameter s_1. The viscous boundary layer thickness is frequency dependent and is proportional to $1/\sqrt{f}$ (see Appendix B). Thus for a given tapering parameter s_1 the cochlear input impedance will become more and more resistive as the frequency decreases.

Figure 3.6:

The effect of tapering in a cochlear model with viscous perilymph ($\eta = 0.02$, $S_0 = 0.02\ cm^2$, $Z_h = SC$): Above approximately $150\ Hz$ Z_c is similar to the no viscosity case (Fig. 3.5). Below that frequency Z_c becomes more and more resistance dominated as tapering increases. As tapering increases, the tube radius in the apical region becomes more comparable to the viscous boundary layer thickness. Thus we conclude that interaction of the reduced radius in the apical region with the viscous perilymph gives rise to R_o in the Lynch *et al.* model. In addition, as tapering is increasing, apical reflection due to the low frequency limit of the cochlear map are diminishing. Thus the presence of viscosity dissipates the apical reflections by a significant amount.

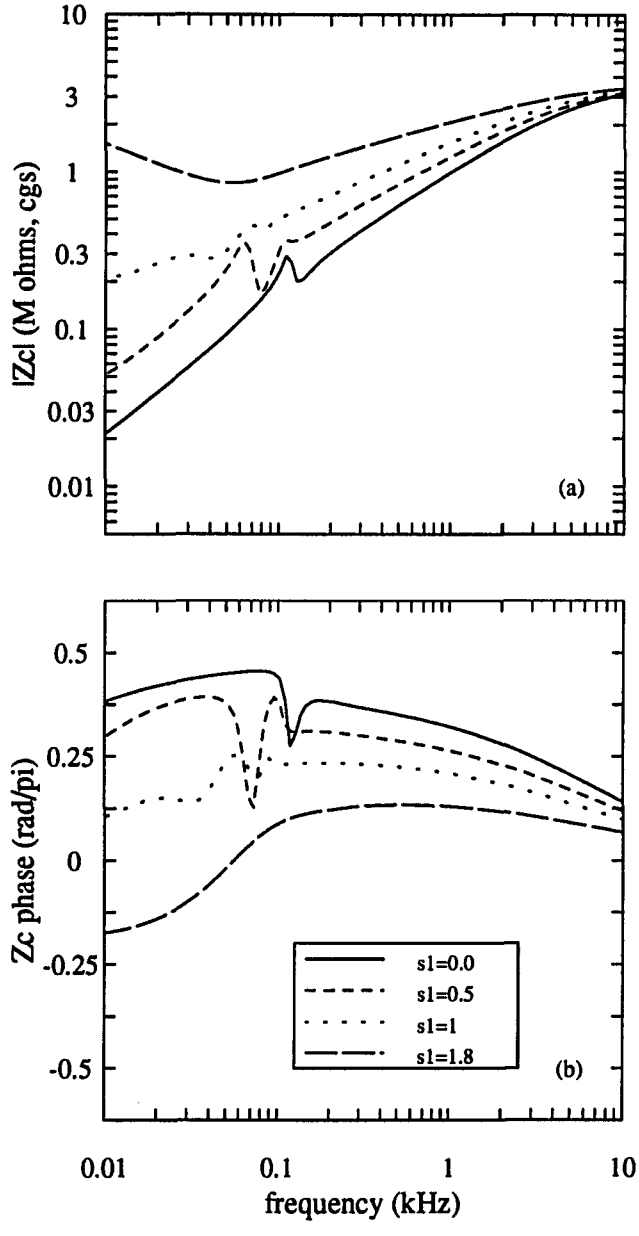

Fig. 3.6: The effect of tapering in a cochlear model with viscous perilymph

If we define f_{bl} to be the frequency at which the viscous boundary layer becomes equal to the tube radius then by setting $r_v = 1$ in Eq. (B.3) we obtain $f_{bl} = 0.5\eta\rho^{-1}S^{-1}(x)$. For $S_0 = 0.0175$ and $s_1 = 1.3$, f_{bl} is 15 Hz at $x = x_L$. Thus near 15 Hz the viscous effects completely dominate. However, viscosity will start to have an effect at frequencies greater than 15 Hz. For the purposes of discussion we have chosen $150\ Hz$ as the frequency below which viscous effects become important. Coincidentally this frequency is close to $f_{CF}^{cl}(x_L)$. This frequency was chosen based on when Z_c was more real rather than mass dominated. For these parameters, r_v the ratio of tube radius to viscous boundary layer is approximately 2.46. If one were to recompute the calculations of Fig. 3.6 with f_{CF}^{cg} then the effects of viscosity below $150\ Hz$ on Z_c would still be observed, but without the complications of reflections below $f_{CF}^{cl}(x_L)$.

Figure 3.7 shows how $|Z_c|$ scales with S_0 for a fixed $s_1 = 1.0$, and with $\eta = 0.02$. The overall shape of $|Z_c|$ is maintained with no significant change in the slope of $|Z_c|$ for each value of S_0. For frequencies above $\approx f_{CF}^{cl}(x_L)$, $|Z_c| \propto S_0^{-\nu}$ and $\angle Z_c$ is, to a first order approximation, independent of S_0. For large S_0, ν is a weak function of S_0. But for $S_0 < 0.03\ cm^2$, ν is constant and is $\approx$ 0.87. Thus, given Z_c at one frequency and the corresponding S_0, one can evaluate the proportionality constant and therefore find $|Z_c|$ for any other S_0 at that frequency.

3.4.3 Effects of the helicotrema with tapering

In Section 3.2 the effects of the helicotrema boundary condition for a constant scalae area model were analyzed. In a similar manner we now analyze the effect of the helicotrema in the tapered cochlear model. In Fig. 3.8 four possibilities are considered: with and without viscosity (WV,NV), and using the two different helicotrema boundary conditions (SC,TI). This gives a four-way comparison. By comparison of Fig. 3.5 to Fig. 3.6 we showed that the introduction of viscosity greatly reduces the low frequency standing waves in a tapered cochlea. Figure 3.8 shows that

Figure 3.7:

The effect of S_0 in a cochlear model with tapering parameter s_1 fixed ($s_1 = 1.0$, $Z_h = SC$): For frequencies above $\approx f_{CF}(x_L)$, scaling $S(x)$ (i.e. by decreasing S_0) effectively results in a proportional translation in $|Z_c|$ with only a small effect on $\angle Z_c$. For this case $|Z_c| \propto S_0^{-\nu}$, where $\nu \approx 0.87$ (see text).

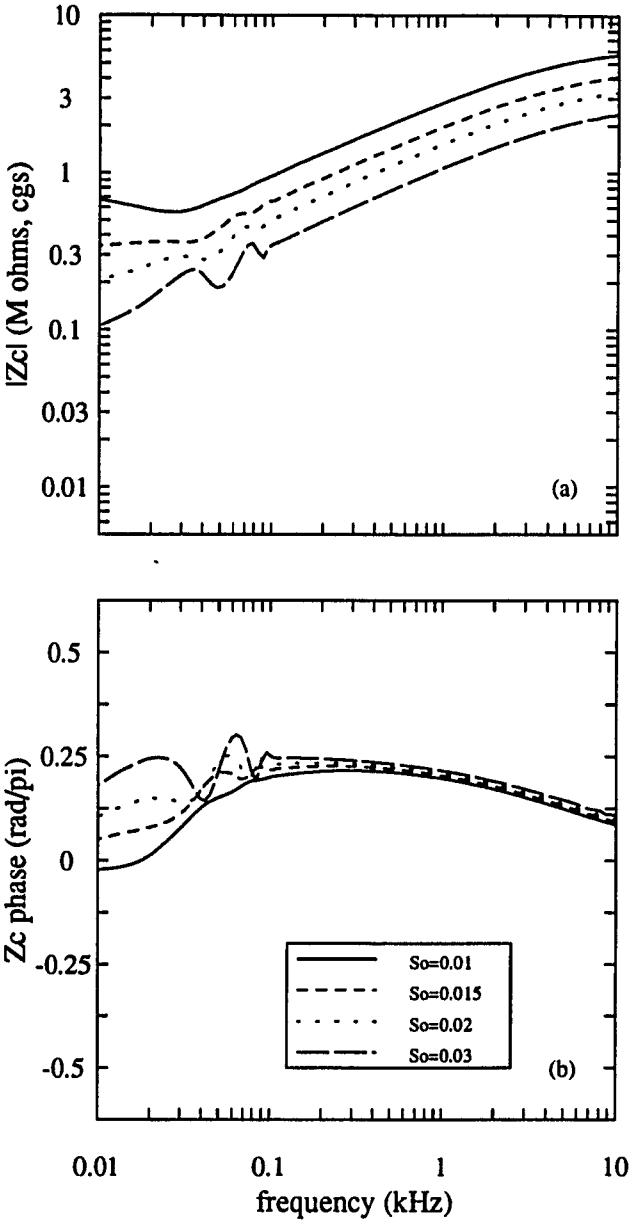

Fig. 3.7: The effect of S_0 in a cochlear model with tapering parameter s_1 fixed

changing the helicotrema boundary condition from SC to TI, in the zero viscosity case, has the effect of reducing the magnitude of the oscillations in Z_c but its effect is not as great as that due to viscosity alone. In addition, for frequencies below 150 Hz, Z_c is resistance dominated in the viscous perilymph case and it is mass dominated when perilymph viscosity is zero. Introducing a TI boundary condition when perilymph viscosity is already present has little effect on Z_c. *We therefore conclude that in the tapered cochlea, the effects due to the viscous perilymph are more significant than the effects due to the acoustic impedance of the helicotrema.* Unless otherwise stated all further calculations of Z_c will be assumed to be with $\eta = 0.02$ and $Z_h = SC$.

3.5 Comparison of tapered scalae area cochlear models

The Koshigoe *et al.* model, is the only model in Table 2.1 that includes the effect of tapering. But as they stated in their paper: "In our approximate analysis, apical reflections are ignored" (Koshigoe *et al.*, 1983, p. 488). Thus their analytic method does not lend itself to the type of analysis we have established in the previous sections where apical reflections can be of considerable importance.

Figure 3.9 compares, for the same set of parameters, our results for the acoustic input impedance with those of Koshigoe *et al.*'s numerical calculations. In this figure only, K_0' was adjusted to match K_0 used by Koshigoe *et al.*. Measured data and Koshigoe *et al.*'s numerical calculations assume a round window stiffness K_{rw}. The round window impedance $Z_{rw}(\omega) = K_{rw}/s$ adds to the cochlear input impedance as a series impedance (Nedzelnitsky, 1980):

$$Z_{crw}(\omega) = \frac{K_{rw}}{s} + Z_c(\omega). \tag{3.5}$$

Nedzelnitsky (1980) concluded that the effect of the round window, in the cat, is important for frequencies below $\approx$ 300 Hz. To fit $|Z_c|$ for frequencies below 40 Hz, where $Z_c \cong Z_{rw}$, Lynch *et*

Figure 3.8:

The effects of the helicotrema and perilymph viscosity in a tapered cochlear model ($S_0 = 0.02, s_1 = 1.0$): As shown here, and in Figs. 3.5 and 3.6, the introduction of viscosity (WV) virtually eliminates the apical reflections that result in the standing waves. A tube impedance (TI), in the no viscosity case, reduces the apical reflections but its effect is not nearly as great as that due to viscosity alone. For frequencies less than approximately 150 Hz, the phase indicates that Z_c is resistance dominated only when viscosity is present. Thus when tapering *and* viscosity are present, a TI model of the helicotrema has a negligible effect.

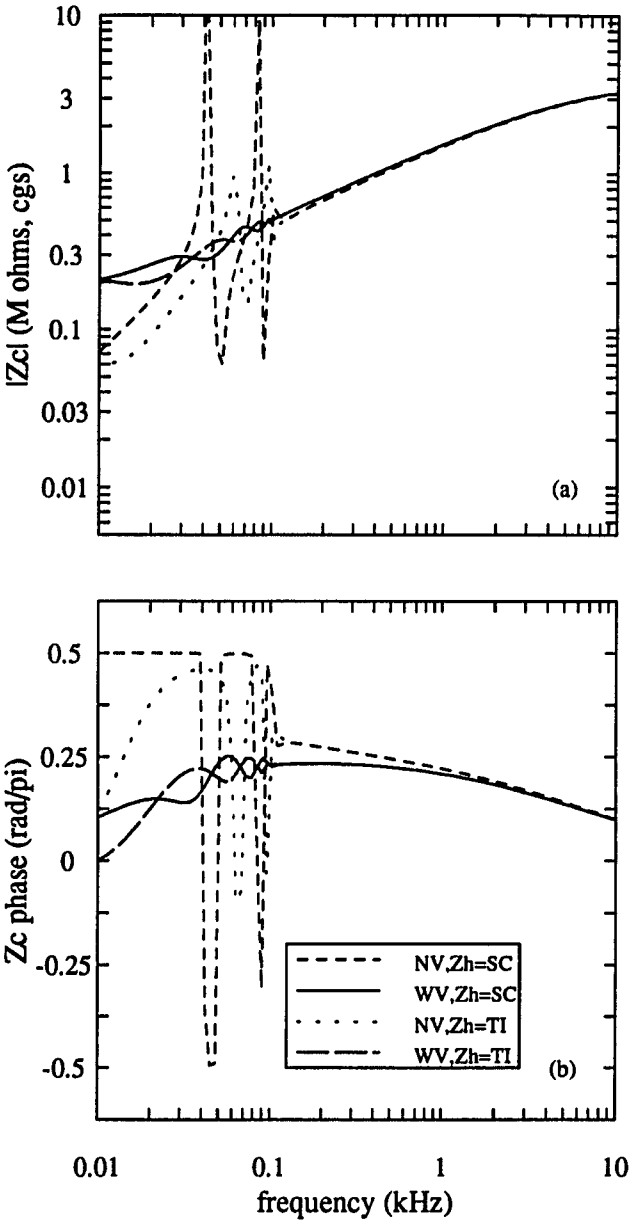

Fig. 3.8: The effects of the helicotrema and perilymph viscosity in a tapered cochlear model

Figure 3.9:

Comparisons of measured data and cochlear models with tapered scalae area: The impedance of the round window $Z_{rw}(\omega)$ has now been added to the model calculations of $Z_c(\omega)$. The sum of these impedances is referred to as $Z_{crw}(\omega)$. Koshigoe *et al.*'s numerical results (their analytical approximations) are from their Figs. 1 and 2. Parameters for both models are: $S_0 = 0.02, s_1 = 1, K_0' = 10^9, \eta = 0.02, Z_h = SC$, and the round window stiffness K_{rw} is 10^8. In the chain-matrix model, Liberman's cochlear map was used. In Koshigoe *et al.*'s calculations, an exponential stiffness was assumed. "Av cat data" is from Lynch *et al.* (1982). Although the chain-matrix calculations are in better agreement with the data than the Koshigoe *et al.* calculations, discrepancies still exist. For example for frequencies above 500 Hz the discrepancy in phase is as large as $\frac{1}{3}\pi$ (60°) and for frequencies below 1 kHz the discrepancy in magnitude is as large as a factor of 2.5 (8 dB). (Note the change in magnitude scale from previous figures).

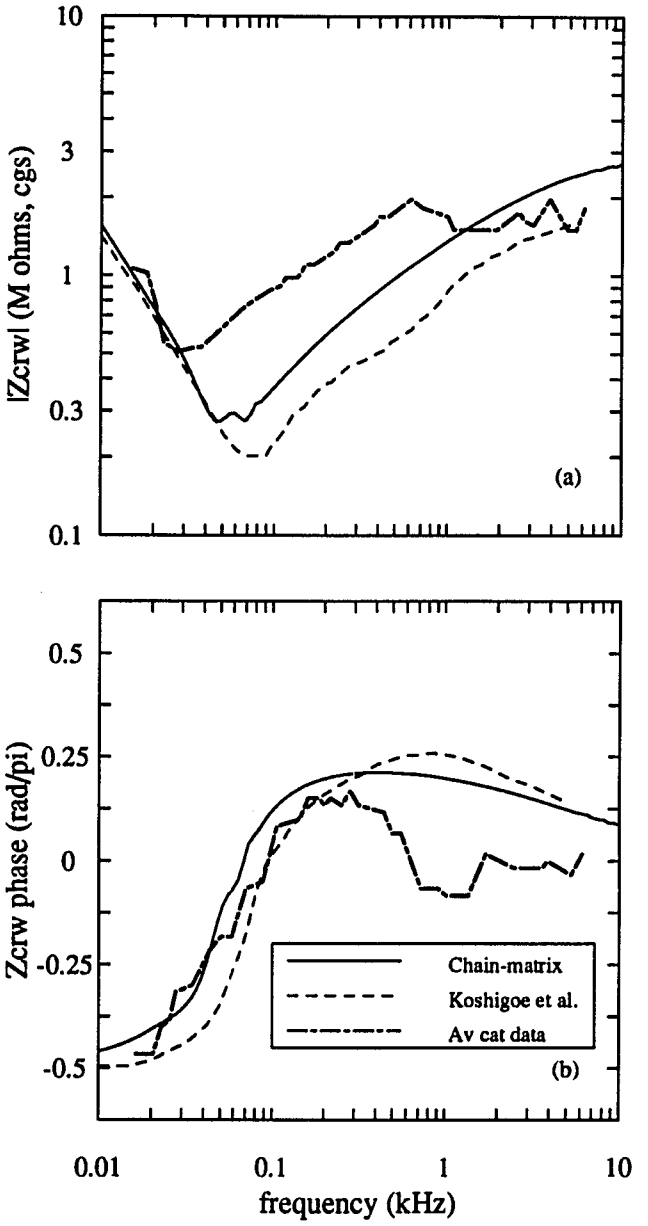

Fig. 3.9: Comparisons of measured data and cochlear models with tapered scalae area

al. (1982) chose a value of 10^8 dyn/cm^5 for the round window stiffness. Unless otherwise stated we will use this value for the round window stiffness. This value of the round window stiffness has an effect on the phase for frequencies up to 70 Hz. Thus, when referring to effects above 70 Hz we will use Z_c and Z_{crw} interchangeably. Unless otherwise stated, all further calculations in this section will include K_{rw}.

From Fig. 3.9 , despite a similar choice of parameters, the chain-matrix model and Koshigoe *et al.*'s model show a ratio of up to 1.7 (4.6 dB) between 0.1 and 8 kHz. The two most obvious explanations for the differences between our and Koshigoe *et al.*'s results is that the Koshigoe *et al.* solution is an approximation solution, while our chain-matrix solution is an exact numerical solution. This approximation has two parts. The *first* is that our numerical solution includes a forward and backward traveling wave, whereas Koshigoe *et al.*'s method includes only a forward traveling wave. Specifically, the Koshigoe *et al.* model ignores reflections due to scalae tapering and apical reflections. *Second* is the approximations for the series impedance they make in finding the solutions.

There is also a significant difference between the conclusions arrived at by the chain-matrix method and those of Koshigoe *et al.* For frequencies above 150 Hz, we have presented evidence that the low frequency increase in $|Z_c|$ is independent of viscosity and is due only to tapering. For frequencies below 150 Hz, the phase indicates that Z_c is resistance dominated due to presence of *both* viscosity and tapering, independent of the helicotrema impedance. Koshigoe *et al.*, on the other hand, argue that it is viscosity alone that is responsible for the rise in $|Z_c|$ below 500 Hz.

3.6 Comparison with measured data

Figure 3.9 compares averaged Z_{crw} obtained by scala vestibule pressure and stapes velocity measurements in anesthetized cats (Lynch *et al.*, 1982) with our model calculations of Z_{crw} (in Lynch *et al.* Z_{crw} is reffered to as Z_c). There is some agreement in $|Z_{crw}|$ for frequencies above 2 kHz but poor agreement in $\angle Z_{crw}$ above 500 Hz. For frequencies below 200 Hz, our theoretical calculations match measured $\angle Z_{crw}$ quite well. But our model $|Z_{crw}|$ is below the average data by as much as a factor of 2.5 (8 dB) in the frequency region between 30 Hz and 1 kHz. Lynch *et al.* estimate their experimental worst-case error to be ± 10 dB; however, the "actual measurement errors are likely to be substantially smaller than these worst-case estimates of error *limits*" (Lynch *et al.*, 1982, p. 113). Shera and Zweig (1991b) have recently made minimum-phase fits to the amplitude and phase of the Lynch *et al.* data. Their calculations indicate that the data stays minimum-phase for approximate deviations of ± 2 dB in amplitude and $\pm 10°$ in phase. Thus although the measurement errors are not exactly known we assume that they are sufficiently small. This indicates that the parameters chosen to calculate our model results need to be re-evaluated.

3.6.1 The appropriate geometric representation

As mentioned previously, the most important parameter that affects the cochlear input impedance is the scalae area function. Thus in this section, we further explore the effect of $S(x)$ on $Z_c(\omega)$. Figure 3.10 shows the various area functions that we use next to calculate $Z_c(\omega)$. To our knowledge the only anatomical measurement of the area function for the cat scala vestibule is one by Dallos (1970). The $S_0 = 0.02\ cm^2$ and $s_1 = 1\ cm^{-1}$ curve is the approximate fit made by Dallos to the measured area function; this is the approximation that we have used to this point. The $S_0 = 0.0175\ cm^2$ and $s_1 = 1.3\ cm^{-1}$ curve is a second approximation to the measured area

function. Discussion of the $S_m(x)$ curve is deferred for the moment. The effect of each of these area functions on $Z_c(\omega)$ is shown in Fig. 3.11.

For frequencies below 1 kHz, we see that a better fit to $|Z_{crw}|$ is obtained with $S_0 = 0.0175$ cm^2 and $s_1 = 1.3$ cm^{-1} than with $S_0 = 0.02$ cm^2 and $s_1 = 1$ cm^{-1}. However even with this area function, our match to averaged phase is still poor for frequencies above 400 Hz. In the experimental data, the phase starts to decrease near 300 Hz becoming negative near 500 Hz and it stays negative for frequencies up to 2 kHz. Above 2 kHz, the phase is approximately zero, indicating that Z_c is more or less resistive. The model Z_{crw}, on the other hand, approaches zero phase gradually, still having an angle of $\pi/10$ radians at 10 kHz. Near 5 kHz there is also a systematic error in $|Z_c|$, becoming as large as 1.8 (5.1 dB) at high frequencies. Since we have shown that the geometry of the cochlea has an important effect on Z_c, perhaps representing $S(x)$ by an exponentially tapered function is not a sufficient approximation for the purposes of accurately calculating the input impedance. Figure 3.11 shows calculations of Z_{crw} using Dallos' measured area function of the scala vestibule, which results in an input impedance that is not significantly different from the one obtained with $S_0 = 0.0175$ and $s_1 = 1.3$. Therefore, the errors as stated above persist.

The scala vestibule area measured by Dallos is for one cat only. In addition, an error bound on the measurement was not provided by Dallos. To better fit the average cochlear input impedance data, we have tried slight perturbations (less than a factor of two) to the measured area function. In the apical region the $S_0 = 0.0175$ and $s_1 = 1.3$ curve has a smaller area than the $S_0 = 0.02$ and $s_1 = 1$ curve. Since the former area function results in a better fit, we have decreased the measured area in the region apical to 0.9 cm; with the exception of the 1.6 cm region, where the area was slightly increased. Figure 3.10 shows that the net effect of these changes results in an area function

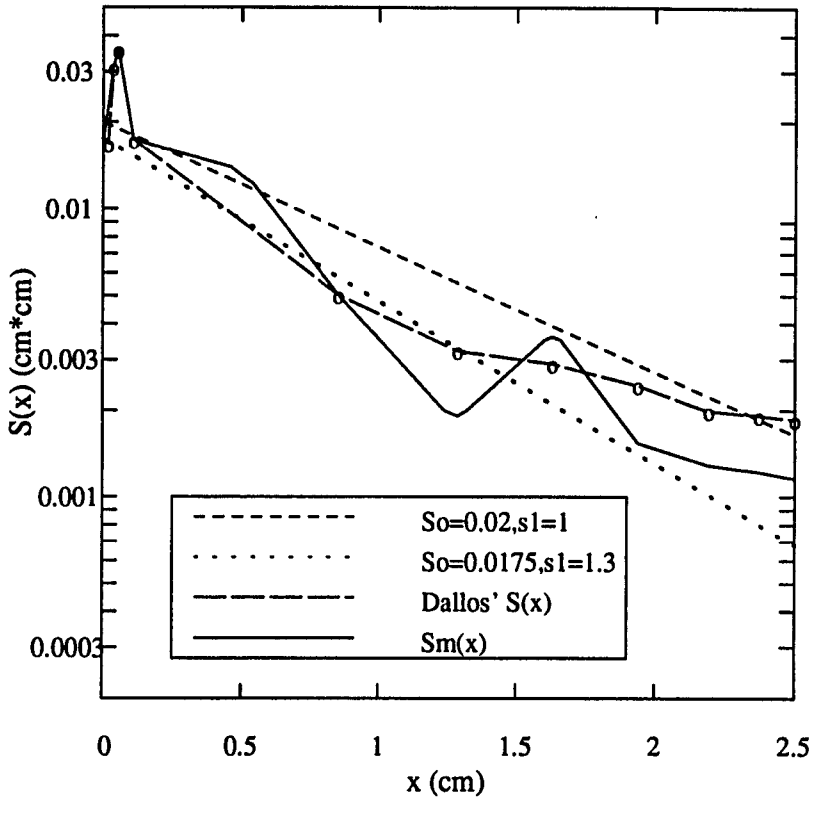

Figure 3.10: *Anatomical measurements of cat scala vestibule area* $S(x)$: The basal end corresponds to $x = 0$ and the apical end of the cochlea corresponds to $x = 2.5\ cm$. The circles indicate anatomical measurements in one cat (Dallos, 1970). The curve with $S_0 = 0.02, s_1 = 1$ is an approximate fit to the measured area function (Dallos, 1970). The curve with $S_0 = 0.0175, s_1 = 1.3$ is another approximate fit to the measured area function. $S_m(x)$ is Dallos' area function heuristically modified (see text) to obtain a better fit to measured $Z_{crw}(\omega)$.

Figure 3.11:

$Z_{crw}(\omega)$ corresponding to the area functions of Fig. 3.10: Going from the $S_0 = 0.02, s_1 = 1$ curve to the $S_0 = 0.0175, s_1 = 1.3$ curve results in a better agreement between the calculated $Z_{crw}(\omega)$ and the measured data. Using the actual measured area function of Dallos yields only a slight improvement. When Dallos' area function is heuristically modified as in $S_m(x)$ of Fig. 3.10 , then there is a better agreement between the calculated $Z_{crw}(\omega)$ and the measured data. The decrease in phase near 300 Hz is due to the local maximum in the area function $S_m(x)$ apical to $x = 0.9\ cm$. $K_{rw} = 10^8$ (Lynch *et al.*, 1982) for all four cases.

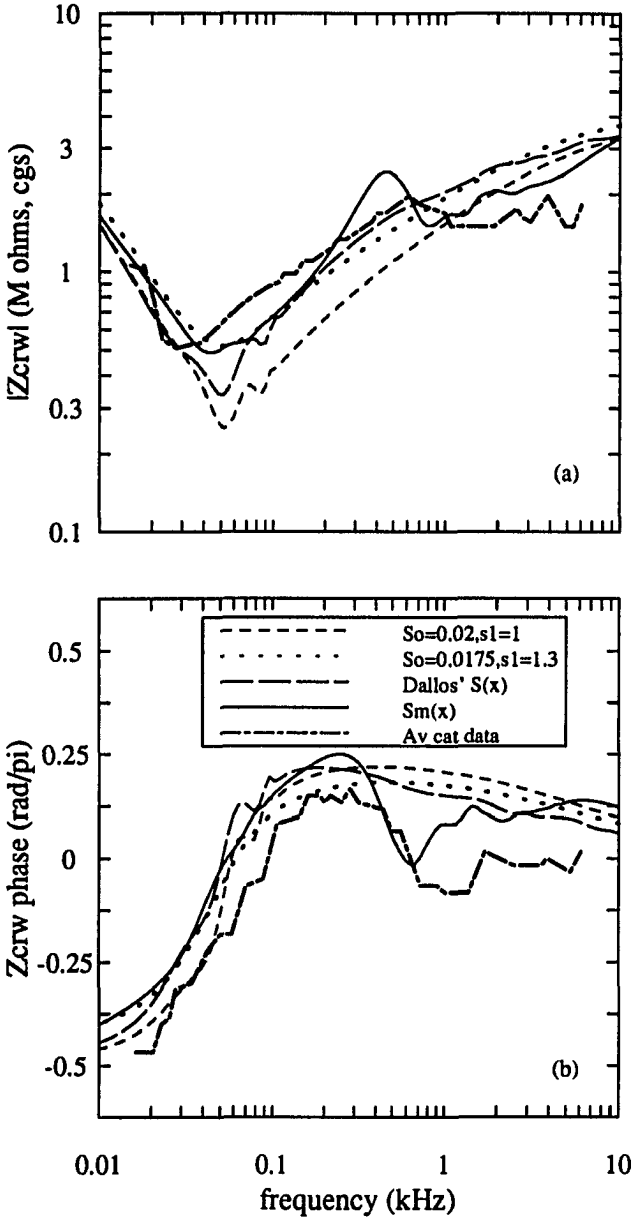

Fig. 3.11: $Z_{crw}(\omega)$ corresponding to the area functions of Fig. 3.10

with a local maximum in the apical region of the cochlea. One important motivation for making these changes comes from the observation that the scalae vestibule area function measurements are not monotonically decreasing in the human cochleae (Wever, 1949, pp. 276-278) (see Fig. 3.14). Figure 3.11 shows that this local increase in the area function gives rise to a sharp decrease in phase above approximately 300 Hz. From Fig. 3.10 we note that there are no area measurements in the $0.1 < x < 0.85$ cm region. Perhaps the area function in this region cannot be approximated by an exponential function as we have assumed. Based on our experience with perturbations of the area at the $x = 0.5$ cm point, we have increased the scalae area by a factor of 1.5 at that point. The result of increasing the area near the $x = 0.5$ cm region is to decrease the magnitude and phase of Z_c above the 3-4 kHz region, which is consistent with the measured Z_c data. The area function with the modifications described above is reffered to as $S_m(x)$ in Fig. 3.10. The input impedance corresponding to $S_m(x)$ is shown in Fig. 3.11. *The resulting cochlear input impedance calculations are in very close agreement with those of the averaged measured data.*

3.6.2 Effect of transducer placement

In calculating the load to the middle ear, one should use the pressure in the scala vestibule at the stapes – as we have done thus far. However, for comparison to measured Z_c data, one should use the pressure inside the scala vestibule in the vicinity of the transducer. Thus we need to know the location of the transducer relative to the stapes. Figure 3.12 shows the results of evaluating Eq. (2.10) at various locations near the stapes, i.e. use $P(x_0)$ instead of $P(0)$. For frequencies below 1 kHz there are virtually no differences in $|Z_{crw}|$ and $\angle Z_{crw}$ as a function of x_0, which we define as the distance from the stapes. But for frequencies above 1 kHz, large differences in $\angle Z_{crw}$ exist as a function of x_0. Figure 3.12 shows that the phase decreases with an increase in x_0. Individual cat data (Lynch *et al.*, 1982) in Fig. 3.13 display negative phase for some of the

high-frequency data points. A change in x_0 is one model parameter that results in a negative phase above 2 kHz. This distance is most likely to be difficult to measure experimentally, and was not reported by Lynch *et al.* (1982). However, Figure 2 of Lynch *et al.* (1982) suggests that $x_0 < 0.2$ *cm*. To calculate the model result show in Fig. 3.13 we have chosen $x_0 = 0.15$ *cm*.

3.7 Inter-animal comparison with the chain-matrix model

Up to now we have been using the Lynch *et al.* averaged Z_c data. The parameters used thus far have proven to capture some of the detail present in the averaged Z_c data. Since averaging of data smears out details, we now wish to compare our results with the individual measurements from which the averaged data was obtained. Figure 3.13 shows the four measurements of Z_c on individual cats by Lynch *et al.* (1982). It is apparent from Figure 3.13 that the individual cats show a large amount of inter-animal variability. Some of the trends present in the averaged data are more pronounced in each of the individual curves. For frequencies above 1 kHz, the individual phase is positive and negative across animals and would tend to average to zero, leaving a real result. *Thus for any given animal, Z_c is not necessarily real at frequencies above 1 kHz.*

The model results shown in Figure 3.13 are obtained by using parameters from the previous sections. The parameters used are: $S_m(x)$ (see Fig. 3.10), pressure measured at location $x_0 = 0.15$ *cm*, $\eta = 0.02$, Z_h = SC, $K_0' = 1.7 \times 10^9$. The round window stiffness K_{rw} was increased to 1.2×10^8. A comparison with individual data shows good quantitative agreement. From our modifications to the area function, albeit in a heuristic manner, we have been able to capture some of the detailed structure of the cochlear input impedance. From this exercise we reach the conclusion that individual animal differences in the scala area result in measurable differences in the cochlear input impedance. It was noted that for frequencies above 1 kHz, the inter-animal

Figure 3.12:

The effect on $Z_{crw}(\omega)$ of placing the pressure transducer at distances x_0 apical to the stapes: The major effect of placing the pressure transducer at different location along the length of the cochlea is in the phase $[S(x) = S_m(x)]$.

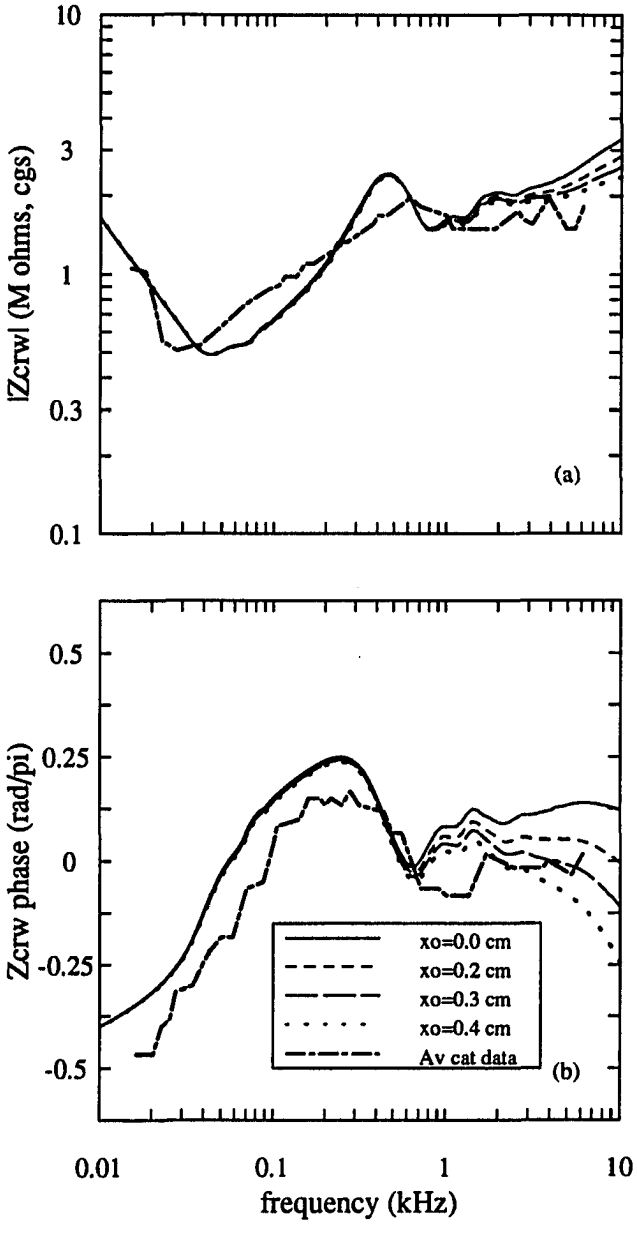

Fig. 3.12: The effect on $Z_{crw}(\omega)$ of placing the pressure transducer at distances x_0 apical to the stapes

Figure 3.13:

Comparison with Lynch et al.*'s measured data:* "cat27", "cat25", "cat18", and "cat7" are measurements of $Z_{crw}(\omega)$ on individual cats (Lynch *et al.*, 1982). The "Av cat data" shown here and in previous figures were obtained by Lynch *et al.* by averaging the individual curves. The individual data shows significant inter-animal variability. For frequencies greater than 1 kHz, the measured phase is distributed on both sides of zero. This indicates that the individual animal phase is not necessarily resistive, at frequencies above 1 kHz, as one would be lead to believe by looking at the phase of the averaged data. From the present study we conclude that one reason for the inter-animal variability in cochlear input impedance is due to inter-animal differences in the scalae area. Calculation parameters are: $S_m(x)$, $K_0' = 1.7 \times 10^9$, $K_{rw} = 1.2 \times 10^8$, and $x_0 = 0.15\ cm$.

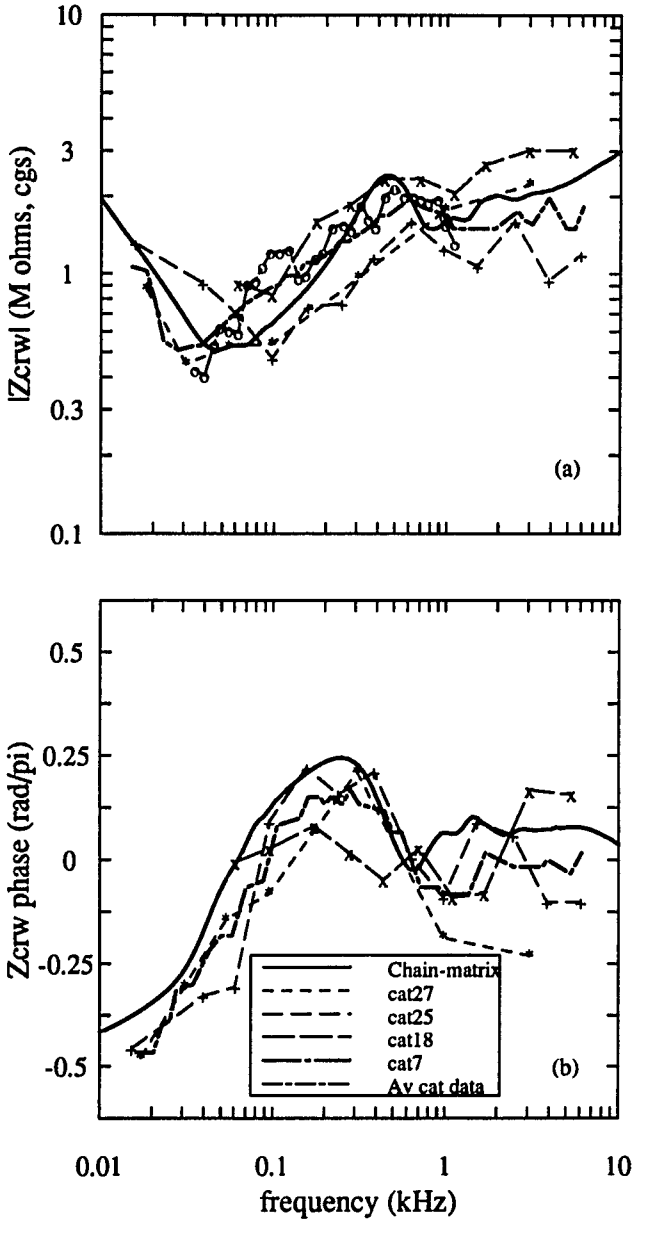

Fig. 3.13: Comparison with measured data

phase is both positive and negative; this variation is most likely due to inter-animal differences in the basal region of the scala vestibule area function, variations in transducer placement, or perhaps errors in animal measurements.

3.8 Extension to other species

To accurately compute the cochlear input impedance we have proposed a cochlear model that requires the specification of species dependent parameters such as: the area function of the vestibule, the cochlear map $f_{CF}(x)$, the length of the cochlea x_L, the BM width function $\beta(x)$, the round window stiffness K_{rw}, and the area of the footplate A_{fp}. In addition, one also needs to specify the physical constants for the perilymph such as: viscosity η, and the density ρ. The parameters chosen thus far were for calculating the cochlear input impedance of the cat. Given the model, we now compute the cochlear input impedance for the guinea pig, man, and the chinchilla, and compare our results to those of the cat, for frequencies up to 70 kHz.

The human cochlear map according to Greenwood (1961) is

$$f_{CF}^{man}(x) = 165.4\left[10^{\frac{2.1}{x_L}(x_L-x)} - 1\right], \tag{3.6}$$

the guinea pig cochlear map (Greenwood, 1990) is

$$f_{CF}^{gp}(x) = 350\left[10^{\frac{2.1}{x_L}(x_L-x)} - 0.85\right], \tag{3.7}$$

and the chinchilla cochlear map (Eldredge *et al.*, 1981) is

$$f_{CF}^{ch}(x) = 112.5\left[10^{\frac{2.24}{x_L}(x_L-x)}\right]. \tag{3.8}$$

The area functions for the cat [$S_m(x)$ of Fig. 3.10], human (Wever, 1949), guinea pig (Dallos,

Parameter	cat	guinea pig	chinchilla	man	units
x_L	2.5[a]	1.85[b]	1.84[c]	3.5[d]	cm
H[g]	0.146	0.161	0.137	0.254	cm
β_0	0.011[f]	0.01[b]	0.023[e]	0.015[h]	cm
β_1	0.56[f]	0.375[b]	0.3[e]	0.329[h]	cm^{-1}
a_h	0.0125[i]	0.0084[e]	0.0248[e]		cm
l_h[j]	0.04	0.0284	0.078		cm
A_{fp}	0.0126[k]	0.014[b]			cm^2
K_{rw}	10^8[k]				dyn/cm^5
K_0'	1.7×10^9	8.3×10^8	4.5×10^8	2.4×10^8	dyn/cm^3

[a] Liberman (1982)
[b] Fernández (1952)
[c] Eldredge *et al.* (1981)
[d] von Békésy (1960)[p 29]
[e] Dallos (1970)
[f] Cabezudo (1978)
[g] $H = 2\sqrt{\frac{S_0}{\pi}}$
[h] Wever (1949)[p 100]
[i] Mulroy (Lynch *et al.*, 1982, note 11)
[j] $l_h = \pi a_h$
[k] Lynch *et al.* (1982)

Table 3.1: *Species dependent parameters:*
For chinchilla and man A_{fp} of the cat were used. K_0' is the basilar membrane stiffness at the base. Anatomical parameters for the helicotrema are not required for man, guinea pig, and chinchilla model calculations since a short circuit helicotrema impedance was used; they are listed here only for comparison to the cat.

1970), and the chinchilla (Dallos, 1970) that we have used are shown in Fig. 3.14. Since round window stiffness measurements for some of these animals are not available, we make comparisons of Z_c rather than Z_{crw}. For this reason, comparisons of our calculated results with measurements of Z_c reported in the literature are meaningful only for frequencies above $\approx$ 70 Hz. Figure 3.15 compares Z_c for cat, human, guinea pig, and chinchilla cochleae in the frequency region between 10 Hz and 70 kHz given the areas shown in Fig. 3.14. The BM stiffness $K'(x)$ was modified for other species, as in the case for the cat, so that the calculated cochlear map coincided with the actual cochlear map of either Eq. (3.6), Eq. (3.7), or Eq. (3.8). The species dependent physical parameters, including the BM stiffness at the base K_0', are shown in Table 3.1.

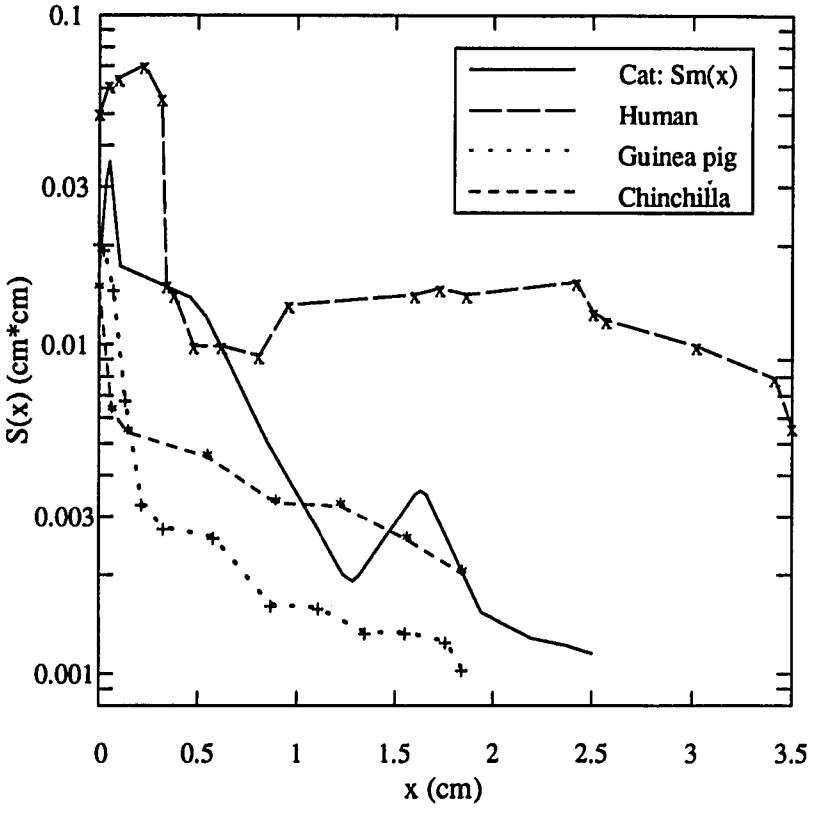

Figure 3.14: *Inter-species comparison of anatomical measurements of the scala vestibule area:* The cat area labeled $S_m(x)$ is from Fig. 3.10 . The human scala vestibule area is from (Wever, 1949). The guinea pig and chinchilla area measurements are from Dallos (1970). The human scala area is the largest and the guinea pig scala area is the smallest.

3.8.1 Human impedance

Our model calculations (Fig. 3.15) show that below 1 kHz the human cochlear input impedance slope is approximately 4 dB/oct, reaching a peak at 1.2 kHz of 1.24 $M\Omega$. Between 1.2 kHz and 10 kHz the model $|Z_c|$ starts to decrease with an approximate slope of -6 dB/oct. In comparison, the cochlear input impedance magnitude measured on human temporal bones, is "flat" for 0.6 kHz $< f <$ 2.2 kHz, and the mean value on eleven temporal bones is 0.7 $M\Omega$ at 1 kHz (Aritomo and Goode, 1987). Estimates of the measurement error are not reported in (Aritomo and Goode, 1987). Thus at 1 kHz our $|Z_c|$ is higher than the measured data by a factor of 1.8 (5.1 dB).

3.8.2 Guinea Pig impedance

The only reported measurements of guinea pig impedance have been by Dancer and Franke (1980). Since phase measurements were not reported in that study, we compare our theoretical results with their magnitude measurements. Franke and Dancer estimated the impedance from pressure measurements in the first turn of the scala vestibule. In the frequency region between 200 Hz and 2 kHz the measured impedance magnitude is approximately 0.4 $M\Omega$. The slope of the measured impedance is approximately 5 dB/oct for the frequency region between 2 kHz and 5 kHz, and the impedance is approximately 0.8 $M\Omega$ near 5 kHz. Above 7 kHz the measured impedance magnitude is approximately 0.4 $M\Omega$. Figure 3.15 shows that this estimate of the magnitude of the impedance is smaller than our theoretical calculations by as much as a factor of $\approx$ 6 (15.6 dB). From Franke and Dancer (1980) Fig. 2, we estimate that their "confidence interval" of 95% corresponds approximately to a measurement error of $\pm$6 dB. Even with this measurement error our results seem to be outside the range of experimental error.

Figure 3.15:

Inter-species comparison and high-frequency effects of $Z_c(\omega)$*:* For frequencies just above $f_{max} = f_{CF}(x = 0)$, Z_c becomes completely mass dominated for all four animals. This is a predictable result, since the mass of the fluid and mass of the organ of Corti dominates in that frequency region. However, the sudden decrease in $|Z_c|$ for ≈ 10 kHz $< f < f_{max}$ is unexpected. Human Z_c is lowest in magnitude, due to its relatively large scalae area, and the guinea pig Z_c is largest in magnitude due to its relatively small scalae area. Since the human scalae area in the apical region is larger than the other animals, the viscous boundary layer is not as significant for human Z_c as it is for the other animals at low frequencies (below 150 Hz). Thus the human Z_c is more mass-like than the other animals studied, as may be seen by the phase. The corresponding scalae areas are shown in Fig. 3.14 . The other model parameters are listed in Table 3.1 ($\eta = 0.02$, $Z_h = SC$).

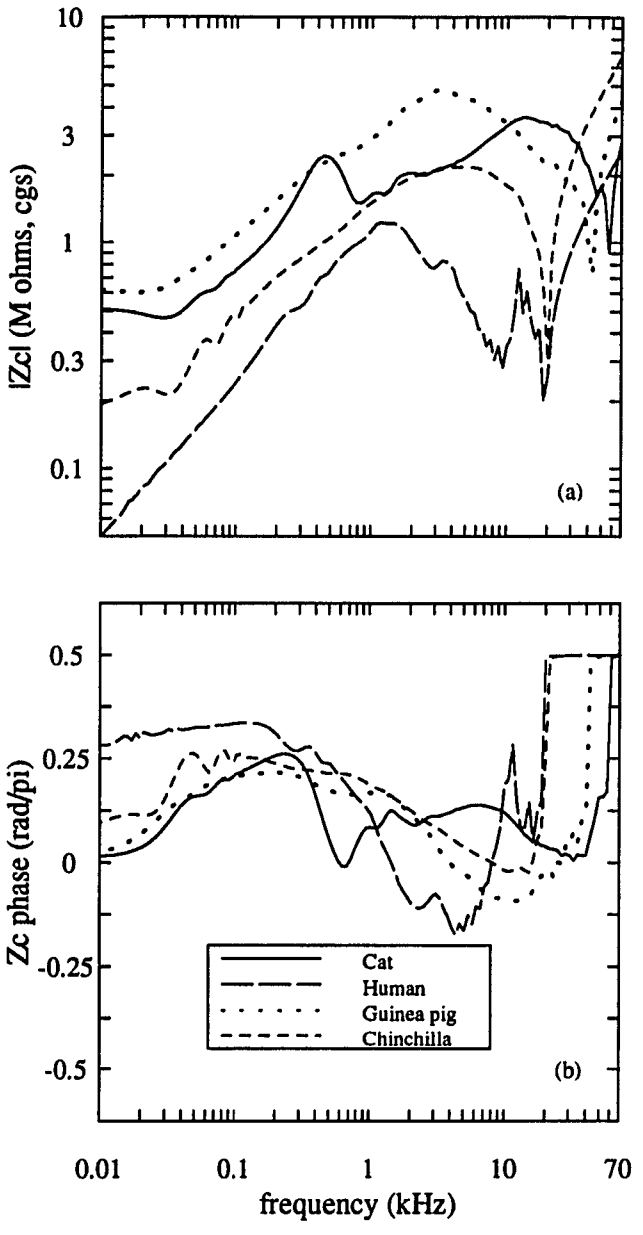

Fig. 3.15: Inter-species comparison and high-frequency effects of $Z_c(\omega)$

3.8.3 Chinchilla impedance

Recently Ruggero *et al.* (1990) have reported measurements of Z_c for the chinchilla. They found an impedance of approximately $0.5 - 0.9\ M\Omega$ in the 1 kHz $< f <$ 15 kHz frequency region, and the impedance decreases with an approximate slope of 7 dB/oct below 1 kHz. Our model calculations are greater than the reported values by as much as a factor of 4.4 (12.9 dB). The measured phase decreases from approximately $\pi/4$ at 300 Hz to approximately $\pi/8$ at 3 kHz, in agreement with our calculations. However, for 3 kHz $< f <$ 18 kHz, the measured phase starts to increase towards π, whereas the model phase continues towards zero. The model phase is $\pi/2$ for $f >$ 20 kHz. In Ruggero *et al.* (1990) the maximum measurement error was not reported. Note that f_{CF}^{ch} is a straight cochlear map but oscillations in Z_c in the model were substantially reduced due to the presence of viscosity and tapering.

3.9 Inter-species comparisons

For stimulus frequencies below 10 kHz, it is observed that of the four species studied, the human impedance is the lowest in magnitude while the guinea pig impedance is highest in magnitude. For the most part, the human scalae area is greater than the other animals, and the guinea pig scalae area is smaller. These results are consistent with our previous observation (Fig. 3.7) that the impedance magnitude is inversely proportional to the scalae area.

3.9.1 Low frequency effects

In the previous sections we concluded that the resistive behavior of Z_c below 150 Hz is due to the interaction of tapering with viscosity. Since the area in the apical region of the human cochlea is significantly larger than other cochleae, the viscous boundary layer thickness is less significant in

the human cochlea; thus the human cochlear input impedance is not as resistive at low frequencies as the other animals studied.

3.9.2 High frequency effects

For 10 kHz $< f <$ f_{max}, where $f_{max} = f_{CF}(x = 0)$, there is a "dip" or decrease in the impedance for all four species. To our knowledge this decrease in model impedance has not been previously observed. In all four cases, Z_c abruptly becomes mass dominated for frequencies above f_{max} of the cochlear map. For the cat, man, guinea pig, and chinchilla this occurs at $f_{max} \approx$ 57, 20.7, 43.8, and 19.6 kHz. Based on heuristic arguments, this mass-dominated region was modeled as M_V in (Lynch *et al.*, 1982, Fig. 23). In the chain-matrix model, the high-frequency effects of the perilymph fluid mass and organ of Corti mass arise in a natural manner.

We shall refer to the decrease and then the increase in $|Z_c(\omega)|$, at the highest frequencies, as the anti-resonance of Z_c. This anti-resonance can be quantified by analyzing $Z_o(x,\omega)$ the characteristic impedance of the cochlea [see Eq. (2.6a)]. Since at high frequencies viscous effects are insignificant we shall carry out the analysis for the inviscid case. If we substitute the approximate form $1/Y'(x,\omega) = H Z_{bm}(x,\omega)/S_0 = \frac{H}{S_0}[K(x)/j\omega + R(x) + M(x)j\omega]$ for the BM shunt impedance, and $Z' = \frac{2\rho}{S(x)} j\omega$ for the series impedance, then the characteristic impedance, at the stapes (denoted by subscript "0"), after some simplifications, is

$$Z_{o0}(\omega) = Z_o(x = 0,\omega) = \sqrt{\frac{2\rho H(K_0 - \omega^2 M_0 + j\omega R_0)}{S_0^2}}. \tag{3.9}$$

It can be shown that Eq. (3.9) reaches a minimum when $\omega = \omega_0 = \sqrt{\frac{K_0}{M_0}}$; at that frequency the magnitude of the characteristic impedance is

$$|Z_{o0}| = \left[\frac{2\rho H R_0 \sqrt{\frac{K_0}{M_0}}}{S_0^2}\right]^{\frac{1}{2}} \tag{3.10a}$$

while the phase of Z_{o0} is $\pi/4$. Note that ω_0 occurs at $2\pi f_{max}$. For frequencies below the anti-resonance frequency

$$|Z_{o0}|_{\omega<<\omega_0} \approx \left[\frac{2\rho H K_0}{S_0^2}\right]^{\frac{1}{2}}, \tag{3.10b}$$

at those frequencies the phase of Z_{o0} indicates that the characteristic impedance is real. At the very high frequencies

$$|Z_{o0}|_{\omega>>\omega_0} \approx \omega \left[\frac{2\rho H M_0}{S_0^2}\right]^{\frac{1}{2}} \tag{3.10c}$$

with a phase of $\pi/2$, indicating that Z_{o0} is mass dominated at the highest frequencies.

Most cochlear input impedance measurements have been for frequencies below 20 kHz. A way of verifying these high frequency results would be to make cochlear input impedance measurements up to and beyond f_{max} of the cochlear map of the specific animal being studied. An important reason for making such measurements is that it would then be possible to extrapolate, within a scale factor, BM parameters such as the stiffness K_0, the mass M_0, and damping parameter R_0, at the stapes.

Another reason is that if it could be measured, the sharp transition in Z_c near f_{max} of the cochlear map would appear to be a sensitive test of a traveling wave in species such as the turtle or the lizard, where the traveling wave properties are in question.

3.10 Discussion

Standing waves exist when there are reflections at both the stapes end and the apical end of the cochlea. The problem of apical reflections has been analyzed in detail. We conclude that the magnitude of apical reflections can be eliminated by using a cochlear map of the form $f_{CF}(x) = A\,[10^{\frac{a}{x_L}(x-x_L)} - 1\,]$. Alternatively, the amplitude of the apical reflections can be substantially reduced by properly accounting for scalae area variations and viscosity in the

cochlear model. In such a model, the apical reflections are dissipated by the viscous boundary layer when it is comparable to the tube radius in the apical region of the cochlea. Eliminating apical reflections obviates the need for an "infinite length" cochlear model. In addition, potential artifacts due to standing waves in non-linear time-domain models can be controlled by eliminating apical reflections.

By modeling the cochlear input impedance, important insight has been gained regarding mechanisms of the cochlea. Specifically, we have shown that the scalae area function $S(x)$ of the cochlea is important when one is interested in accurately calculating $Z_c(\omega)$. The effect of viscosity is significant for frequencies below those where the viscous boundary layer thickness is comparable to the radius of the scalae in the apical region. For the cat, chinchilla, and guinea pig, this occurred at approximately $150\ Hz$. The helicotrema boundary condition has been a point of conjecture in cochlear mechanics. We have shown that the helicotrema acoustic impedance has an insignificant effect on $Z_c(\omega)$ in comparison to the effects of tapering and viscosity. We conclude that the helicotrema can be approximated as an acoustic short circuit without altering cochlear dynamic results, assuming tapering and viscosity are properly accounted for in the cochlear model. Traditionally the helicotrema is considered to be the small hole at the apex of the cochlea. However, our model calculations show that acoustically, the helicotrema extends well into the cochlea.

In answer to the question: What physical mechanisms give rise to R_o of Fig. 2.1? We conclude that tapering increases the impedance magnitude and inclusion of perilymph viscosity results in the impedance becoming real as $f \rightarrow 0$. For the cat, chinchilla, and guinea pig the impedance is dominated by the real component for frequencies below approximately $150\ Hz$. Therefore the notion that the input impedance depends only upon the properties of the BM close to the stapes, such as in the WKB approximation, is not consistent with the results derived in the present work

Stated in other terms, the reflected wave component is an important and a necessary part of the cochlear input impedance calculation.

We have shown that accurate calculations of the cochlear input impedance requires accurate specifications of the scala vestibule and scala tympani area functions. A further verification of this result would require more cochlear input impedance measurements along with corresponding anatomical measurements of the area functions.

Sondhi (1981) conjectured that it is possible to gain insight about important BM parameters, such as the BM stiffness function $K(x)$, from $Z_c(\omega)$. Testing this idea, with a constant height cochlear model, did not prove to yield physically reasonable results for the stiffness function (Sondhi, 1988). Alternatively, under the assumptions of full knowledge of the BM stiffness $K(x)$ derived from the cochlear map, it might be possible to recover the area function $S(x)$ from the input impedance measurements by Sondhi's acoustic inverse method.

3.11 Summary

A non-uniform transmission line model of the cochlea is formulated as a cascade of two-port chain-matrices. This model includes the effects due to the spatial variations in scalae area, the viscous perilymph, spatial variations in the basilar membrane partition, and the impedance of the helicotrema.

Figure 3.16 graphically depicts some of the main points of this chapter. The curve with (S=0.0167 cm^2) is the only curve with constant scalae area. The other curves are with an area that is a close approximation to anatomical measurements of the scalae area $S_m(x)$. It is clear from Fig. 3.16 that, for frequencies below about 1-2 kHz, the magnitude of the cochlear input impedance with a constant scalae area diverges from the model calculations with realistic scalae area. For

Figure 3.16:

Summary of results: $Z_c(\omega)$ with constant scalae area, no viscosity, and a helicotrema short circuit is labeled as (S=0.0167,NV,SC). The sudden jump in Z_c near 100 Hz is due to apical reflections resulting from the low frequency limit of the cochlear map $f_{CF}^{cl}(x_L)$. The other calculations of Z_c use the more realistic scalae area $S_m(x)$ of Fig. 3.10. For frequencies below about 1-2 kHz the constant scalae area model magnitude of Z_c diverges from the model calculations with realistic scalae area. For all cases having scalae area $S_m(x)$, model results are in good agreement with measured data for frequencies above 150 Hz (see Fig. 3.13). Below $f_{CF}^{cl}(x_L)$, the large oscillations in Z_c are due to apical reflections. Adding a tube impedance (TI), for the helicotrema, has the effect of changing the nature of the reflections, but it fails to remove them. After including perilymph viscosity (WV), two important result emerge for frequencies below 150 Hz: First, the phase indicates that Z_c is resistance dominated. Second, the apical reflections have dissipated. Viscous effects are important when the scalae radius becomes comparable to the viscous boundary layer.

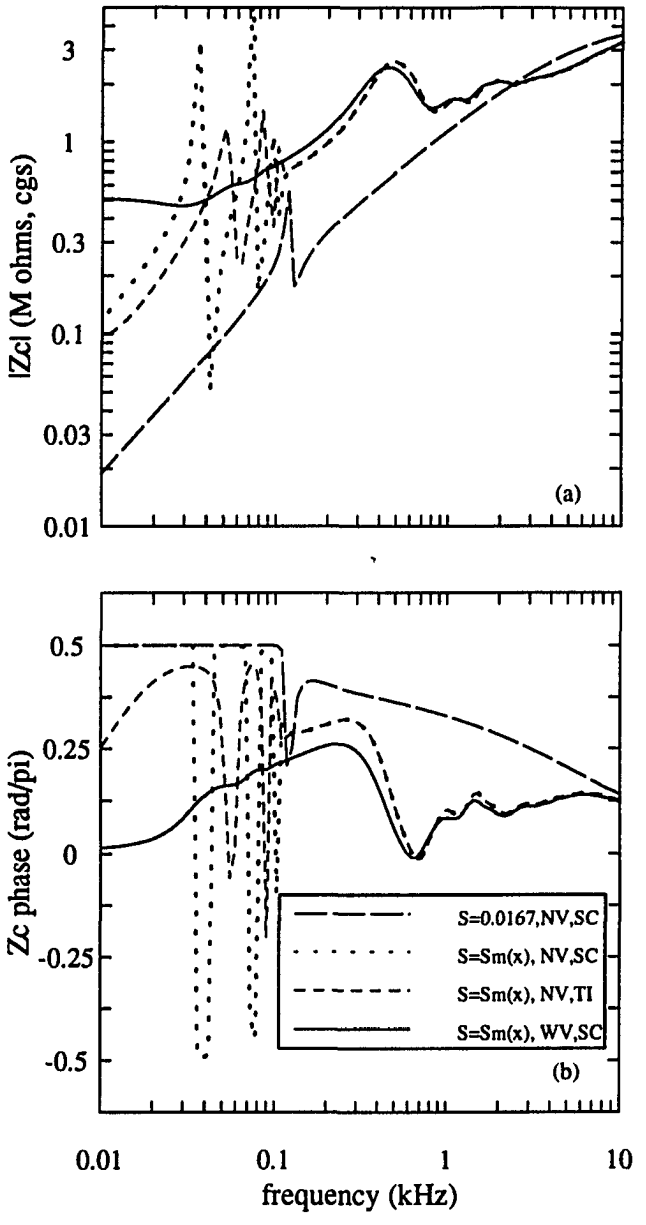

Fig. 3.16: Summary of results

frequencies above 150 Hz, there is good quantitative agreement between the data and our model calculation with a realistic scalae area (see Fig. 3.13). The amplitude oscillations in Z_c below $f_{CF}^{cl}(x_L)$ are present in both the constant scalae area model and the model with the realistic scalae area. These oscillations indicate the presence of apical reflections. In the realistic scalae area case, the magnitude of the reflections are much greater due to an increase in impedance-mismatch between the scalae and the helicotrema. Although adding a tube impedance, for the helicotrema, affects the nature of the apical reflections it fails to remove them. When perilymph viscosity is included in the model, two important effects are observed for frequencies below 150 Hz: First, the impedance starts to become more and more resistive as frequency decreases. Second, the apical reflections have dissipated. These effects are due to the viscous boundary layer becoming comparable to the scalae radius in the apical region of the cochlea.

Chapter 4

Modeling the "surgically modified" middle ear

Introduction

A signal presented in the ear canal is transmitted through the middle ear to cochlea, and then to the auditory nerve. In addition it is now known that a small fraction of the energy measured in the earcanal has its origin in the cochlea. In both cases the middle ear is the structure that serves as an interface between the air-filled ear canal and the fluid-filled cochlea. As stated in Chapter 2, in order to understand the bidirectional flow of energy in the cochlea, it is necessary to have a good model of the middle ear and of the cochlear input impedance. The later was the subject of Chapters 2 and 3. In the present Chapter both mechanistic aspects as well as functional aspects of the middle ear are investigated.

Middle ear mechanics goes as far back as the time of Helmholtz (1885). He based many of his conclusions on measurements and observations of the middle ear anatomy. Further studies that characterize the mechanical interconnections of the middle ear ossicles to the eardrum and cochlea were made by von Békésy (1960), Wever and Lawrence (1954) and others. In addition to anatomical and mechanical descriptions many other forms of measurements have become

available on humans and other animals since the time of Helmholtz. These include measurements of earcanal impedance, umbo velocity, stapes velocity, etc, resulting in an evolution of middle ear models.

An important noninvasive measurement is the ear canal impedance. Middle ear models based on earcanal impedance measurements have been abundant in the hearing literature (Zwislocki, 1957; Onchi, 1961; Moller, 1961; Flanagan, 1962; Zwislocki, 1962; Moller, 1965; Shaw and Stinson, 1981; Lynch, 1981; Shaw and Stinson, 1983; Tonndorf and Pastaci, 1986; Matthews, 1983; Kringlebotn, 1988; Shera and Zweig, 1989). However, accurate earcanal impedance measurements above 6-8 kHz have been sparse. To our knowledge impedance measurements near the cat tympanic membrane made by Allen (1986) are the only ones that go as high as 33 kHz. Similar measurements by Lynch (1981) are for frequencies below 20 kHz, and by Tonndorf and Pastaci (1986) for frequencies below 15 kHz.

Our goal of middle ear modeling is to obtain a model that accurately describes the mechanics of the physiological system. Lumped-element modeling provides a readily interpretable framework for modeling middle ear mechanics (Onchi, 1949; Zwislocki, 1957; Moller, 1961). Given the driving point impedance at the eardrum we will obtain parameters that characterizes the measured data. In a typical middle ear model there are many parameters that need to be estimated. One possible methodology, to "uniquely" estimate parameters, is to make "surgical modifications" along the ossicular chain and cochlea. Measurements by Allen (1986) have been made with "surgical modifications" in a systematic manner. Thus his data will be used to model the mechanical properties of the eardrum and ossicles.

The organization of this Chapter is as follows: To acquaint the reader with the literature we first introduce an anatomical representation for the cat middle ear. Subsequently, a phenomenological

representation and then a corresponding specific circuit for the middle ear is presented. Next the impedance data is presented in increasing order of complexity, from which parameters for the model will be extrapolated. First the "interrupted incus" data are modeled. Next the "drained cochlea" data are modeled. Finally the "intact" data are modeled using parameters from the previous two models and results for the cochlear input impedance from Chapter 3. Subsequent to this the cat middle ear cavities are modeled using the chain-matrix method (validation of the chain-matrix model for a cavity is deferred until Chapter 5). The model for the middle ear cavities is combined with the eardrum impedance model to obtain a comprehensive model of the cat middle ear.

4.1 The middle ear model

The middle ear serves to couple acoustic energy of the ear canal to the cochlea. This coupling is necessary because there is an acoustic impedance mismatch between the air filled ear canal and the much higher impedance of the fluid filled cochlea. Figure 4.1 shows a simplified anatomical representation for the cat middle ear. In this figure the *Pinna Flange* and external auditory meatus have been resectioned.

Acoustic energy in the earcanal sets the eardrum in motion. Motion of the eardrum is transmitted to the cochlea by three bones, known as the *ossicles*. They are called the malleus, incus, and stapes. Motion of the eardrum causes the malleus to move, resulting in a rotational motion of the incus. The force produced by the incus at the stapes results in a piston like motion of the stapes footplate (oval window). This sets the cochlear fluids into motion. The cochlea fluids and the organ of Corti are assumed to to be incompressible; thus volume displacement of the oval window results in an equal volume displacement of the round window located in the bulla cavity.

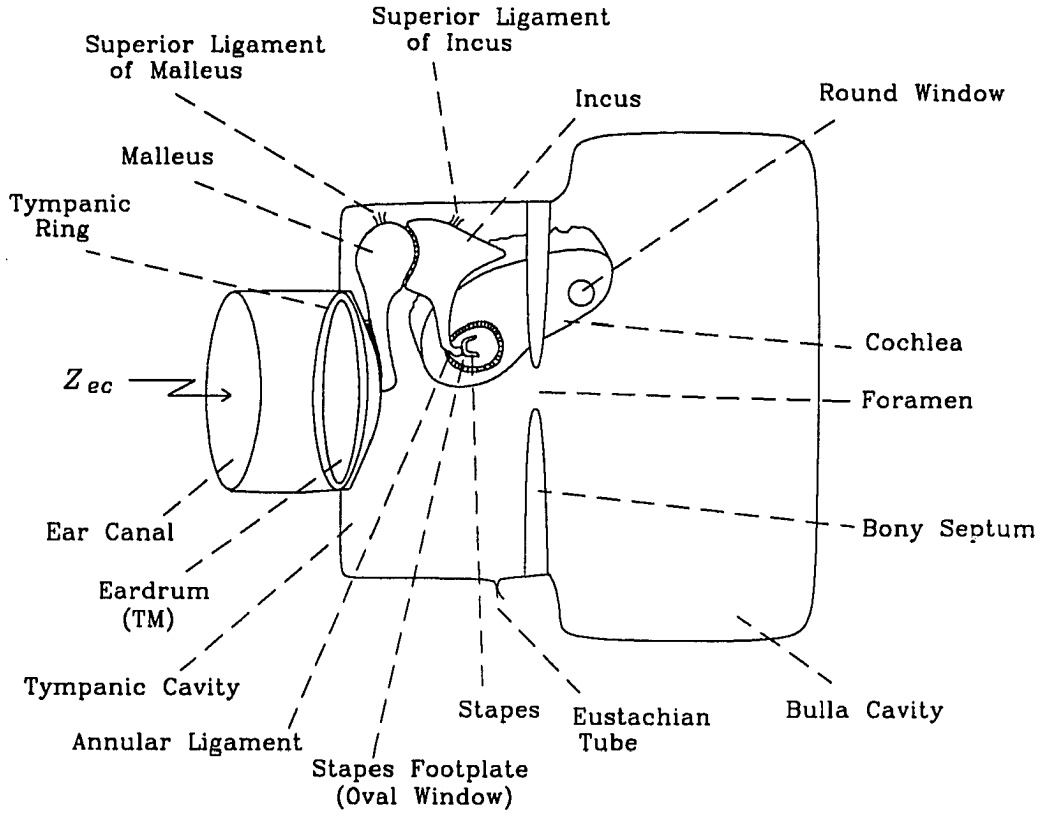

Figure 4.1: *Simplified anatomical representation of the cat middle ear:* Sound pressure difference between the ear canal and the tympanic cavity results in motion of the eardrum (tympanic membrane). This results in motion of the three ossicles malleus, incus, and stapes. The malleus and the incus are suspended from the tympanic cavity walls by the *superior ligament of malleus* and *superior ligament of incus*. There are other ligaments that connect the ossicles to the cavity walls, but for the sake of simplicity they are not shown in this figure. The tympanic cavity is connected to the bulla cavity by a small opening called the foramen; this opening is formed by the bony septum. The Eustachian tube is shown in its normally closed position. Impedance measurements are made by placing a microphone/receiver transducer assembly close to the tympanic ring.

4.1.1 Phenomenological representation

To better quantify the above description, a phenomenological representation of the cat middle ear anatomy is shown in Fig. 4.2 . This model is intended to capture details of middle ear mechanics from impedance measurements made at the tympanic membrane (TM). Difference between the model of Fig. 4.2 and previous middle ear models of Zwislocki (1962), Lynch (1981), Shaw and Stinson (1981), Matthews (1983), and others is that in present model the pressure seen by the round window is that of the bulla cavity rather than the tympanic cavity. There are topological similarities between the model of Fig. 4.2 and middle ear models by Shera and Zweig (1989) and Peake *et al.* (1991). The main differences between those models and the present one lies in the formulation for the cavities, the physiological mechanisms attributed to some of the elements, and more importantly the estimated parameters. We now discuss the physiological mechanism for each of the "boxes" in Fig. 4.2 .

We assume that the component of the eardrum impedance that is coupled to the ossicles is $Z_{dc}(\omega)$ and the component of the eardrum impedance that is coupled to the tympanic cavity, but is uncoupled from the ossicles, is $Z_{du}(\omega)$. A review of the anatomical and mechanical properties of the eardrum can be found in (Robert *et al.*, 1982). The impedances of the malleus and incus are Z_m and Z_i. The interconnection between these two bones is referred to as the incudo-malleolar joint. The impedance of this joint is referred to as Z_{jim}. Similarly, the shunt impedance due to slippage between the incus and stapes, known as the incudo-stapedial joint, is $Z_{jis}(\omega)$. These joints are believed to be species dependent.

In most rodents such as guinea pig, chinchilla, etc. (Dallos, 1973, p. 5), man (Gyo *et al.*, 1987), and other animals, it is believed that the malleus and incus bones are fused together. In animals such as the cat (Guinan and Peake, 1967), squirrel monkey (Rhode, 1971), and others,

there is experimental evidence of slippage between the two bones.

In man (Zwislocki, 1962) there is some evidence of slippage at the incudo-stapedial joint. To our knowledge there is no experimental evidence regarding slippage between incudo-stapedial joint for the cat. Z_{jis} is included in our model for the sake of generality.

The stapes impedance is $Z_s(\omega)$ and the annular ligament impedance is $Z_{al}(\omega)$. The annular ligament is flexible and it keeps the stapes attached to the cochlea. The "load" to the middle ear is the cochlea. Input impedance of the cochlea is $Z_c(\omega)$. The impedance of the round window is $Z_{rw}(\omega)$.

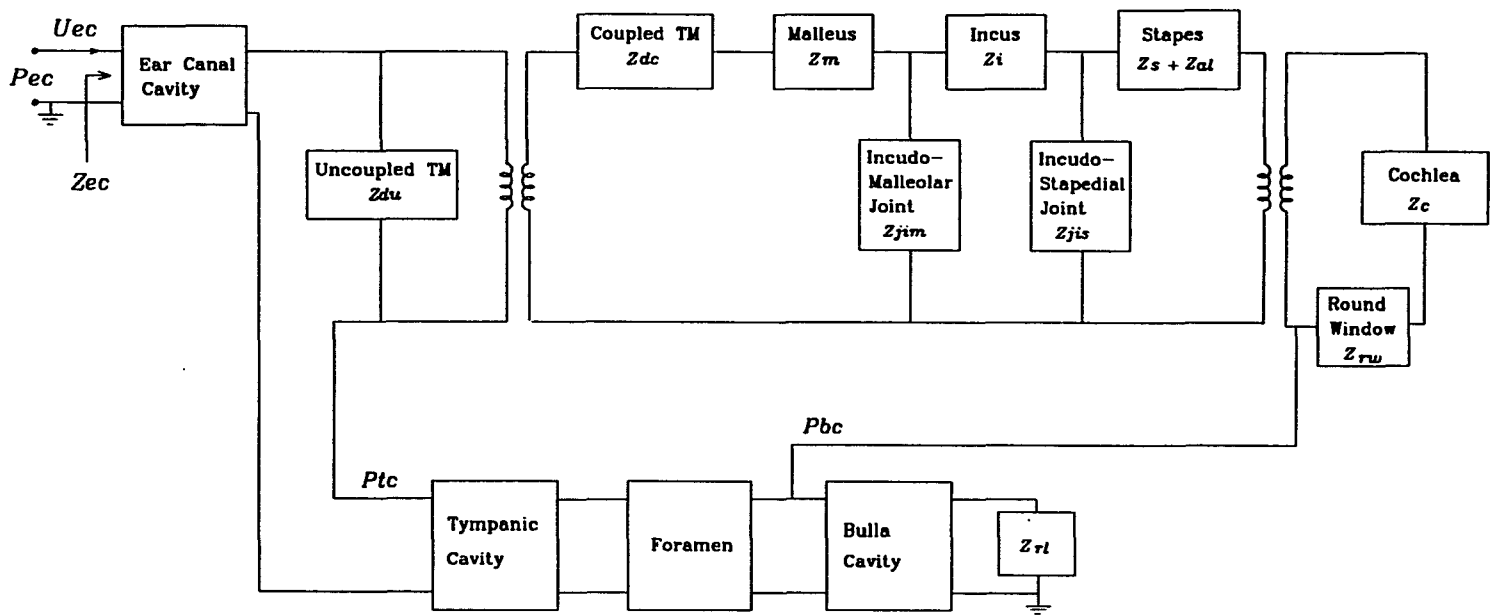

Figure 4.2: *Phenomenological representation of the middle ear:* Salient anatomical features of the middle ear are functionally represented here by a "box". The transformers provide the necessary dimensional transformation. The complicated motion of the eardrum is functionally represented by two types of motion: one that is coupled to the ossicles and the other is uncoupled from the ossicles but drives the middle ear cavities. The earcanal cavity is modeled as a cylindrical tube of length l_{ec} and diameter d_{ec}. The middle ear cavities are modeled as cylindrical tubes of lengths l_{tc}, l_f, l_{bc} and diameters d_{tc}, d_f, d_{bc} for the tympanic cavity, foramen, and the bulla cavity. The radiation impedance seen by the bulla cavity is $Z_{rl}(\omega)$.

In the cat the volume of the middle ear is divided into two cavities by a partition called the bony septum. The cavity directly behind the eardrum cavity is the tympanic cavity; the pressure in this cavity will be reffered to as $P_{tc}(\omega)$. The other cavity is called the bulla cavity; the pressure in the this cavity is reffered to as $P_{bc}(\omega)$. Communication between the two cavities is possible by a small oval shaped hole in the bony septum. Since the round window is located in the bulla cavity the pressure seen by the round window is P_{bc}. In humans the total middle ear volume is also divided into two chambers, but it is believed that there is no partition between the two volumes. As a result, differences in the pressures of the two cavities are expected to be much smaller than those in the cat.

The chain-matrix model for a cavity with a variable cross-sectional area is to be used to represent the middle ear cavities and the ear canal. Viscous and thermal losses are explicitly included in the chain-matrix model. Further discussion of the chain-matrix model of a cavity and experimental measurements on some sample cavities is deferred until Chapter 5. In the present Chapter we assume that the chain-matrix model in valid without further proof.

The auditory meatus has been resectioned and thus the space between the tympanic ring and the measurement location is approximated as a cylindrical tube with length l_{ec} and diameter d_{ec}.

The middle ear cavity impedance is modeled as three cylindrical tubes with a radiation impedance. The first tube represents the tympanic cavity with diameter d_{tc} and length l_{tc}. The second tube is not really a tube but a narrow passage called the foramen; this passage can be approximated as a tube with a short length l_f and diameter d_f. The third tube represents the bulla cavity with length l_{bc} and diameter d_{bc}. The radiation load seen by the tympanic cavity Z_{rl} depends on the condition of the experiment. When the bulla cavity is intact an open circuit condition exists and thus $Z_{rl} \rightarrow \infty$. When the cavities are surgically removed then there is a finite radiation load seen by that cavity.

4.1.2 Specific representation

To mathematically describe the middle ear one can write the equations of motion for each anatomical entity of the middle ear. Alternatively, by using dynamical analogies the mechanical system can be represented by an analog electrical network (Beranek, 1954; Olson, 1958; Pierce, 1989). Since electrical network representations are readily interpretable, we shall use them to describe the impedances of the eardrum and the ossicles. Such a network corresponding to the phenomenological model of the middle ear model is shown in Fig. 4.3 . The specific middle ear model of Fig. 4.3 is similar to that of Lynch (1981) and Matthews (1983). A good review of the relationship between this model and previous middle ear models is found in Shera and Zweig (1991a).

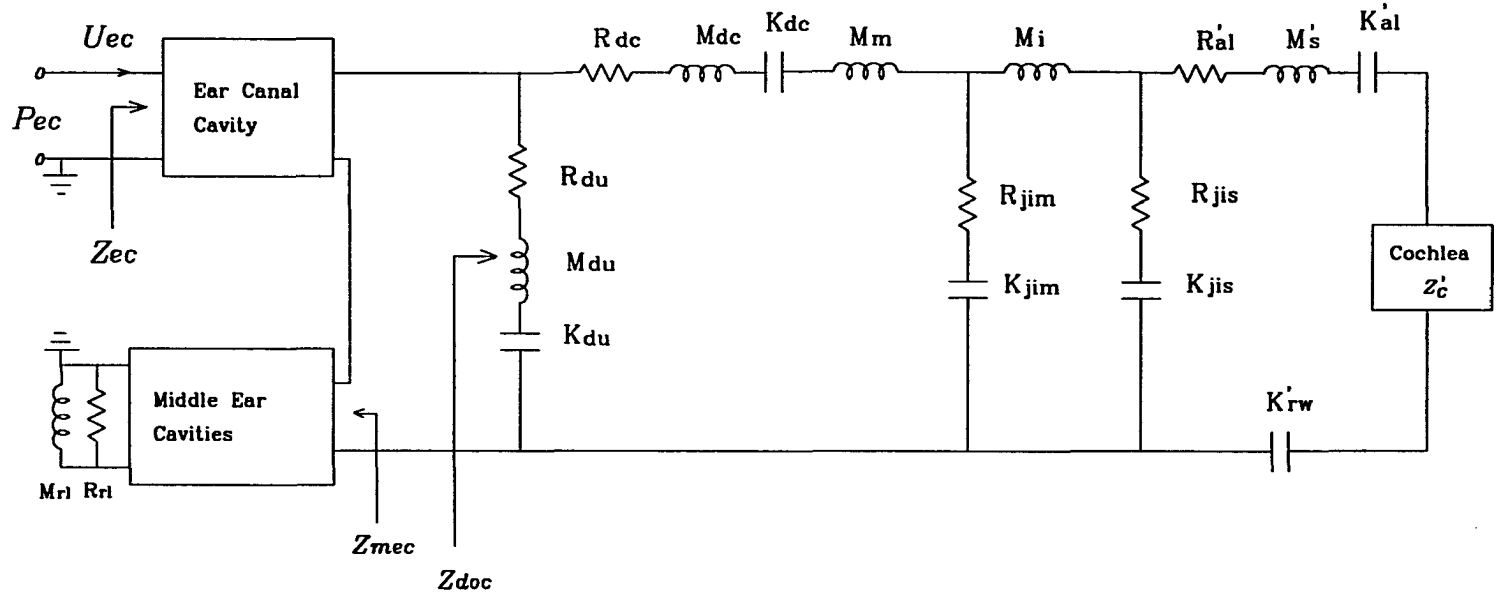

Figure 4.3: *Specific implementation for the phenomenological representation of the middle ear:* The cochlear input impedance is obtained from the chain-matrix cochlear model of the previous Chapters. The eardrum and the ossicles are modeled by lumped-parameter elements. The primes indicate that those impedances have been transformed to the eardrum side by the transformer ratio. In combining the impedance of the middle ear cavities with the impedance of the eardrum we have assumed that they can be connected in series; the validity of which is discussed in Sec. 4.8. The cavities are modeled as chain-matrices that include visco-thermal losses and effects resulting from non-planer wave propagation due to a constriction such as the foramen. When the bulla cavity is resectioned, Z_{rl} is approximated by the parallel combination of $j\omega M_{rl}$ and R_{rl}. For the closed bulla case $Z_{rl} \rightarrow \infty$.

In Fig. 4.3 the combined impedances of the eardrum, ossicles, and cochlea are shown to be connected in series with the impedance of the middle ear cavities. The validity of the series model has been experimentally tested by making various surgical modifications to the cat middle ear anatomy (Lynch, 1981). Such a network representation requires the assumption that the pressure on the middle ear cavity side of the round window is the pressure in the tympanic cavity (P_{tc}). Anatomically the round window is located in the bulla cavity and thus the actual pressure seen by the round window is that of the bulla cavity (P_{bc}). From the eardrum impedance point of view, the nature of the errors made in making the assumption that the round window is located in the tympanic cavity is limited to a small frequency region. This point is further discussed in Sec. 4.8.

The impedance due to the middle ear cavities will be reffered to as $Z_{mec}(\omega)$. For the cochlear input impedance $Z_c'(\omega)$ we use the frequency dependent results of the previous Chapters. The prime indicates that the impedance has been transformed to the eardrum side of the transformer ratio. The rest of the boxes shown in Fig. 4.2 are each represented in Fig. 4.3 by an R, M, K series network, where R represents the damping (due to internal losses), M represents the inertance (due to mass), and K is the stiffness of the particular middle ear structure. All elements referred to will be in *cgs* units.

4.1.3 Network synthesis

The problem of network synthesis from a given driving-point impedance is a classical one in analog circuit theory. Some of the most important concepts are presently reviewed.

There are several general procedures in network synthesis: the Brune procedure, the Darlington procedure, the Bott-Duffin procedure, and the Cauer method. All of these describe a method for synthesizing a network from a positive real (p.r.) driving-point impedance. By p.r. we mean that the real part of the driving-point impedance is non-negative for all frequencies. With the exception of measurement noise, the driving-point impedance measured in the earcanal indicates that it is p.r. for all frequencies. The Brune procedure and the Darlington procedure require the use of mutual inductances (ideal transformers) as part of the network. Bott and Duffin were the first to prove that it is possible to realize p.r. functions without the use of transformers. In Cauer's method the driving-point impedance and transfer function are important. In this method a ladder network is synthesized by removal of poles and/or zeros. A more complete analysis of these network synthesis procedures can be found in (Weinberg, 1962, Chap. 10), (VanValkenburg, 1964), and others.

The procedures briefly mentioned above generally assume no knowledge of the mechanisms of the system under consideration. As a result, application of different procedures results in different forms for the network. In this sense the synthesized network is not unique. For the problem at hand *the particular network is necessitated by physical principals* and hence the physical network of Fig. 4.3 . The difficulty lies in estimating the parameters and verifying the accuracy of the chosen topology. An informal procedure for estimating the parameters will be described in Sec. 4.3.4.

4.2 The cat eardrum impedance data

The eardrum impedance data that we shall use to estimate the middle ear parameters is shown in Fig. 4.4 (Allen, 1986). The bulla cavity was opened as wide as possible and the bony septum that separates the bulla cavity and the tympanic cavity was removed. Subsequently, a calibrated pressure transducer and probe-tube microphone assembly were placed close to the tympanic ring (typically less than 4-5 mm from the eardrum).

The impedance measurement technique will be described in Chapter 5. In summary, a calibration technique allows estimation of the Thévenin equivalent source parameters for the pressure transducer. With these parameters the impedance is calculated from pressure measurements of the unknown cavity by a simple pressure divider rule. The resulting impedance is the impedance of the unknown load normalized by the characteristic impedance of the transducer Z_{ot}. The normalized earcanal impedance will be reffered to as $Z_{ec}(\omega)$.

The measurements shown in Fig. 4.4 are to 33 kHz. It is noted that such high frequency measurements were not previously available. One of the factors that determines the high frequency limit for these measurements is the frequency at which the pressure transducer starts to roll-off. In this particular case the pressure transducer started to roll-off at approximately 20 kHz (Allen, 1986).

Recall that the system is calibrated with cylindrical tubes having hard walls. The ear canal geometry is more complicated than that of cylindrical tubes. In addition, the complicated motions of the eardrum may, in theory, excite higher-order modes (Rabbitt, 1990). Under these conditions it is possible for higher order modes to propagate short distances and possibly have an effect on the impedance measurements. Based on some simple calculations Lynch (1981, p. 147) has shown that these higher-order modes are evanescent near the location of the transducer assembly.

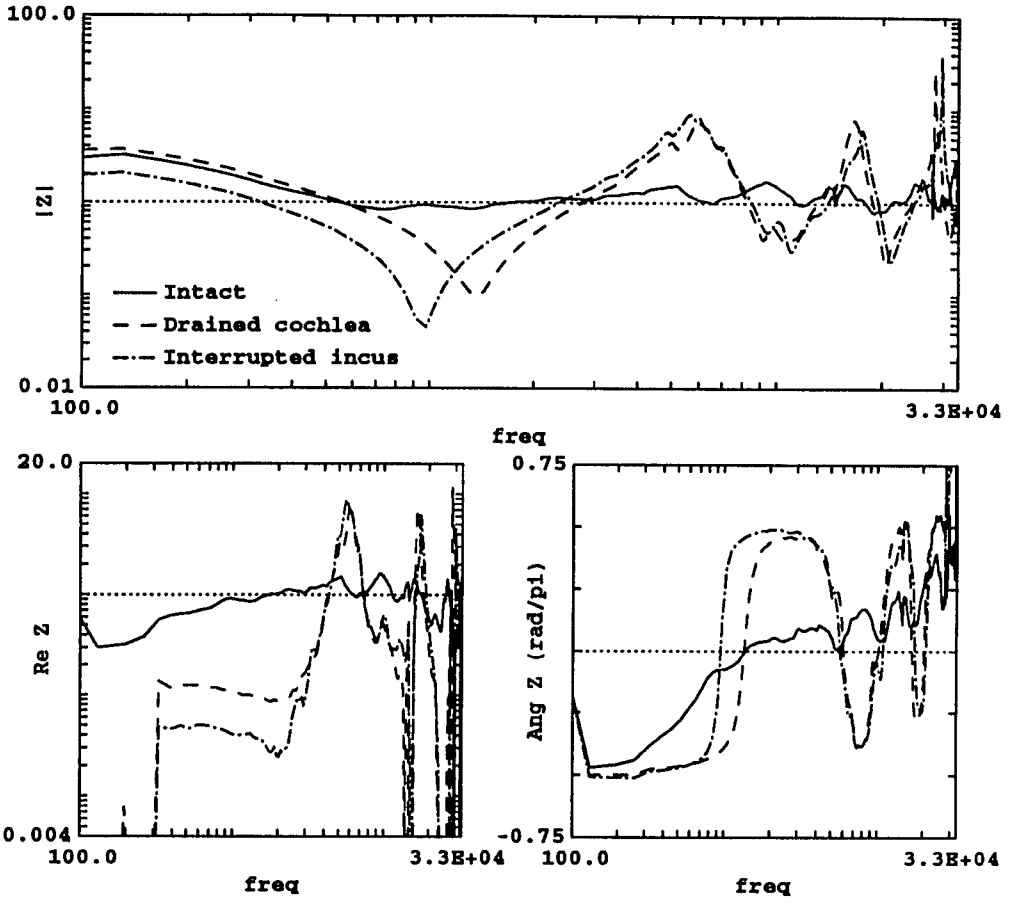

Figure 4.4: *The "surgically modified" earcanal impedance measurements (Allen, 1986):* All measurements were made with the bulla cavity wide open and the bony septum removed. (1) "Intact" – ossicles and cochlea in normal state (Z_{ec}^{i}), (2) "Drained cochlea" – scala vestibule and scala tympani perilymph removed (Z_{ec}^{dc}), (3) "Interrupted incus" – Cut incus away from stapes (Z_{ec}^{ii}). The magnitude of the impedance normalized to the characteristic impedance of the transducer assembly is shown in the upper panel. The lower left panel shows the real part of the normalized impedance. The scale in the real part was adjusted so as to display the full range of the curves. The right panel shows the phase angle in multiples of π units. The frequency range is from 100 Hz to 33 kHz. All subsequent figures showing impedances will follow this format.

There are three measurement conditions shown in Fig. 4.4 . These measurements were made, with the tympanic cavity and bulla cavity wide open, in the following order:

- Cochlea and middle ear ossicles "Intact" $Z_{ec}^{i}(\omega)$.
- Perilymph removed – "drained cochlea" $Z_{ec}^{dc}(\omega)$.
- Cut incus from stapes – "Interrupted Incus" $Z_{ec}^{ii}(\omega)$.

Note that when the incus is cut, the impedance of the annular ligament Z_{al}, stapes Z_s, and the cochlea Z_c may no longer be observed at the eardrum. Thus the complexity of eardrum impedance is reduced to that of the eardrum, malleus and incus. In the drained cochlea case the complexity increases from the previous case by the addition of Z_{al} and Z_s. And finally in the intact case the complexity is further increased by the load Z_c placed on the stapes. Consequently, we will begin our modeling efforts with the least complicated data – that is in reverse order of the measurements.

4.2.1 Reflectance domain

Up to now we have presented the data in the impedance domain. Very often transforming the impedance to the reflectance domain offers an understanding of the data that is not possible in the impedance domain. The normalized impedance $Z_{ec}(\omega)$ and reflectance $R_{ec}(\omega)$ are related by the *bilinear transformation*:

$$R_{ec}(\omega) = \frac{Z_{ec}(\omega) - 1}{Z_{ec}(\omega) + 1}. \tag{4.1}$$

The magnitude of the reflectance is sensitive to $\Re e[Z_{ec}]$ (Smith, 1944). For example if Z_{ec} is lossless then $|R_{ec}|$ is one for all frequencies. We will use the notation $\Re e[Z_{ec}]$ and $\Im m[Z_{ec}]$ to indicate the real and imaginary parts of Z_{ec}.

One interpretation of reflectance is that it is the complex ratio of the reflected wave to the

incident wave. Thus it is possible to obtain information regarding the amount of delay in the reflected wave from the phase of the reflectance.

Khanna and Tonndorf (1969), Rosowski *et al.* (1986), and others have shown that calculations of power are somewhat correlated with threshold of hearing. Thus there is some evidence that the cochlea is a detector of power. It can be shown that the relationship between reflectance as calculated by Eq. (4.1) and the average normalized real power W_t/W_o absorbed at the eardrum is simply (Carlin and Giordano, 1964, Sec. 4.3)

$$\frac{W_t(\omega)}{W_o(\omega)} = 1 - |R_{ec}(\omega)|^2, \tag{4.2}$$

where W_t is the power transmitted to the ossicular chain, cochlea, and middle ear cavities, and W_o is the power generated by the pressure transducer. Because measures of reflectance are meaningful in their own right and because power calculations can be easily made from the reflectance calculations we will only make calculations of reflectance in this study.

The impedance Z_{ec}^{ii} when transformed to reflectance will be reffered to as R_{ec}^{ii}; similarly for R_{ec}^{dc} and R_{ec}^{i}. These reflectance domain calculations will be shown as we model each case.

4.3 Interrupted incus

The effect of cutting the incus is that there are no impediments to the motion of the tip of the incus; as a result there is no force developed at its free end. This effectively corresponds to an acoustic short circuit to ground (zero pressure). In the literature this is referred to as the "interrupted incus" case. The anatomical representation corresponding to this case is shown in Fig. 4.5 . The circuit diagram corresponding to the "interrupted incus" case is shown in Fig. 4.6 . Since bulla and tympanic cavities are exposed to the atmosphere, the MEC impedance is approximated as a short

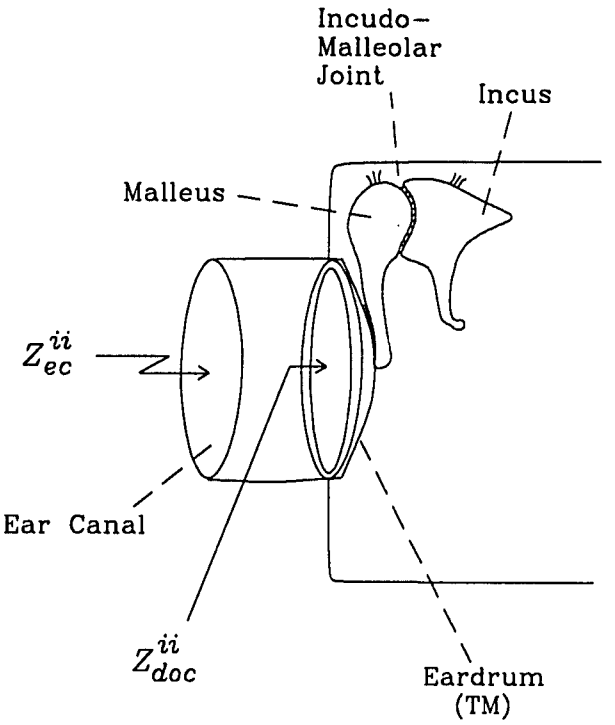

Figure 4.5: *Anatomical representation for the "interrupted incus" case:* In this case the end of the incus is free to move without an impedance at its tip; this is equivalent to an acoustic short circuit. $Z_{doc}(\omega)$ is the impedance of the eardrum with open cavities. Z_{ec}^{ii} is the impedance measured in the earcanal for this case.

circuit. In the section that follows we estimate the unknown parameters for the circuit of Fig. 4.6 .

4.3.1 Estimating the parameters

To a first order approximation, the phase of the impedance data and the slopes of the magnitude of the impedance Z_{ec}^{ii} in Fig. 4.4 indicate that the impedance consists of stiffness dominated regions and mass dominated regions. The impedance data can be approximated with straight line approximations having −6 db/oct slopes for the compliance dominated regions and +6 db/oct slopes for the mass dominated regions.

Recall that the impedance shown in Fig. 4.4 has been normalized by the characteristic

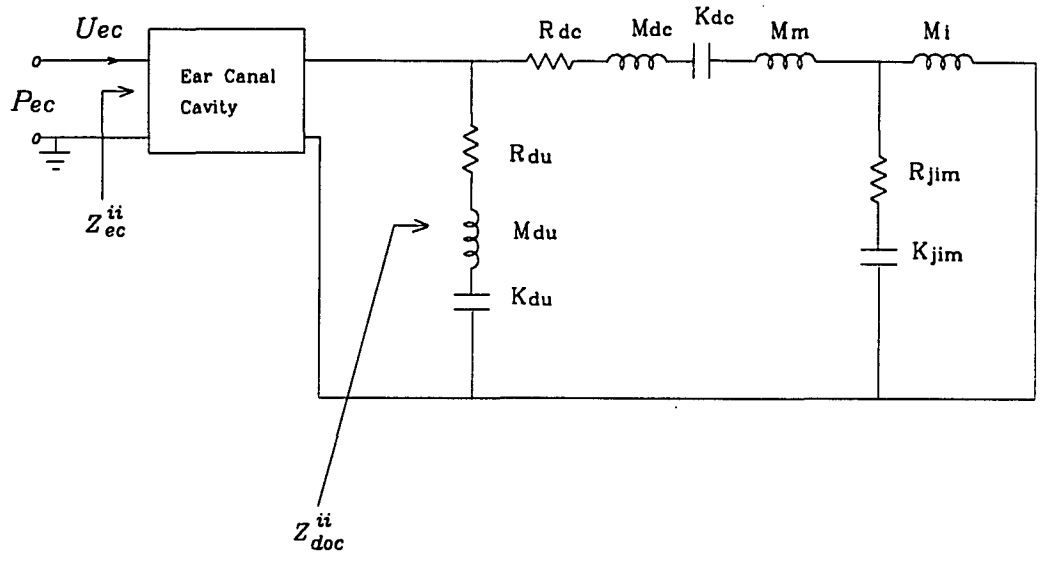

Figure 4.6: *Circuit diagram for the "interrupted incus" case:* Each element here corresponds to a particular anatomical entity in Fig. 4.5 . There are eleven parameters that need to be evaluated. Mass of the malleus M_m and the coupled eardrum mass M_{dc} are considered as a single parameter. The tympanic cavity is exposed to the atmosphere and thus Z_{mec} is approximated as a short circuit.

impedance of the measurement transducer $Z_{ot} = \rho_a c_a / A_t$. Where $\rho_a c_a = 40.87$ at $27 \pm 10\ ^\circ C$ and A_t the area of the transducer is 0.1018 cm; this results in $Z_{ot} \approx 401\ dyne - sec/cm^5$.

The impedance Z_{ec} of a compliance dominated region is $K/j\omega$. Unnormalizing the impedance by Z_{ot} results in $|Z_{ec}| = Z_{ot}\ K/\omega$. Thus the stiffness components are estimated according to

$$K = \omega \frac{|Z_{ec}|}{Z_{ot}}. \tag{4.3}$$

The mass components are similarly estimated according to

$$M = \frac{|Z_{ec}| Z_{ot}}{\omega}. \tag{4.4}$$

Using the above equations $K_{dc}, K_{du}, M_{dc}, M_{du}$ were estimated. The value for R_{dc} was chosen to

match $\Re e[Z_{ec}^{ii}]$ for frequencies below approximately 1 kHz, i.e.

$$R_{dc} = Z_{ot}\Re e[Z_{ec}^{ii}]. \tag{4.5}$$

R_{du} was initially chosen arbitrarily. These parameters were subsequently adjusted to obtain a good fit to the impedance data. The optimized parameters are listed in the first part of Table 4.1. The measured impedance and corresponding model result is shown in Fig. 4.7 . Discussion of how the other parameters are evaluated is found in section 4.3.3.

4.3.2 Frequency region below 5 kHz

For frequencies below approximately 5 kHz, Z_{ec}^{ii} is dominated by Z_{dc}. In the frequency region between 100 Hz and 1 kHz the impedance is dominated by the stiffness K_{dc}. Between 1 kHz and 5 kHz it is dominated by the mass M_{dc}. $|Z_{ec}^{ii}|$ reaches a minimum when the reactive components of Z_{dc} cancels. The frequency where this occurs is

$$f_{dc} = \frac{1}{2\pi}\sqrt{\frac{K_{dc}}{M_{dc}}}. \tag{4.6}$$

At frequency f_{dc} the impedance is due mostly to R_{dc}.

In its normal state, the eardrum is a cone shaped structure. However, when the malleus is cut the eardrum starts to lose its conic shape and tends to "crinkle" (Allen, 1990). Thus the stiffness in the coupled portion of the eardrum K_{dc} is mostly due to the stiffness of the the superior ligaments and some component of it is due to the eardrum itself. Since the two mass components M_{dc} and M_m appear in series, we have combined them into a single mass M_{dc}.

4.3.3 Frequency region above 5 kHz

For frequencies above approximately 5 kHz the behavior of the measured earcanal impedance is quite complicated. It is dictated by Z_{du}, Z_{jim}, and Z_m. For stimulus frequencies between approximately 5 kHz and 8 kHz the impedance is dominated by K_{du}. For frequencies above approximately 12 kHz it is dominated by M_{du}.

In the 8-12 kHz frequency region the magnitude, real part, and the phase of Z_{ec}^{ii} are non-monotonic. In Fig. 4.7 this non-monotonicity appears as a "bump" and for brevity we shall refer to it as such. Initially this bump was thought to be artifactual. However, such impedance measurements on other cats (unpublished data) also show a similar bump in the 10 kHz vicinity. This has lead us to believe that this bump is not an artifact but is due to some physical mechanism. We shall refer to this bump as Z_b in the impedance domain. We will argue that the physical mechanism for this impedance is slippage between the incudo-malleolar joint.

Initially it was thought that Z_b was due to the impedance of the open cavities behind the eardrum. In fact by assuming M_i to be much smaller than M_m (i.e. short circuiting Z_{jim}) we were able to somewhat replicate the bump by choosing appropriate dimensions and radiation load for the tympanic cavity. However, based on Guinan and Peake's (1967) experimental observation that there is slippage between the cat incudo-malleolar joint for frequencies above approximately 8 kHz, it would appear that Z_{jim} may play an important role in Z_{ec}. Subsequent to this realization we were able to obtain parameters for Z_{jim} and M_i that resulted in a good fit to the measured Z_{ec}^{ii}.

Thus far two different hypothesis have been put forth to characterize Z_{ec}^{ii} in the 8-12 kHz frequency region. The model with incudo-malleolar slippage resulted in a better fit to the measured data. Based on this and attempts to model other data, such as Z_{ec}^{dc} and Z_{ec}^{i}, the evidence that Z_b is due to slippage of the incudo-malleolar joint appears stronger.

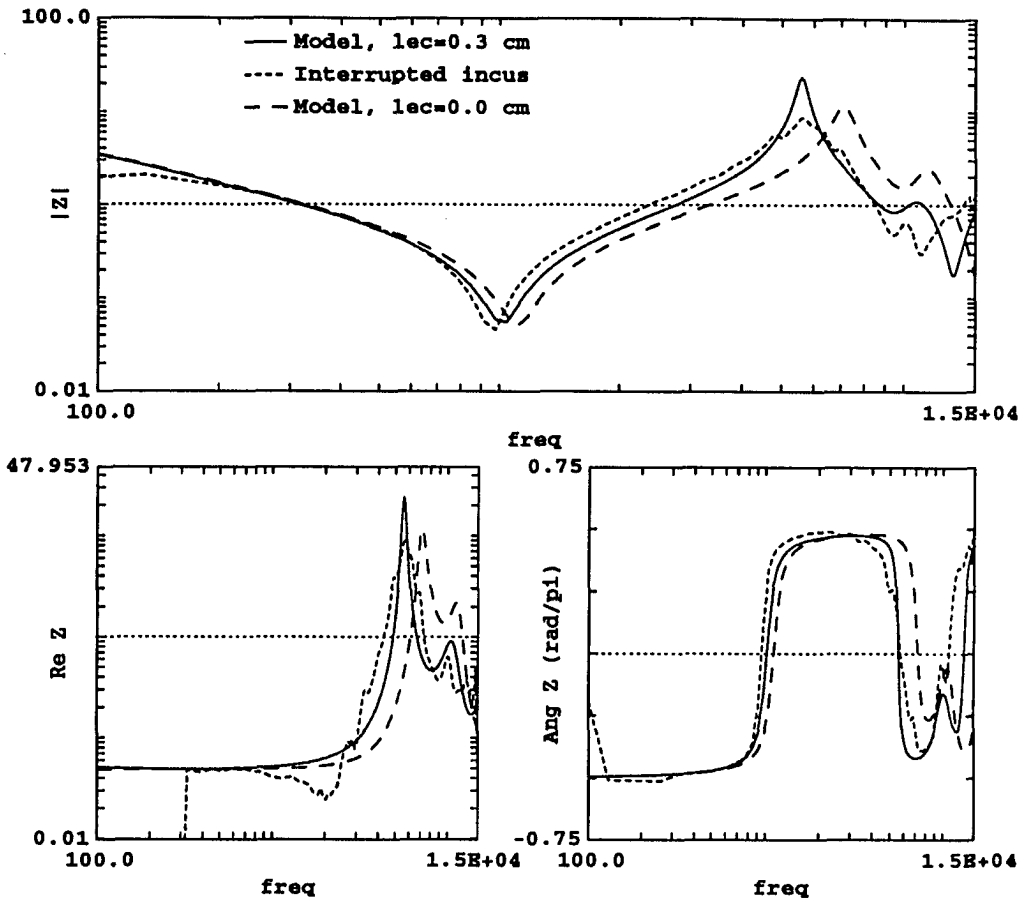

Figure 4.7: *Comparison of model impedance and measured impedance for the "interrupted incus" case (Z_{ec}^{ii}):* The frequency range is from 100 Hz to 15 kHz. The data is labeled "interrupted incus". For frequencies below 5 kHz the impedance is dominated by the coupled portion of the eardrum impedance Z_{dc}. Above 5 kHz the eardrum impedance depends on other factors. In both magnitude and real part of the data there is a nonmonotonic transition in the frequency region between 8 kHz and 12 kHz. This behavior in the impedance is due to slippage between the malleus-incus joint Z_{jim}. The two model calculations are for a ear canal length l_{ec} of 0.3 *cm* and 0.0 *cm*.

Impedance of Fig. 4.7 after transforming to the reflectance domain is shown in Fig. 4.8 . Since the impedance is p.r. the magnitude of the reflectance $R_{ec}(\omega)$ must be less than one. Below 300 Hz $\Re e[Z_{ec}^{ii}]$ is less one due to low-frequency measurement noise, thus $|R_{ec}^{ii}|$ is greater than one for those frequencies.

The magnitude of the reflectance $|R_{ec}^{ii}|$ is between 0.9-0.95 in the 300 Hz to 7 kHz frequency region. Starting at 7 kHz $|R_{ec}^{ii}|$ starts to decrease, reaching a minimum of about 0.25 near 10 kHz. Above 10 kHz $|R_{ec}^{ii}|$ starts to increase. At the frequency where $|R_{ec}^{ii}|$ is a minimum the phase of R_{ec}^{ii} goes through a nonmonotonic transition.

Stiffness K_{jim} and mass M_i form a resonant circuit with resonance frequency at f_b. This resonance is what causes the minimum in $|R_{ec}^{ii}|$ and the "bump" in phase of R_{ec}^{ii}. Thus the minimum in reflectance is due to slippage between the incudo-malleolar joint. The parameters for Z_{jim} and M_i were adjusted until model results and data were in good agreement in the reflectance domain. These parameters are found in the first part of Table 4.1. For the parameters chosen, f_b is approximately 8.4 kHz. In the model f_b is approximately 10 kHz. Because stiffness and mass of Z_{dc} contribute to the effective values for K_{jim} and M_i, f_b is higher than predicted. The minimum value of $|R_{ec}^{ii}|$, at f_b, is a function of R_{jim}. Thus it appears that it is possible to measure the effect of the incudo-malleolar joint, for the interrupted incus case, from impedance measurements at the eardrum.

For frequencies above about 10 kHz, the magnitude of the reflectance R_{ec}^{ii} for the model and data are in good agreement, while the phase of the model reflectance is higher than of the data by as much as $\frac{3}{4}\pi$. The real part of earcanal impedance $\Re e[Z_{ec}^{ii}]$ for the model and data are in good agreement for all frequencies shown. However the phase and the magnitude of Z_{ec}^{ii} are not in good agreement for frequencies above about 12 kHz. This points out the inadequacies of the model

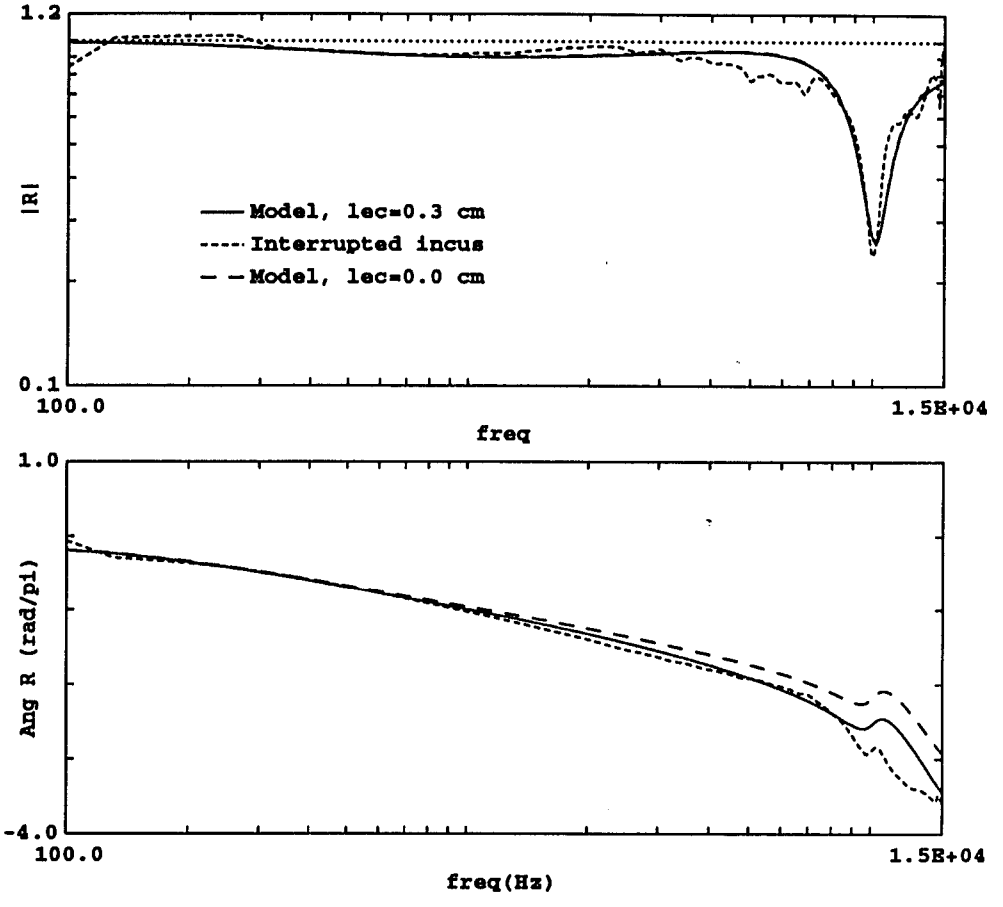

Figure 4.8: *Reflectance (R_{ec}^{ii}) corresponding to the "interrupted incus" impedance:* The non-monotonic behavior in the 8-12 kHz frequency region of the impedance domain is shown here to have a pronounced effect on the magnitude of the reflectance. The phase clearly indicates that the primary effect of ear canal length is to add delay.

in being able to characterize the imaginary part of the "interrupted incus" earcanal impedance Z_{ec}^{dc} for frequencies above 10 kHz. It for this reason that we have limited our model results to frequencies below 15 kHz. The behavior of the earcanal impedance and reflectance is dominated by the uncoupled portion of the eardrum impedance Z_{du} for frequencies above approximately 5 kHz. Thus a change in the transformer ratio in a frequency dependent manner is not likely to fix the problem.

One possibility for the error in $\Im m[Z_{ec}^{ii}]$ is that the parameters need to be further modified. A more likely alternative is that the $Z_{du} = R_{du} + j\omega M_{du} + K_{du}/j\omega$ is an inadequate model for the uncoupled portion of the eardrum impedance. Experimental evidence, for stimulus frequencies above 3-4 kHz and SPL's above 90 dB (Khanna and Tonndorf, 1972), suggest that the eardrum vibrations are complicated. In order to characterize the complicated motions of the eardrum a more complete characterization for Z_{du} is needed. It is possible, and even likely, that for frequencies above 10 kHz, Z_{du} cannot be modeled by a lumped parameter description (Rabbitt and Holmes, 1988; Rabbitt, 1990).

One way to isolated the uncoupled eardrum impedance is to make eardrum impedance measurements, for frequencies as high as 20-30 kHz, with zero velocity through the coupled portion of the eardrum (see Fig. 4.6). This is referred to as the "blocked malleus" condition. The malleus can be blocked by "gluing" it to the walls of the middle ear cavity. To our knowledge measurements as such are not available in the literature. Thus it is not possible to model the eardrum impedance at the highest frequencies without further measurements.

4.3.4 Effect of the space between transducer and eardrum

Two different model calculations for Z_{ec}^{ii} are shown in Fig. 4.7 . The curve with $l_{ec} = 0$ cm corresponds to the impedance of the eardrum without any influence due to cavities (open circuited)

Table 4.1: *Estimated parameters for Z_{doc}:* In each case the impedance is the sum of the impedance due to each element, i.e.: $Z = R + K/j\omega + j\omega M$. The effective transformer ratio T_r is needed to transform Z_{al}, Z_s, and Z_{rw} to the eardrum side.

Description	Function	R ($dyn - sec/cm^5$)	K (dyn/cm^5)	M (g/cm^4)
Uncoupled TM	Z_{du}	45	8×10^7	0.0085
Coupled TM	Z_{dc}	20	9×10^5	0.013
Incus	Z_i	0	0	0.0054
Incudo-malleolar joint	Z_{jim}	60	1.5×10^7	0
Annular Ligament	Z_{al}	1.1×10^5	5.5×10^9	0
Stapes	Z_s	0	0	3.3
Round window	Z_{rw}	0	1.2×10^8	0
Incudo-stapedial joint	Z_{jis}	∞	∞	∞
Transformer ratio	$T_r = 76$	(*dimensionless*)		

Z_{doc}. The curve with $l_{ec} = 0.3\ cm$ corresponds to our model estimate of Z_{ec}^{ii} (Z_{doc} with the earcanal cavity). The effect of the earcanal tube is a translation in impedance to lower frequencies.

The group delay is

$$\tau_{gd} = -\frac{\partial \phi(\omega)}{\partial \omega}, \tag{4.7}$$

where $\phi(\omega)$ is the phase of the reflectance. Figure 4.8 shows that the effect of the space between the transducer and the eardrum is to increase the slope of the phase of R_{ec}^{ii}. In the above equation, an increase in the slope of the phase corresponds to an increase in the group delay. Although not shown here, the group delay for R_{ec}^{ii} was computed for the cases $l_{ec} = 0\ cm$ and $l_{ec} = 0.3\ cm$. As expected, the case with $l_{ec} = 0.3\ cm$ was found to have a larger group delay than the case with $l_{ec} = 0\ cm$. The magnitude of the reflectance for the two cases is virtually indistinguishable. Thus when viewed in the reflectance domain, it is clear that the effect of the space between the

transducer assembly and the tympanic membrane is to add delay to the reflected wave.

4.4 Drained cochlea

In the "drained cochlea" case the cochlea is attached to the stapes, as in the normal case, but with perilymph removed from the scala vestibule and scala tympani. Thus, the difference between the "interrupted incus" measurement condition and that of the "drained cochlea" is that in the later the incus is no longer acoustically short circuited to ground. In the drained cochlea case the load to the incus is the input impedance of the drained cochlea Z_c^{dc}, the impedance of the annular ligament $Z_{al} = R_{al} + K_{al}/j\omega$, and the impedance of the stapes $Z_s = j\omega M_s$.

With the perilymph drained, the characteristic impedance [see Eq. (2.6a)] of the cochlea at the stapes is

$$Z_{co}^{dc} = \sqrt{\frac{4\rho_a K_0'}{S_0}}. \tag{4.8}$$

That viscous and thermal effects are insignificant when the cochlea is air-filled has been assumed in Eq. (4.8). Using $\rho_a = 1.18 \times 10^{-3}\ g/cm^3$ for the density of air, $K_0' = 1.7 \times 10^9\ dyn/cm^4$ for the BM stiffness at the base, and $S_0 = 0.02\ cm^2$ for the area at the base of the cochlea we obtain $Z_{co}^{dc} \approx 2 \times 10^4\ dyn - sec/cm^5$. For comparison, the cochlear input impedance Z_c^{dc} was computed for the drained cochlea case using thermodynamic constants of air for the chain-matrix method developed in Chapter 2. Magnitude and phase of Z_c^{dc} were found to be frequency dependent. The drained cochlea input impedance Z_c^{dc} is mass dominated for frequencies below approximately 1 kHz at which point it reaches a maximum magnitude of approximately 1.8×10^4. Above 1 kHz Z_c^{dc} oscillates and goes in and out of the mass and stiffness dominated regions.

Lynch *et al.*'s (1982) experimental averaged value for R_{al} is 2×10^5; an order of magnitude greater than Z_{co}^{dc}. Thus the impedance of the air filled cochlea does not represent much of a load

to the stapes in the drained cochlea case. We shall use 2.7×10^9 and 3.3 for K_{al} and M_s (Lynch *et al.*, 1982) as initial values.

4.4.1 The transformer ratio

Measurements made by Lynch *et al.* were made on the stapes side. In order to see the effect of Z_c, Z_s, and Z_{al} on the eardrum side, the transformer ratio T_r must be evaluated. Impedances are transformed to the eardrum side by dividing by T_r^2; for example $Z_c' = Z_c/T_r^2$.

There are several factors that contribute to the transformer ratio. These include the ratio of the areas of the tympanic membrane to the oval window, the lever ratio due to the malleus and incus, and buckling due to the conical shape of the tympanic membrane. All of these factors depend on the particular anatomy. Thus it is species dependent, animal dependent, and it may also depend on the physiological state of the animal. It is perhaps for these reasons there is not general agreement on what the transformer ratio should be (Pickles, 1988, pp 15-23).

Using holographic techniques Khanna and Tonndorf (1972) have reported displacement patterns of the eardrum surface. All their measurements were for levels above 90 dB SPL. For a stimulus frequency of 600 Hz, and levels as high as 115 dB SPL, the eardrum seems to move without multimoding. But for frequencies above 3-4 kHz their measurements show that the eardrum motion "breaks up", suggesting that the eardrum multimodes. Khanna and Tonndorf, however, did not report the SPL used corresponding to each stimulus frequency. If at the higher frequencies the multimoding of the TM were due to level dependent effects, then the observations would seem to indicate non-linear phenomena. The effect of multimoding, whatever its cause, on the transformer ratio is unclear. Presently we assume that the transformer ratio T_r as it pertains to impedances of the cochlea, stapes, and annular ligament is independent of frequency.

4.4.2 Comparison with data

Allen's impedance measurements were made on the eardrum side and consequently it is only possible to estimate parameters for $Z_s = M_s$ and $Z_{al} = R_{al} + K_{al}/j\omega$ when they have been converted to the eardrum side by the transformer ratio T_r. Since none of the four parameters are known for this particular cat, they were adjusted simultaneously to obtain a fit to the data. It is important to explicitly evaluate T_r in order to calculate Z_c' from Z_c for the "intact" cochlea case of section 4.5.3. Final parameter values used to compute the model are listed in Table 4.1. Model results and measured data for Z_{ec}^{dc} are shown in Fig. 4.9 .

For frequencies below approximately 2 kHz Z_{ec}^{dc} is dominated by the stiffness of the K_{al}. The annular ligament resistance R_{al} was chosen to match $\Re e[Z_{ec}^{dc}]$ for frequencies below 2 kHz. Above about 4-5 kHz Z_{ec}^{dc} and Z_{ec}^{ii} are approximately the same.

The impedance Z_{ec}^{dc} transformed to the reflectance domain is shown in Fig. 4.10 . In the frequency region between 300 Hz and 7 kHz, magnitude of R_{ec}^{dc} has gone from a minimum of approximately 0.9 in the interrupted incus case to a minimum of approximately 0.8 for this case. This decrease in reflectance is due to an increase in $\Re e[Z_{ec}]$. A large portion of this in the model is due to R_{al}. *Thus there is a decrease in reflectance is due to dissipation of energy in the annular ligament.*

Near 10 kHz, model $\Re e[Z_{ec}^{dc}]$ is higher than the data by approximately a factor of two; other than this, agreement between model and data $\Re e[Z_{ec}^{dc}]$ is fairly good. For frequencies above approximately 10 kHz, agreement between model and data phase for Z_{ec}^{dc} is poor. This manifests itself as an error in the phase of R_{ec}^{dc} by as much as $\frac{2}{3}\pi$ and a slight error (less than 3 dB) in the magnitude of R_{ec}^{dc} for frequencies above 10 kHz. As pointed out in the previous section, these model errors are due to inadequacies of the uncoupled portion of the eardrum Z_{du}.

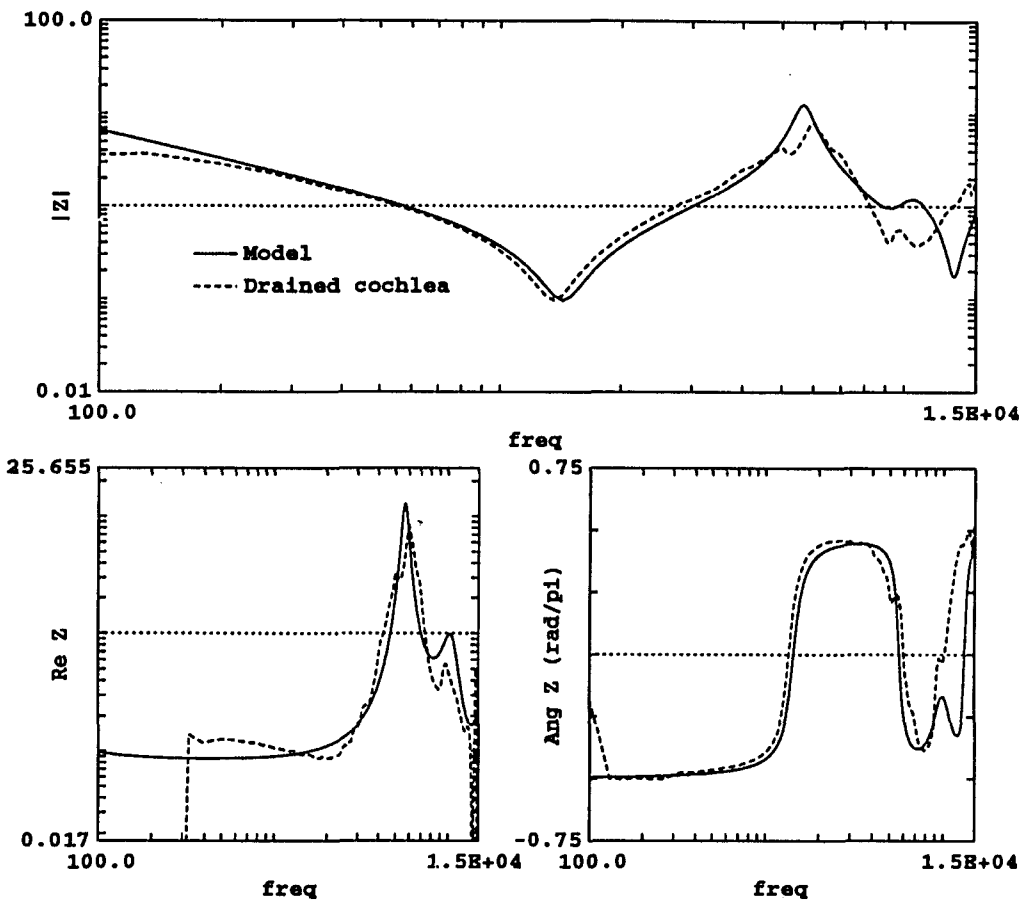

Figure 4.9: *Earcanal impedance for the "drained cochlea" case:* For frequencies below approximately 2 kHz Z_{ec}^{dc} is dominated by the impedances of the annular ligament and the stapes. Above 4-5 kHz the measured impedance is approximately the same as Z_{ec}^{ii}.

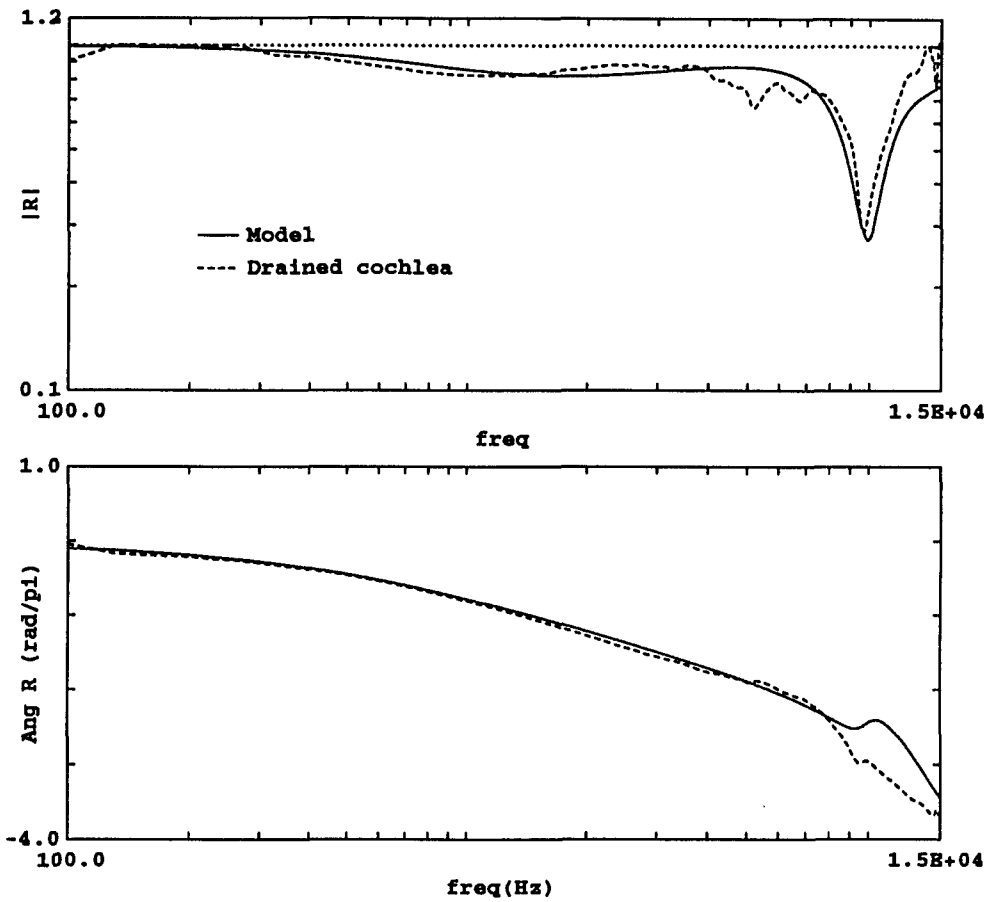

Figure 4.10: *Reflectance for the "drained cochlea" case:* In comparison to the "interrupted incus" case, the addition of the annular ligament resulted in a decrease in reflectance magnitude to a minimum of approximately 0.8 for frequencies between 300 Hz and 7 kHz and an increase in phase for frequencies between 300 Hz and 4 kHz.

4.5 Intact ossicles and cochlea

In the "intact" case, the ossicles and the cochlea are unaltered from their normal operation. In this case, the load to the stapes is the impedance of the fluid filled cochlea $Z_c(\omega)$. Properties of Z_c were extensively studied in Chapters 2 and 3. We have used the result of cat Z_c from Fig. 3.16 having a realistic scala area $S_m(x)$ and including viscous perilymph. It was transformed to the eardrum side by $Z_c' = Z_c/T_r^2$. All other parameters were from the drained cochlea case.

4.5.1 Mass of the vestibule

Note that in our middle ear model the mass of the vestibule M_v is not present. Lynch *et al.*'s (1982, p 126) model included M_v. They attributed M_v to nonuniform velocity distribution of the fluid near the entrance of the cochlea. Their estimate of M_v is more than an order of magnitude greater than M_s. Zwislocki's (1962, p 1520) M_v is attributed to the mass of perilymph between the oval window and the point at which the basilar membrane begins. Our own model computations of the cochlear input impedance in section 3.9 for frequencies up to 70 kHz resulted in a mass like behavior for frequencies above f_{max} of the cochlear map (57 kHz for the cat). But below f_{max} no mass like behavior was observed. Consequently we have not included M_v in our model and do not feel that this mass is experimentally justified.

4.5.2 Comparison with data

The model and measured eardrum impedance for the "intact" case Z_{ec}^i are compared in Fig. 4.11 . In comparison with Fig. 4.9 *it is clear that the effect of the cochlear input impedance on impedance measured at the eardrum is quite significant.*

The transformation from impedance of Fig. 4.11 to reflectance is shown in Fig. 4.12 . When this figure is compared with Fig. 4.10 it is evident that without the fluid filled cochlea, most of the

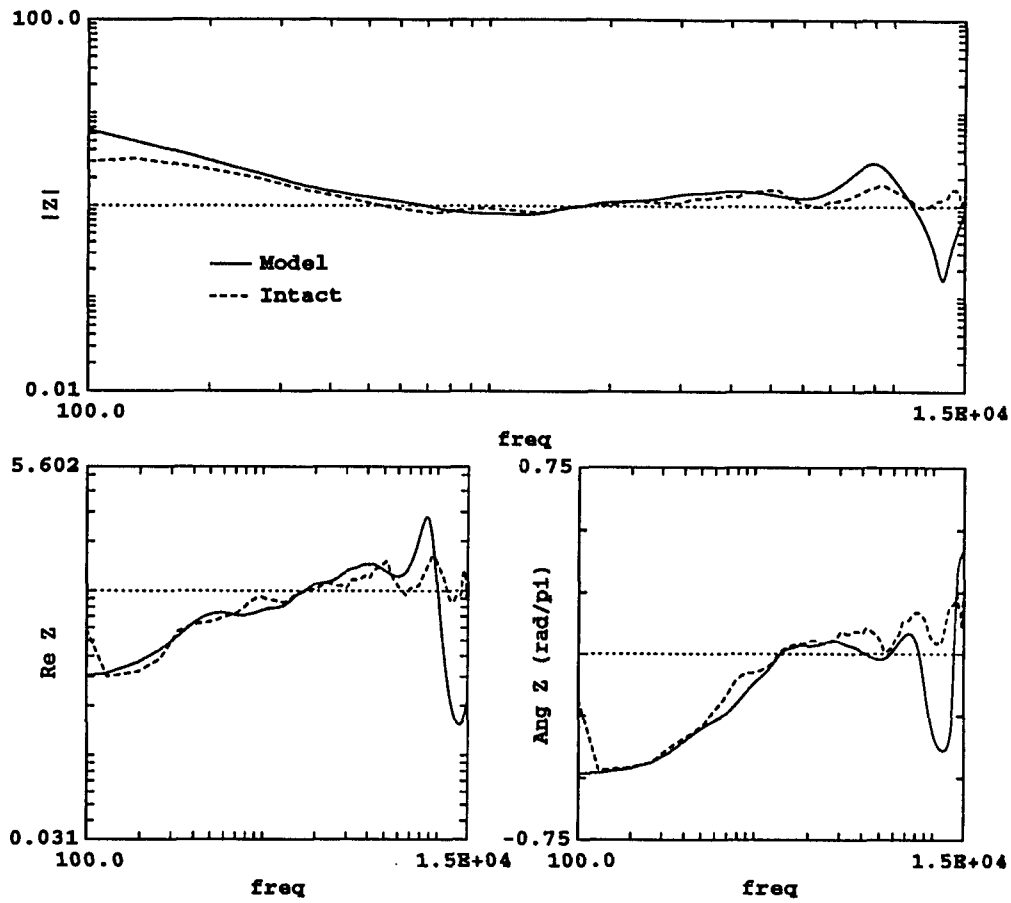

Figure 4.11: *Earcanal impedance with "intact" ossicles and cochlea:* In the intact case the impedance of the cochlea is added to that of the drained cochlea case. Cochlear input impedance for the cat was calculated with a realistic scalae cross-sectional area and viscous perilymph (see text). For frequencies between 400 Hz and 10 kHz, the normalized impedance magnitude is seen to fluctuate around the characteristic impedance of the transducer tube in both the model and data. For frequencies between 100 Hz and 10 kHz, the real part of the eardrum impedance changes by about a factor of 5 (14 dB).

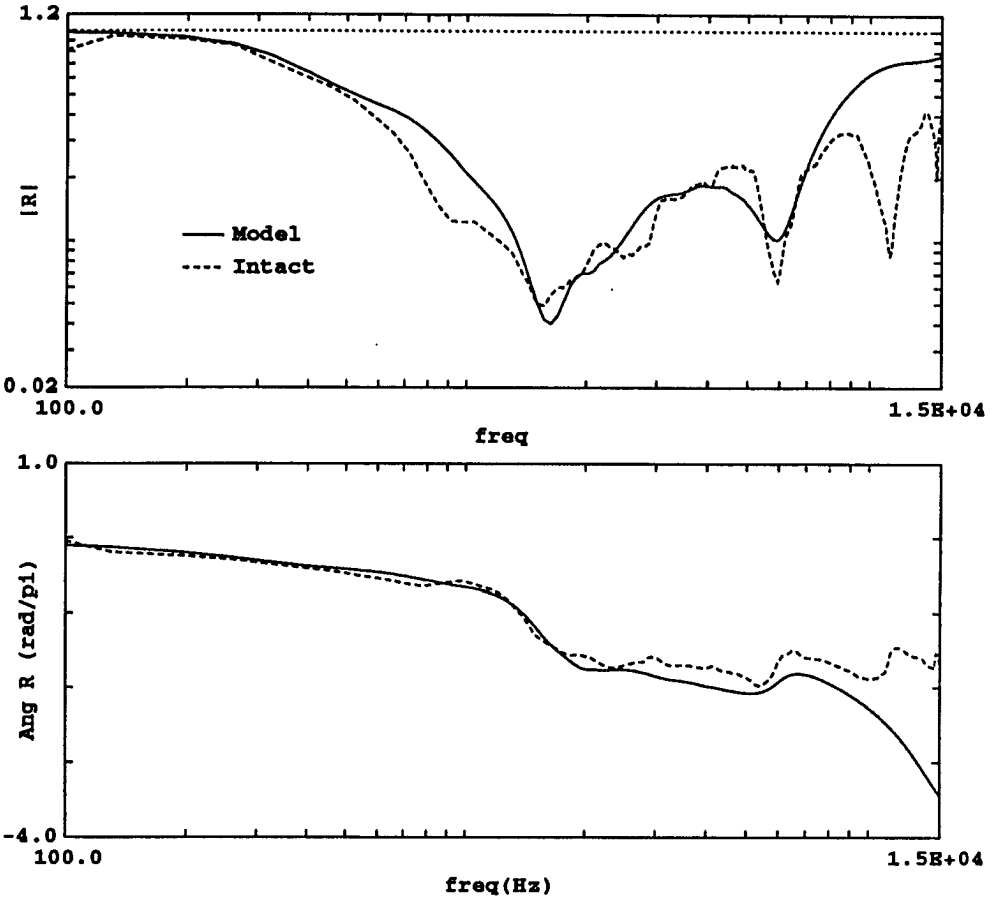

Figure 4.12: *Earcanal reflectance with "intact" ossicles and cochlea:* With the an intact cochlea the reflectance magnitude decreases by almost 30 dB in the 1.6 kHz frequency region. This decrease in reflectance magnitude is due to the impedance of the cochlea. The data and model deviate for frequencies above approximately 10 kHz. (Note the change in magnitude scale from previous figures).

energy in the earcanal is reflected at the eardrum. *When the load to the stapes is a normal cochlea, a much larger portion of the incident sound (20% vs. 97% at 1.6 kHz) is transmitted through the middle ear and into the cochlea.* A more extensive discussion of the effect of the cochlear input impedance is found in the next section.

All three ear canal impedance measurements indicate that for frequencies above 10 kHz our middle ear model no longer works. At this point it is not clear why this is so. Some possible explanations are: (1) An insufficient number of degrees of freedom in model of Z_{du}, (2) Evanescent higher-order modes near the measurement plane, or (3) Measurement and/or calibration errors. We will restrict all subsequent calculations to frequencies below 10 kHz.

4.5.3 Effect of cochlear input impedance on earcanal measurements

In calculating the earcanal impedance (and reflectance) we used the cochlear input impedance as calculated by the chain-matrix method of Chapters 2 and 3. In this section the effect of different assumptions for the cochlear input impedance on model calculations of the earcanal impedance and reflectance is further analyzed. Three different models for Z_c will be investigated: the chain-matrix calculations of Chapter 3, Lynch *et al.*'s (1982) experimentally based model, and Allen's (1979) theoretical model for Z_c. These three models decrease in level of complexity and assumptions.

The difference between Lynch *et al.*'s and Allen's WKB model for Z_c is that in the former there is a resistor R_0 in series with the mass component M_0. This resistor has a significant effect on the magnitude of Z_c for frequencies below 500 Hz, but affects the phase of Z_c over a much wider range of frequencies (see Fig. 3.4). In Lynch *et al.*'s model, the real part of Z_c starts to become dominant for frequencies above approximately 500 Hz, whereas in the WKB model, the real part of Z_c starts to become dominant for frequencies above approximately 5 kHz. Allen's

WKB model for Z_c was formulated for a zero viscosity, constant scalae area cochlear model, and it is representative of Z_c for most constant scalae area cochlear models.

Model calculations of Z_c for the tapered case are somewhat more complicated (see Fig. 3.16). In this Chapter when we refer to the tapered case we mean that the cross sectional area, used to calculate Z_c, is one that corresponds most closely to the cat anatomy (see S_m of Fig. 3.10). Magnitude of Z_c for the tapered case increases from a value of approximately 0.5 $M\Omega$ at 10 Hz to a value of approximately 3 $M\Omega$ at 500 Hz. Above 500 Hz the magnitude at first decreases and then it increases. The corresponding phase increases from approximately 0° at 10 Hz to approximately $\pi/4$ near 300 Hz. Above 300 Hz, the phase at first decreases and then it is nonmonotonic. The phase of Z_c above 1 kHz fluctuates and on the average it is approximately $\pi/8$.

Three model calculations for the earcanal impedance for the "intact" case (Z^i_{ec}) are shown in Fig. 4.13 . The curve corresponding to the tapered area calculations for Z_c is our best model fit to the "intact" case from Fig. 4.11 . From Fig. 4.13 it is clear that with the WKB model for the cochlear input impedance the real part of Z^i_{ec} is in error from the measured data by as much as 13-14 dB for frequencies below 1 kHz. This is consistent with the fact that the WKB model for Z_c and measured Z_c are in error by approximately the same amount. With a WKB model for Z_c, errors as big as approximately 15 dB exist in measured magnitude and model magnitude of Z^i_{ec} for frequencies above 1 kHz. The corresponding phase is in error by as much as $\frac{3}{8}\pi$. These errors in impedance translate to much larger errors in the reflectance domain.

The reflectance domain calculations for the "intact" case R^i_{ec} are shown are shown in Fig. 4.14 . With the WKB model for Z_c the maximum error in magnitude of R^i_{ec} is approximately 24 dB near 1.5 kHz. There is also a zero in R^i_{ec} with the WKB Z_c between 6-7 kHz. This zero due to cancellation of imaginary components in Z_c and the middle ear impedance.

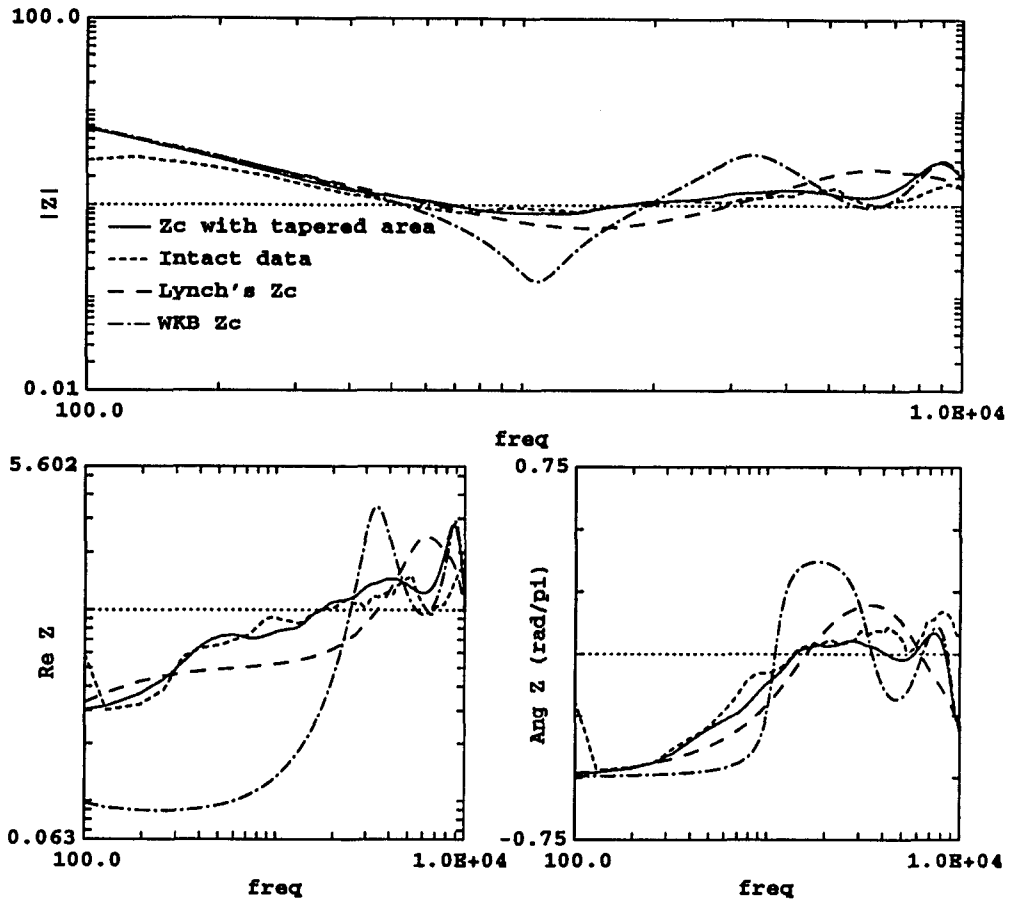

Figure 4.13: *Effect of the cochlear load Z_c on earcanal impedance:* The eardrum impedance is computed using three different models for the cochlear input impedance $Z_c(\omega)$. The tapered area calculations were made with the chain-matrix cochlear model that takes into account the scalae cross-sectional area variations and visco-thermal losses. In contrast to the chain-matrix model, the WKB model for Z_c (Allen, 1979) was based on the assumptions of no viscosity and constant cross-sectional area. The WKB model is representative of Z_c for cochlear models with constant cross-sectional area. *This figure shows that tapering and viscosity of the cochlea have an important effect on the impedance measured at the eardrum.* Lynch's (1982) model for Z_c, based on averaged measurements, is in closer agreement with our model calculations than the WKB solution. Some differences exist due to averaging of data. These differences are seen to be more pronounced in the reflectance domain.

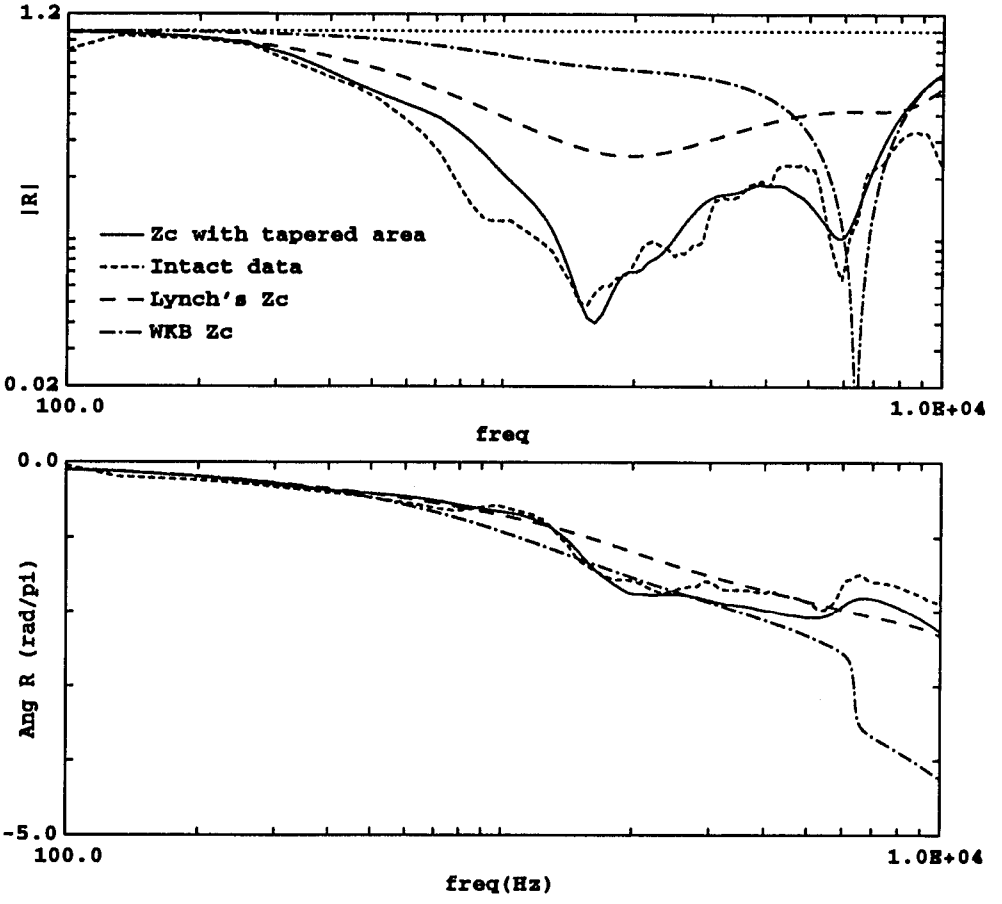

Figure 4.14: *Effect of the cochlear load Z_c on earcanal reflectance:* When a tapered cochlear model is used then the calculated reflectance magnitude is seen to be significantly less than when a constant cross sectional area cochlear model (WKB Z_c) is used. The calculated reflectance with Lynch's model for Z_c lies between the other model results shown. The fine structure in the reflectance magnitude is due, in part, to the fine structure of the cochlear input impedance.

When Lynch *et al.*'s model for Z_c is used, deviations in impedance and reflectance are somewhat reduced, but still quite large. The error in impedance magnitude and real part of the impedance is less than 6 dB. The error in phase is less than $\frac{1}{8}\pi$. The corresponding maximum error in magnitude of R^i_{ec} is approximately 15 dB near 1.5 kHz.

The calculation with tapered Z_c is able to model the fluctuations present in the measured impedance and reflectance. For example, near 1.5 kHz the slope of the phase of the "intact" reflectance R^i_{ec} increases in both the model and the data. Above 6 kHz the slope of the phase of R^i_{ec} goes from being negative at first to positive and then negative again. Neither the WKB model nor Lynch *et al.*'s model for Z_c is able to replicate the fine structure of the reflectance magnitude and phase. Recall that the middle ear model for the three cases is exactly the same. Thus, we conclude that *the fine structure observed in earcanal reflectance, with the intact cochlea and middle ear, is due, in part, to the fine structure of the cochlear input impedance.*

4.6 The effect of the cochlea on the motion of the stapes

Parameters for the ossicular path of the middle ear were based on "surgically modified" as well as "intact" eardrum impedance measurements. In order to verify that this method of estimating the parameters leads to reasonable middle ear parameters, calculations of measurable quantities, other than eardrum impedances, should agree with those measurements without any modifications to the estimated parameters.

An important measurement is the stapes displacement for a given earcanal sound pressure. This measurement is not available for the specific cat studied thus far. However, the earcanal pressure to stapes displacement transfer function has been measured for frequencies up to 10 kHz in other laboratories (Guinan and Peake, 1967; Tonndorf and Khanna, 1967). We shall use the

data of Guinan and Peake (1967) to compare our calculated results.

Figure 4.15 shows the stapes displacement per unit earcanal pressure as measured by Guinan and Peake (1967) on four cats. Also shown is the stapes transfer function calculated from the middle ear model. To analyze the effect of the cochlear input impedance, the stapes transfer function is calculated using three different cochlear models: (1) model for Z_c of chapter 3 that explicitly takes into account scalae area variations and perilymph viscosity, (2) Lynch *et al.*'s model for Z_c based on measured data, and (3) Allen's (1979) theoretical model for Z_c based on the WKB approximation of a constant scalae cross sectional area cochlear model with inviscid perilymph. Note that as in Fig. 4.13 the middle ear model did not change, only the model used to represent Z_c has changed.

All three model results are approximately the same for frequencies below about 300 Hz. Near 1 kHz there is a resonance in the stapes displacement for the model computation with the WKB $Z_c(\omega)$. When the chain-matrix model or the Lynch *et al.* model for $Z_c(\omega)$ is used, the resonance is no longer observed. The phase of the stapes motion, corresponding to the WKB model for Z_c, changes rapidly whereas for the other Z_c models and in the measured data the decrease in phase is gradual. The tapered cochlea model presents a much higher resistive load to the middle ear than the WKB model does; as the result the resonance with the tapered cochlea model is damped out to a much greater degree than the WKB cochlear load.

In comparison to the data all three model computations show a larger stapes displacement by a factor of about 1.6 (4.1 dB). Since the error is for frequencies below 800 Hz, one can expect that the parameters of the elements that dominate in this frequency region need to be modified. The elements that dominate in this frequency region are K_{dc} and K_{al}. Adjustment of these parameters could result in a better agreement with the measured ear canal to stapes transfer function. But if

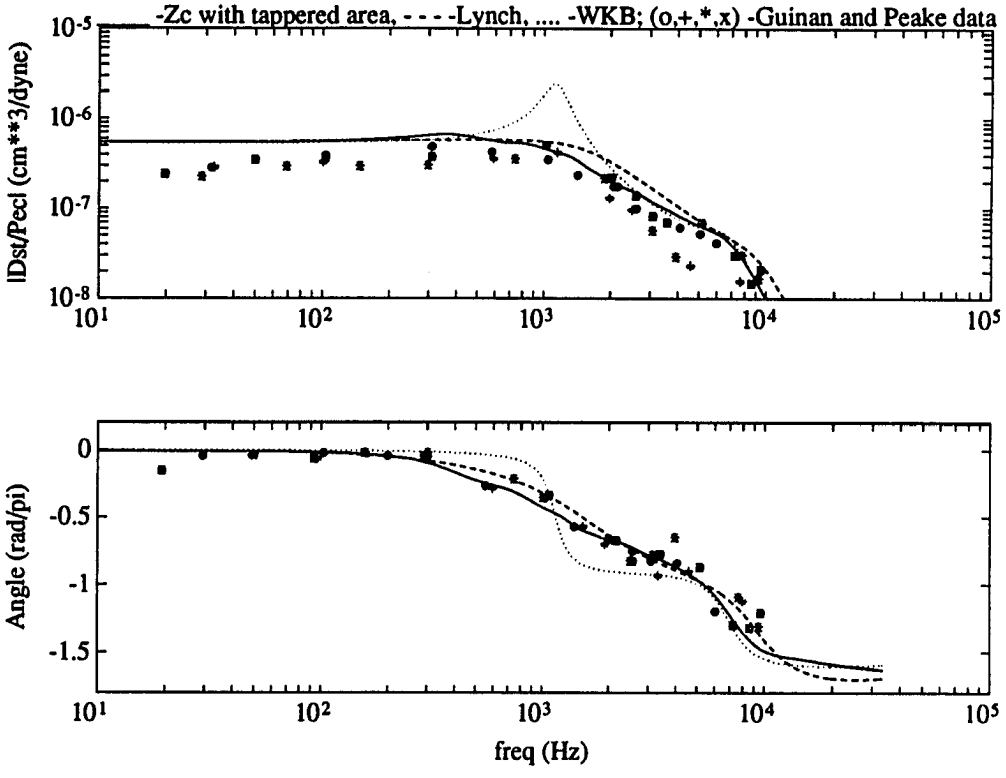

Figure 4.15: *The stapes displacement for different Z_c model assumptions:* The top figure shows the stapes displacement per unit of SPL at the eardrum. The bottom figure shows the phase of the stapes displacement relative to the pressure at the eardrum. The three different models for Z_c used to compute the eardrum impedance for Fig. 4.13 were also used to compute the stapes transfer function. The measured data are from Guinan and Peake (1967).

adjustments were to be made to K_{dc} or K_{al} then the match to the eardrum impedance would not be as good. Recall that the model parameters were not explicitly adjusted to fit this data. Since an estimate of the measurement error was not reported by Guinan and Peake we do not know at this point know which is in error.

4.7 The middle ear cavities

The assumption up to now has been that the space in the back of the eardrum is fully vented to the atmosphere. Thus $Z_{mec}(\omega)$, the impedance of the middle ear cavities, was short circuited to acoustic ground. In the normal condition there are a set of cavities behind the eardrum called the middle ear cavities (MEC). Experimental observations on cat (Moller, 1965; Lynch, 1981; Tonndorf and Pastaci, 1986), rabbit (Moller, 1965), guinea pig (Zwislocki, 1963) and other animals, indicate that these cavities have an important effect on the impedance measured at the eardrum. By making modifications to the middle ear cavities, systematic changes in the middle ear transmission have been observed in cat (Moller, 1965; Guinan and Peake, 1967; Tonndorf and Pastaci, 1986), chinchilla (Ruggero *et al.*, 1990), as well as other animals. Thus a middle ear model, without the middle ear cavities, would be an incomplete one.

Despite these experimental observations, it is not clear what role the middle ear cavities play in auditory performance. Anatomical observations indicate that there are considerable differences in sizes and shapes of the MEC in various species. Consider the following two experimental observations. *First*, impedance measurements at the eardrum of many different animals indicates that there is a high Q (=center frequency/bandwidth) resonance due to the MEC. It has been observed that the high Q resonance in impedance is accompanied by a comparable decrease in both the stapes motion (Guinan and Peake, 1967) and the cochlear microphonic (Dallos, 1973, p. 1191

Second, the pressure transfer function measured from free-field to the cat tympanic membrane indicates that there is a pressure gain of approximately 15-20 dB near 3.5-4 kHz (Wiener *et al.*, 1966). It can be argued that the auditory threshold, when measured with respect to the pressure at the eardrum, is increased due to the bulla resonance. However, when the auditory threshold is measured with respect to the free-field pressure then the auditory threshold remains relatively "flat" in the frequency region of the bulla resonance. Putting these two experimental observations together one might conclude that the effect of the earcanal pressure gain is compromised by the increase in impedance due to the MEC (Dallos, 1973, pp 117-126). This line of reasoning relies on the observation that there is no increase in the auditory threshold that is comparable to the resonance observed in the impedance.

A closer inspection of the auditory threshold data shows that it is sampled but at a few frequency points. Owing to the sharp resonance in the impedance, if a threshold measurement is not made at the frequency at which resonance occurs, then the auditory threshold might appear somewhat "flat."

Another possible reason for the MEC might be that they compensate for certain aspects of middle ear anatomy that the eardrum and ossicles were not to able to adapt to. For example, in order to increase the stiffness measured at the eardrum either the stiffness of the eardrum can be increased, or a volume having a stiffness greater than that of eardrum can be placed behind the eardrum. Thus without the middle ear cavities, either the auditory threshold of a given species would be somewhat different, particularly at frequencies below approximately 4-5 kHz, or the middle ear anatomy would have evolved to be somewhat different than what it is.

One of the aims of this section is to formulate a model for the MEC based on the dimensions of those cavities. One motivation for this is to show that signal processing performed on acoustic

signals by the middle ear cavities, in the cat auditory pathway, depends mostly on the particular geometry of the MEC and the interconnection between those cavities.

4.7.1 A physically based model for the middle ear cavities

In the cat, the tympanic membrane is part of the lateral wall of the tympanic cavity. The middle ear ossicles and the cochlea are contained within the tympanic cavity. In the normal condition, the tympanic cavity is separated from the bulla cavity by a bony septum. A small oval shaped hole in the bony septum allows communication between the two cavities.

A model for representing cavities with variable cross-sectional areas will be developed in Chapter 5. This model is called the chain-matrix model for cavities. The validity of the chain-matrix model will be experimentally verified in that chapter of the thesis. In this chapter we will use that model to represent the middle ear cavities. In summary, our model represents a cavity having variable cross-sectional area, as a series of tubes each of constant diameter. Each of these tubes is represented as a ABCD chain-matrix. As in the cochlea model, the matrices include viscous and thermal boundary layer effects on the surface of the cavity walls. Our model explicitly takes into account two-dimensional effects due to sudden jumps in cross-sectional areas. This is done by including the so called "Karal correction" (Karal, 1953). Using this model, it will be show that dimensions of the MEC play an important role when studying acoustic properties of the MEC.

The shape of the cat bulla and tympanic cavities are complicated. The more accurately one can specify the dimensions of the cavities, the more accurate the model approximation. As a first order approximation we represent the bulla cavity as a cylindrical tube with length l_{bc} and diameter d_{bc}. The tympanic cavity is similarly represented with length l_{tc} and diameter d_{tc}. The bony septum, with the hole that forms the foramen, will be represented as an a tube of length l_f and diameter d_f.

In the past, middle ear cavities have been modeled by compliance representing the volumes

of the cavities (Zwislocki, 1962; Peake and Guinan, 1967; Moller, 1983; Shera and Zweig, 1989); lengths and diameter were not explicitly considered to be important. Also, losses in previous models were based on heuristic parameter fits to observed impedances. Since our model for the middle ear cavities includes visco-thermal boundary layer effects at the walls of the cavities, the losses arise in a natural manner in this model. A limitation of previous lumped-parameter representations for the MEC is that they are valid only in a limited frequency region of below 6-8 kHz (Lynch, 1981, pp 160-164). The chain-matrix formulation is a distributed-parameter representation and thus it can be expected to hold at frequencies above 8-10 kHz.

4.7.2 Estimating parameters for the middle ear cavities

Lynch (1981) found mean volumetric measurements on 12 cat bulla and tympanic cavities to be 0.217 cm^3 and 0.675 cm^3, with standard deviations of 0.056 and cm^3 and 0.141 cm^3. To our knowledge, more detailed geometrical data, such as the surface area of the cavities or the approximate lengths and diameters of each cavity, are not available in the literature. Consequently, we have chosen the lengths and diameters to match the poles and zeros of the measured impedances of the middle ear cavities. This will be done under the constraint of the measured volumes.

Based on pressure measurements in the MEC and at the eardrum, the impedance of the MEC for the "normal" condition as well as "surgically modified" conditions have been estimated (Lynch, 1981, Chap. II, Figs. 24-26). The particular cases studied were:

- Intact MEC – Z_{mec}
- Bulla cavity opened widely – Z_{bo}
- Plugged foramen – Z_{pf}.

We briefly summarize Lynch's results: Measurements of the intact middle ear cavity impedance

(Z_{mec}) indicates the presence of a high Q pole (resonance) near 4.5 kHz and a zero (anti-resonance) near 2.2 kHz. For frequencies below $\approx$ 2 kHz, Z_{mec} is compliance dominated. For frequencies above $\approx$ 5 kHz, Z_{mec} has some minor 'fluctuations' but is for the most part compliance dominated. When the bulla cavity is opened widely, and the foramen is left intact, then the zero disappears and the pole shifts to a lower frequency of approximately 3.5 kHz. For frequencies below $\approx$ 3 kHz, Z_{bo} is mass dominated. For frequencies above $\approx$ 4 kHz, Z_{bo} also has some minor 'fluctuations' in it but is largely compliance dominated. The Q of Z_{bo} appears to be slightly greater than that of Z_{mec}. When the foramen is closed-off, by sealing it with a plug, then the resonance in the measured impedance is no longer observed. For frequencies below $\approx$ 15 kHz Z_{pf} is compliance dominated.

There are three lengths (l_{tc}, l_f, l_{bc}) and three diameters (d_{tc}, d_f, d_{bc}) that need to be evaluated in order to calculate the impedance of our middle ear cavity model. In an attempt to uniquely identify the dimensions of the cavities, we have attempted to model the impedance for all three cases.

Since Z_{pf} is compliance dominated for most of the measured frequency region, we can only extract information regarding the volume of the tympanic cavity. We are not modeling any specific cavity impedances and thus we can let this be a free parameter (confined to Lynch's measured volumetric range for the tympanic cavity). This leaves us with Z_{bo} and Z_{mec} to model.

Recall that our model for the MEC consists of a cascade of three chain-matrices. By assuming an infinite impedance for the radiation load and multiplying out the three chain-matrices one obtains, after some algebraic manipulations, an analytic expression for the driving point impedance

$$Z_{mec}(\omega) = \frac{N(\omega)}{D(\omega)}, \qquad (4.9a)$$

where

$$N(\omega) = 1 + \frac{Z_{o2}}{Z_{o3}}\tanh(\gamma_2 l_2)\tanh(\gamma_3 l_3) + \frac{Z_{o2}}{Z_{o1}}\tanh(\gamma_1 l_1)\tanh(\gamma_2 l_2) + \frac{Z_{o1}}{Z_{o3}}\tanh(\gamma_1 l_1)\tanh(\gamma_3 l_3), \tag{4.9b}$$

and

$$D(\omega) = Z_{o1}[\frac{1}{Z_{o2}}\tanh(\gamma_1 l_1) + \frac{1}{Z_{o1}}\tanh(\gamma_3 l_3) + \frac{1}{Z_{o1}}\tanh(\gamma_1 l_1)\tanh(\gamma_2 l_2) + \frac{Z_{o2}}{Z_{o3}}\tanh(\gamma_1 l_1)\tanh(\gamma_2 l_2)\tanh(\gamma_3 l_3)]. \tag{4.9c}$$

In the above equation γ_i is the propagation constant and l_i is the length of the i^{th} tube. The characteristic impedance for each tube Z_{oi} is $\rho_a c_a / A_i$, where A_i is the area of the tube. The poles of Z_{mec} are at frequencies where the denominator of Eq. (4.9) is zero. The zeros of Z_{mec} are at frequencies where the numerator of Eq. (4.9) is zero. Due to the complex nature of the numerator and denominator of Eq. (4.9) it is difficult get an intuitive feel for how the zeros and poles of Z_{mec} are related to the dimensions of the cavities. Equation (4.9) for Z_{mec} is without the Karal correction. If Karal correction is included in the analytic solution then the equation becomes intractably complicated.

The anatomical difference between Z_{mec} and Z_{bo} is that there is a hole in the later case while that hole is replaced by bone when the MEC are intact. From a model point of view this translates into a radiation load of a hole for the open bulla case and impedance of bone for the intact middle ear cavity case. Thus an equation similar to that of Eq. (4.9) can be written for Z_{bo}. However, such an equation would be more complicated than that for Z_{mec}. Since an analytic expression for Z_{mec} did not give us much of an insight, we have not attempted to derive an analytic expression for Z_{bo}.

Note that the cavity dimensions do not change when the bulla has been opened. Thus modeling

Table 4.2: Estimated lengths, diameters, and volumes for the middle ear cavities.

	diameter (cm)	length (cm)	volume (cm^3)
Tympanic cavity	0.7	0.7	0.27
Foramen	0.2	0.075	2.3×10^{-3}
Bulla cavity	1.0	0.85	0.67

the two cases does not seem to help determine the dimensions of the cavities uniquely. However, by modeling both cases with a single set of cavity dimensions, one has greater confidence in the parameters obtained.

The cavity dimensions were adjusted until the model poles and zeros were within the experimentally observed poles and zeros of Z_{mec}. The parameters chosen are listed in Table 4.2. Results for the intact middle ear cavity case and two "surgical modifications" to the MEC are shown in Fig. 4.16 . Also shown in Fig. 4.16 is the intact middle ear cavity impedance Z_{mec} without the Karal correction. The impedances shown in Fig. 4.16 have been normalized to the characteristic impedance of the tympanic cavity ($\rho_a c_a / A_t \approx 106$, where A_{tc} is cross-sectional area of the tympanic cavity).

Also shown in Fig. 4.16 is the real part of the middle ear cavity impedance. In the model the viscous and thermal boundary layer effects on the surface of the middle ear cavity impedance give rise to the real part of the impedance. Measurements of the cat middle ear cavity surface area are not know. If such measurements were know, then they would help further constrain the parameters of the middle ear cavity model.

A few general statements, in the spirit of perturbation analysis, can be made at this point regarding the effect of the dimensions of the cavities on Z_{mec}. As expected, increasing either l_{bc} or l_{tc} will decrease the first zero frequency (f_z) and the first pole frequency (f_p) of Z_{mec}. Increasing

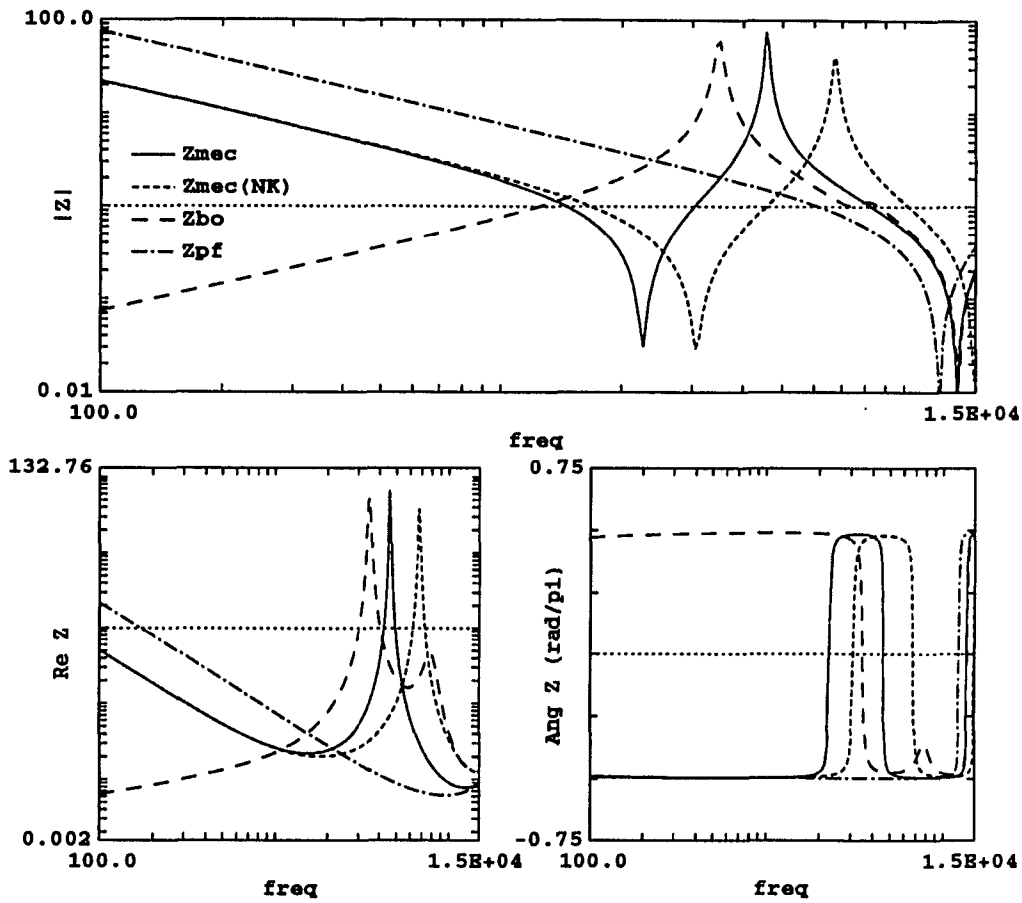

Figure 4.16: *Modeling the middle ear cavities that have been "surgically modified": Z_{mec}* is the impedance of the intact MEC; it was computed by including the effects of the non-planer wave propagation by using the Karal correction. Z_{mec} (NK) is also for the intact MEC but without the effect of the Karal correction. Z_{bo} is the impedance of the bulla open condition. Z_{pf} is the impedance of the plugged foramen condition.

l_{bc} shifts f_p more than it does f_z. Increasing d_{tc} increases f_z, but decreases f_p. Increasing d_{bc} decreases both f_z and f_p. In our parameter modifications we found f_z and f_p to be very sensitive to the foramen dimensions. Increasing the length l_f of the foramen resulted in a decrease in f_z and a larger shift in f_p. Increasing d_f increased both f_z and f_p. *Including the Karal correction in the model shifts both f_p and f_z to lower frequencies by almost half an octave.* Since the Karal correction is a function of the ratio of the areas, changing any of the diameters will have an effect on the Karal correction.

4.7.3 The foramen

We have observed that the foramen dimensions have an important effect on the impedance behind the eardrum. We presently investigate what possible role this curious structure might play in shaping the acoustic properties of the middle ear cavities.

Measurements of the foramen on five cats indicate $0.2\ cm < d_f < 0.3\ cm$, and $0.15\ cm < l_f < 0.2\ cm$ (Lynch, 1981, p. 165). Based on these measurements, Lynch modeled the foramen as a cylindrical tube with length $0.2\ cm$ and diameter $0.3\ cm$. Tonndorf and Pastaci (1986) hypothesized that the foramen is a tube "practically without depth". Our own model finding is that the foramen is approximately $0.075\ cm$ in depth (approximately the thickness of the average human thumbnail) is consistent with Tonndorf and Pastaci's hypothesis regarding the foramen.

In our model, the tympanic cavity, the foramen, and the bulla cavity are each represented as a chain-matrix. These matrices are formulated under the assumption of plane-wave propagation in cylindrical tubes. Table 4.2 shows that there is a decrease in diameter in going from the tympanic cavity to the foramen. There is also an increase in diameter in going from the foramen to the bulla cavity. The sudden changes in diameter (or equivalently in area) give rise to effects that are not modeled by theories of plane-wave propagation. As is experimentally shown in Chapter 5 the

two-dimensional effects can be modeled if one includes the so called Karal corrections to the plane wave theory.

Effects due to the Karal correction can most easily be illustrated in the reflectance domain. The impedance of Fig. 4.16 , when converted to the reflectance domain, is shown in Fig. 4.17 . There we have plotted the group delay [see Eq. (4.7)] of the reflectance instead of the phase. A wave launched at the input of a cavity will be reflected and will propagate back towards the transducer/microphone assembly when it encounters a change in impedance. The group delay is a measure of the round trip travel time of the reflected wave.

In the open bulla case, the magnitude of the reflectance is 0.95 below 6 kHz, at which point it starts to decrease, reaching a minimum of $\approx$ 0.62 near 8 kHz. The reflectance magnitude is $\approx$ 0.97 again for frequencies above 9.5 kHz. We used the impedance of an infinite baffle (Beranek, 1954, p. 124) for the radiation load at the end of the bulla cavity. The low value of the reflectance magnitude in the 8 kHz region is due to losses in the the real part of the radiation impedance. The magnitude of the reflectance is greater than about 0.95 for all other cases considered.

In the plugged foramen case, a reflectance occurs due to the end of a straight cylindrical tube. Thus the group delay shows a "flat" response. One can recover the acoustic length at a given frequency according to:

$$L_a(f) = \frac{\tau_{gd}(f)c_a}{2}. \tag{4.10}$$

Where $\tau_{gd}(f)$ is the group delay at frequency f. From Fig. 4.17 we estimate that τ_{gd} is 0.0403 ms for the plugged foramen case. The calculated acoustic length of 0.6997 cm is in close agreement to the physical length of 0.7 cm. The group delay, and thus the acoustic length, is frequency dependent for the other cases. It can be shown that the group delay is periodic in frequency. For high frequencies (between 10-15 kHz) the group delay for the other three cases approaches the

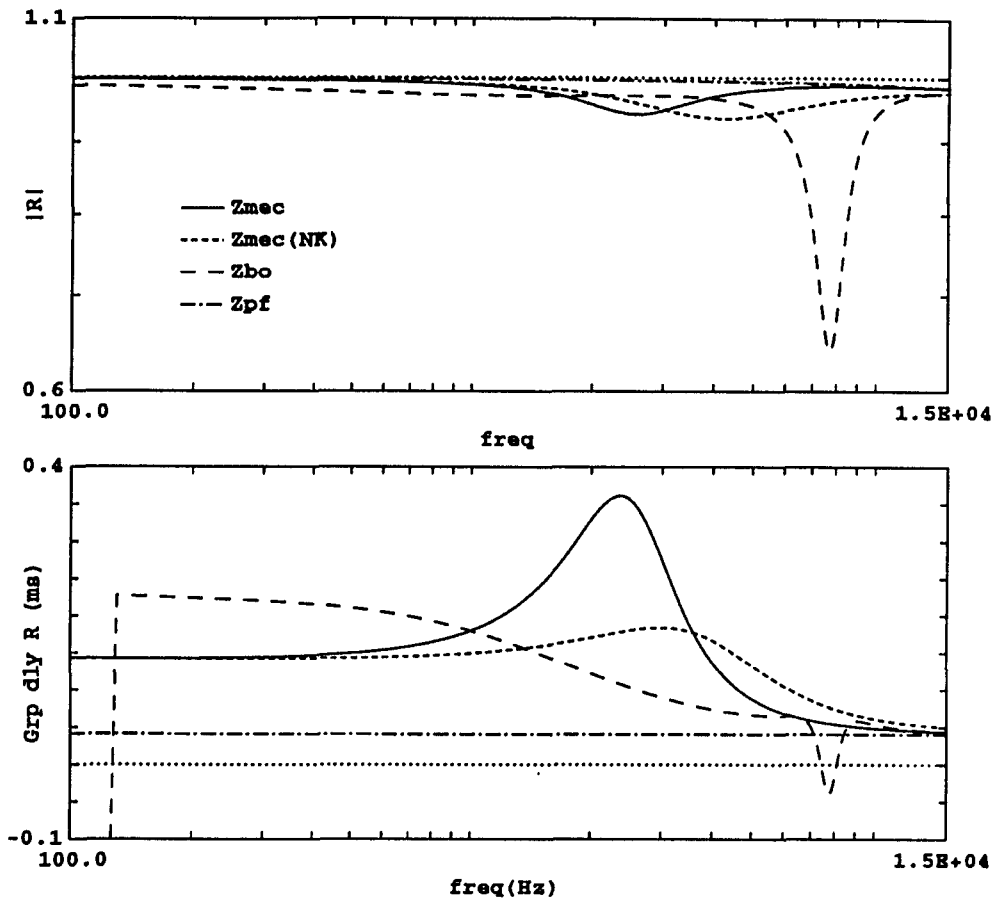

Figure 4.17: *Middle ear cavity reflectance:* Note that the group delay of the reflectance (in milli seconds) is shown in the lower panel. When the Karal correction is included in the calculations then the group delay increases, by as much as a factor of two, in the frequency region between 400 Hz to about 3.5 kHz. This indicates that the effect of the non-planar wave propagation is to increase the acoustic length of the MEC by as much as a factor of two. For frequencies below 1 kHz, the open bulla case has an acoustic length greater than when it is closed. For frequencies between 10-15 kHz the other cavities behave acoustically as if they were plugged at the foramen.

group delay of the plugged foramen case. This indicates that in this frequency region, the MEC behave as if they were plugged at the foramen.

The total physical length for the two cavities and the foramen is 1.625 cm. For the open bulla case τ_{gd} decreases from approximately 0.23 ms for low frequencies to less than 0.075 ms at frequencies above 5 kHz. This correspond to a decrease in the acoustic length from about 4 cm at low frequencies to less than 1.3 cm for frequencies above 5 kHz. At low frequencies, the acoustic length is greater than the physical length because the bulla cavity is open and thus sound is not reflected back towards the source at the end of the cavity. For frequencies above 7 kHz, the group delay starts to decrease rapidly and is approximately -0.045 ms at 7.8 kHz. Above this frequency the group delay increases, eventually becoming positive again. Measures of group delay are not always meaningful when the function being analyzed is not an all-pass function (Papoulis, 1962). Since the reflectance magnitude is significantly less than one in the frequency region between 6 kHz and 9.5 kHz, it is not an all-pass function in that frequency region and thus the negative group delay.

Also shown in Fig. 4.17 are model computations for Z_{mec} with the Karal correction and, for comparison, without the Karal correction. The group delay for the Karal correction case is greater than the case without Karal correction for frequencies above $\approx$ 400 Hz and below $\approx$ 3.5 kHz. Thus *the Karal correction increases the effective acoustic length of the cavities in that frequency region.* The maximum group delay for the no Karal correction case is approximately 0.18 ms, corresponding to an acoustic length of 3.123 cm, at about 3 kHz. The maximum group delay for the case with the Karal correction is $\approx$ 0.36 ms, corresponding to an acoustic length of 6.246 cm, at about 2.3 kHz. Thus, the Karal correction increases the acoustic length by a factor of two near 2.3 kHz. Above 3.5 kHz $\tau_{gd}(f)$ for the Karal correction case is slightly less than the case without

the Karal correction.

Having analyzed some of acoustical properties of the foramen we wish to address the question: Why is the bony septum in the cat middle ear cavity there? To answer this question we compute the cavity model for the case when bulla is closed but without the bony septum. This is compared to the case when the MEC is intact. Figure 4.18 shows these model computations in the impedance domain. Note that model computations are for frequencies up to 30 kHz. This was done to look at the effect of the septum at very high frequencies.

In making these model computations, the diameter of the foramen was changed from its previous value of 0.2 cm to 1.0 cm corresponding to the diameter of the bulla cavity (this simulates the scraping away of the bony septum). With the bony septum removed there are two resonant frequencies, one at about 10 kHz and another one at about 20 kHz. When a bony septum is introduced in the MEC then the 10 kHz resonance shifts to a lower frequency of about 4.5 kHz and the 20 kHz resonance shifts to a higher frequency of about 26 kHz.

The foregoing analysis suggests that the foramen in the bony septum of the cat is there, in part, to increase the effective acoustic length of the middle ear cavities in a limited frequency region. The net result of this increased acoustic length is a shift in the bulla resonance frequency. The structure of the bony septum is such that the lower bulla resonant frequency shifts down in frequency by a factor of about 2.2, and the upper bulla resonant frequency shifts up in frequency by a factor of about 1.3. The geometry of the cat middle ear cavities are not exactly those of cylindrical tubes and thus the exact effect of the foramen can be expected to be slightly different from these predictions. As is seen by the close correspondence in the low frequency (below 1 kHz) limit of both model computations, the cavity resonances are modified virtually without affecting the total volume of the cavity. To our knowledge impedance measurements of animal

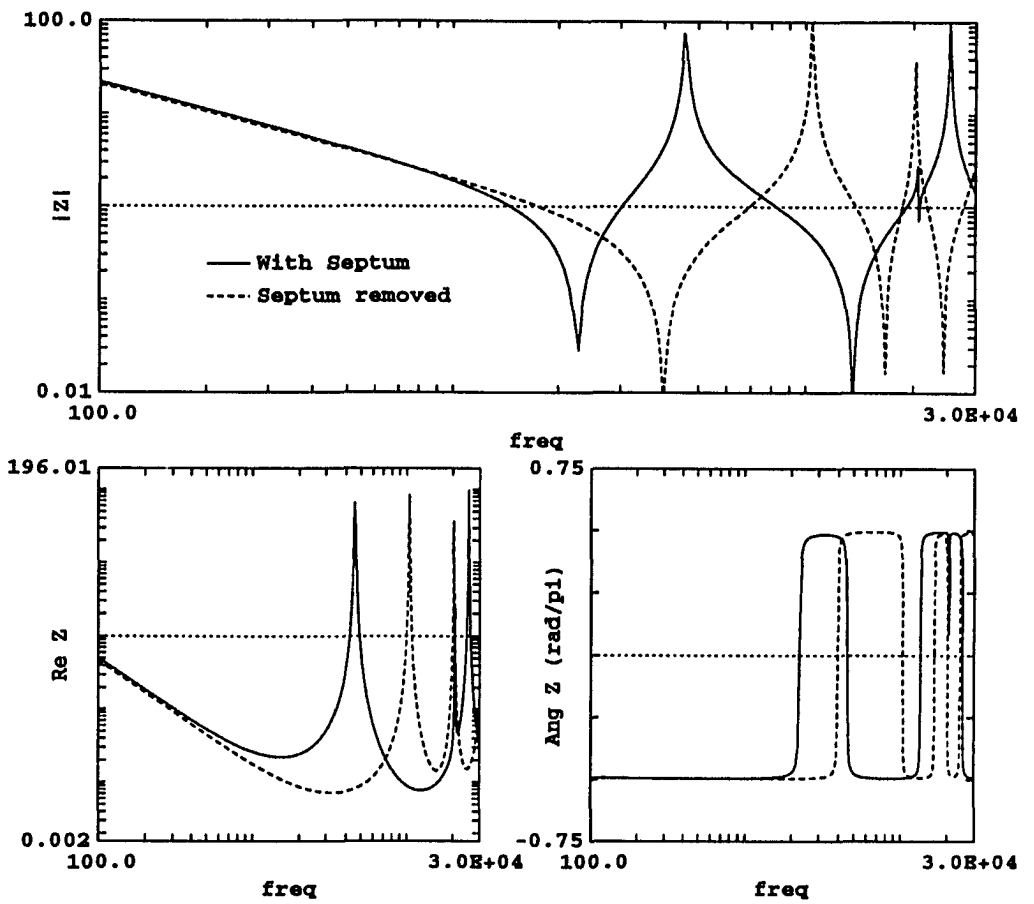

Figure 4.18: Comparison of middle ear cavity impedance with the bony septum and without the bony septum: Note that model computations are shown for frequencies up to 30 kHz. As shown in the previously there is bulla resonance near 4.5 kHz. This figure clearly shows that with the bony septum intact, there is a second bulla resonance near 26 kHz. When the bony septum is removed, the first bulla resonance shifts up to about 10.2 kHz, while the second bulla resonance shifts down to about 20 kHz. The low frequency limit (below 1 kHz) of the impedance indicates that the volumes of the two cavities are virtually identical. The slight difference is due to the relatively small volume of the bony septum.

MEC without the bony septum and with bulla cavity closed do not exist in the literature.

4.8 A comprehensive model for the cat middle ear

A model for the impedance measured at the eardrum with the assumption that the middle ear cavities are exposed to the atmosphere has been developed. In addition, a model for the middle ear cavities with the assumption that the eardrum is removed has been formulated. In the normal case these two impedances interact with each other in a way that significantly affects the hearing ability of any given animal. In this section the two model impedances are combined into a single model for the cat middle ear.

4.8.1 Combining the eardrum and middle ear cavity impedances

The long standing hypothesis for combining the impedance of the MEC and the eardrum impedance has been that the two form a series network. Examples of such a configuration can be found in models formulated by Zwislocki (1962), Moller (1965), Peake and Guinan (1967), Shaw and Stinson (1983), and others. The validity of this hypothesis is presently examined.

Recall that the MEC are a cascade of two cavities with the bony septum separating them. The series network model hypothesis requires that the pressure seen by the round window is the pressure of the tympanic cavity. In most animals with a bony septum between the MEC, the round window is located in the bulla cavity (Dallos, 1973, p. 5). Therefore the actual pressure seen by the round window is that of the bulla cavity. This conflict would seem to make the series model circumspect.

A definitive test of this issue would be to compare the eardrum impedance with the round window in the bulla cavity, and with the round window moved to the tympanic cavity. It is however not possible to do such an experiment. An alternative to this is to look at other measurements and

model results. The later will be discussed in the next section. Since we are questioning the effect of the bulla cavity pressure versus the tympanic cavity pressure, it would be important to consider the relative amplitude of these quantities. For example, if the tympanic cavity pressure relative to the eardrum pressure is small, and the bulla cavity pressure relative to the eardrum pressure is also relatively small, then the location of the round window is not likely to affect the eardrum impedance. On the other hand, if the pressures in either cavities are comparable to the pressure at the eardrum, then one can expect there to be some effect due to the particular location of the round window.

Lynch (1981, Chap. II, Figs. 14-16) measured the pressure in the tympanic cavity and the bulla cavity relative to the eardrum pressure (P_{tc}/P_{ec} and P_{bc}/P_{ec}). Magnitudes of both P_{bc}/P_{ec} and P_{tc}/P_{ec} are approximately -10 dB for frequencies below 1 kHz. Above about 1 kHz, $|P_{tc}/P_{ec}|$ starts to decrease reaching a minimum of approximately -31 dB at 2.1 kHz and then increasing to about 2 dB at 5 kHz. Above 5 kHz, $|P_{tc}/P_{ec}|$ decreases; between $10-20$ kHz, it fluctuates in the -10 dB vicinity. On the other hand $|P_{bc}/P_{ec}|$ is -10 dB, for frequencies up 5 kHz. Above 5 kHz, $|P_{bc}/P_{ec}|$ has two sharp minima; one at 8 kHz with a value of -44 dB, and one at 18 kHz with a value of -35 dB. At about 12 kHz and 25 kHz, there are two maxima in $|P_{bc}/P_{ec}|$ with values for both being approximately -10 dB.

Our interpretation of the above experimental observations are that the pressure in the tympanic cavity is comparable to the pressure at the eardrum for frequencies between 3-7 kHz. The pressure in the bulla cavity is typically less than -10 dB. Thus the effect of putting the round window in the tympanic cavity is likely to result in eardrum impedance calculation errors more in the 3-7 kHz frequency region than the other frequencies. Thus we conclude that the series model for the eardrum impedance and MEC impedance is reasonable except possibly in the 3-7 kHz

frequency region. It is conceivable that placing the round window in the tympanic cavity has a more pronounced effect on the transfer functions, such as that between the eardrum pressure and scala vestibule or scala tympani pressure. We have not attempted to analyze this yet. Peake *et al.* (1991) have recently hypothesized that the pressure differences between the oval window and the round window accounts for the residual hearing above about 2 kHz when there is no sound stimulus to the stapes via the ossicular chain (i.e. under the conditions of missing or interrupted ossicular chain due to damage).

4.8.2 Comparison with data

The middle ear cavity impedance for the intact case Z_{mec} and with the two "surgical modifications" shown in Fig. 4.16 were first unnormalized by the characteristic impedance of the tympanic cavity ($\rho_a c_a / A_{t_c}$). The eardrum impedance calculations Z^i_{ec} shown in Fig. 4.11 were unnormalized by the characteristic impedance of the transducer tube ($\rho_a c_a / A_t$). Under the assumption that the series network model for Z^i_{ec} and Z_{mec} is a valid one, we have combined the two unnormalized impedances. The resulting model impedances, renormalized by the characteristic impedance of the transducer tube, are shown in Fig. 4.19 .

Lynch made measurements on several cats with "surgical modifications" to the MEC with the eardrum impedance intact. We will thus compare our model calculations with Lynch's measurements.

First, Lynch's results are briefly summarized: Measurements of the intact MEC (Z^i_{mec}) indicate the presence of a high Q resonance in the impedance. The resonant frequency varied from 4-5 kHz while the Q_3, defined to be the ratio of the center frequency to the -3 dB bandwidth, varied from 11.0 to 18.3, with a mean of 14.0. When the bulla cavity is opened widely then the resonance in the measured impedance (Z^i_{bo}) shifts to a lower frequency of approximately 3.5 kHz. As is

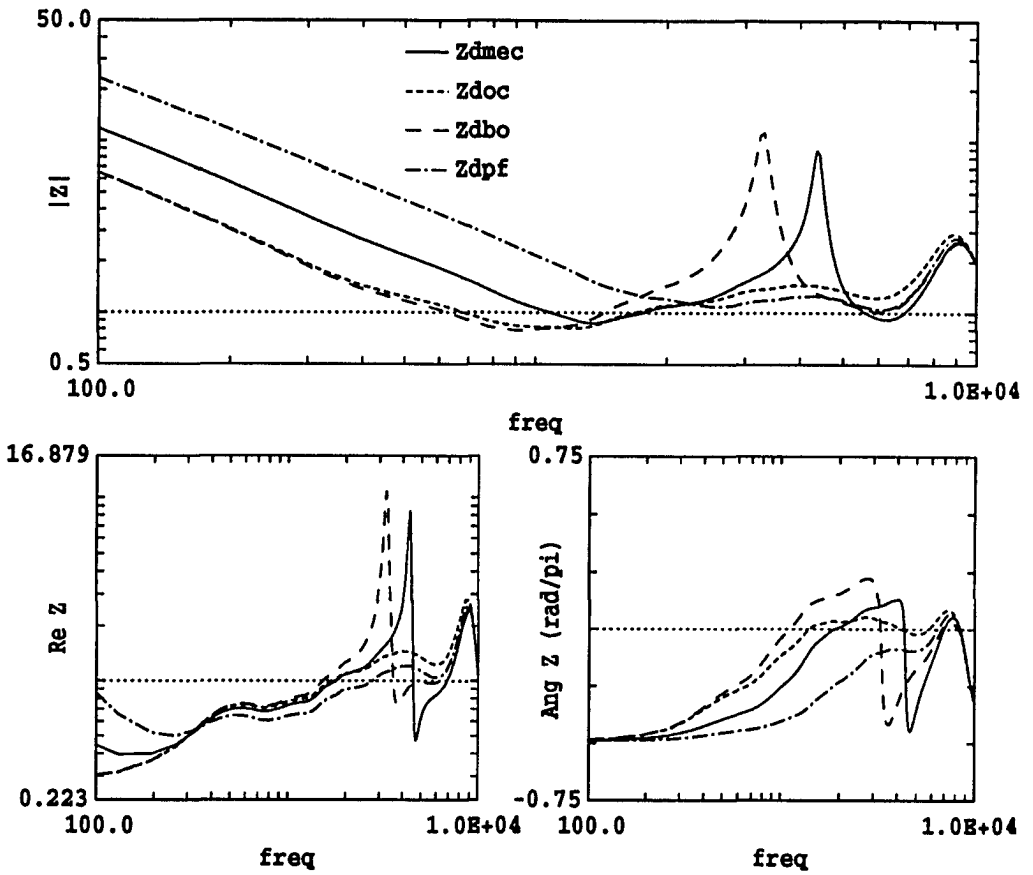

Figure 4.19: *Eardrum impedance with various manipulations on the middle ear cavity:* $Z_{d_{oc}}$ is eardrum impedance with open cavities. Each of the middle ear cavity impedances of Fig. 4.16 were combined with Z_{doc} under the assumption that the two impedances can be connected in series. These model computations are in good agreement with cat eardrum impedance measurements made with similar modifications on the MEC by Lynch (1981).

to be expected, opening of the bulla is accompanied by a decrease in impedance of about 3 dB, relative to Z^i_{mec}, at frequencies below approximately 1 kHz. According to Chapter II, Fig. 8 of Lynch's thesis the Q_3 of Z^i_{bo} appears to be slightly greater than that of Z^i_{mec}. When the foramen is closed-off, by sealing it with a plug, then the resonance in the measured impedance is no longer observed. This time the impedance increases by approximately 6 dB, relative to Z^i_{mec}, for frequencies below approximately 2 kHz.

Although Lynch made the measurements on several cats, the measurements shown for cat TJL-53L in Chapter II, Fig. 8 of his thesis, are representative of his findings. We will thus refer to that figure. Measurements on a specific cat, rather than averaged measurements of several cats, is preferred because averaging tends to "smear-out" the features we are interested in modeling. For comparison to our model calculations we also list the magnitude of the measured impedance at a few important frequencies for that particular cat. $|Z_{mec}|$ at 100 Hz is approximately $6.3 \times 10^3\ dyne - sec/cm^5$. From now on we will use $k\Omega$ to denote $10^3\ dyne - sec/cm^5$. $|Z_{mec}|$ is $\approx$ 4.4 $k\Omega$ at the resonant frequency of about 4.3 kHz. $|Z_{bo}|$ is $\approx$ 3.6 $k\Omega$ at the resonant frequency of about 3.1 kHz.

The phase of the impedance calculations shown in Fig. 4.19 is $\approx -90°$ for frequencies below 300 Hz for all three calculations. This indicates that all three impedances are compliance dominated below 300 Hz. Z_{pf} appears to be compliance dominated for frequencies up to 1 kHz. The normalized magnitude of Z_{mec} at 100 Hz of $\approx$ 10.1 corresponds to an impedance of 4.05 $k\Omega$. This is a factor of about 0.64 (−3.88 dB) smaller than the measured data.

The point of resonance for Z_{mec} occurs at 4.2 kHz with a normalized magnitude of 9.3. This corresponds to an impedance of $\approx$ 3.7 $k\Omega$ (hence forth, references to actual impedances rather than normalized impedance will be made). The calculated Q_3 for the intact MEC is $\approx$ 20. This

Q_3 is higher than most of the measured Q_3's. The magnitude of Z_{bo} is $\approx 5.2\ k\Omega$ at the resonant frequency of about 3.1 kHz. The calculated Q_3 for the open bulla case is ≈ 10. The model calculations show that the relative magnitude of Z_{bo} to be greater than that of Z_{mec} by a factor of 1.4 (2.9 dB) at the resonant frequency. In comparison with the measured data, the magnitude of Z_{bo} is less than the magnitude of Z_{mec} by a factor of 0.82 (−1.72 dB).

At the resonant frequencies both intact cavity impedance Z^i_{mec} and bulla open impedance Z^i_{bo} go through a reversal in phase that is characteristic of resonators. In the region where the resonances of the MEC are dominant, the real part of the eardrum impedance with intact MEC ($\Re e[Z^i_{mec}]$) and the real part of the eardrum impedance with bulla cavity open ($\Re e[Z^i_{bo}]$) are greater than just the eardrum impedance (Z_{doc}) by almost an order of magnitude.

For stimulus frequencies above 5 – 6 kHz, the calculated eardrum impedance with the MEC is slightly lower. Deviations, of less than 7 dB between the impedance measured with the MEC intact and with the MEC completely exposed to the atmosphere occur in the frequency region between 5 – 20 kHz (Lynch, 1981, Chap. II, Fig. 8). Trends in the model and data are in agreement, further indicating that the assumption of the series model is a valid one.

In the previous figures we have looked at impedances as well as reflectance; we presently analyze the effect of the MEC from the reflectance perspective. Figure 4.20 shows the reflectance corresponding to the impedance of Fig. 4.19 . When the magnitudes of the impedances and the magnitude of the reflectance are compared, the following general observation is made: whenever the impedance is increased due to the MEC, or some manipulation of the MEC, the magnitude of the reflectance increases. For example, at the frequencies were there are resonances in Z_{mec} and Z_{bo}, and thus an increase in impedance, the reflectance magnitude increases from about 0.2 to about 0.9.

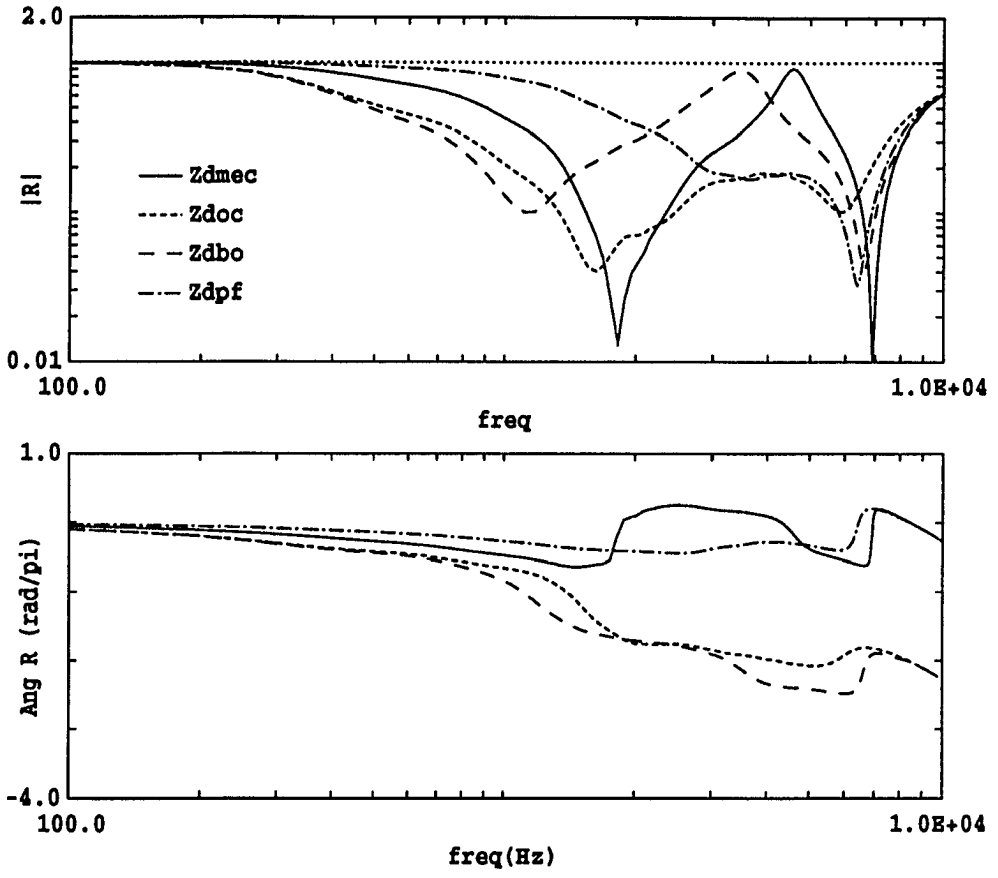

Figure 4.20: *The manipulations of the middle ear cavities viewed from the reflectance domain:* Z_{doc} is for the open cavities case. Generally speaking, for frequencies below about 6 kHz a cavity behind the eardrum results in an increase in the reflectance magnitude. When the cavity behind the eardrum is closed, the phase of the reflectance decreases.

Furthermore, for stimulus frequencies below about 6 kHz, the effect of placing any of the MEC behind the eardrum increases the reflectance magnitude. The only exception to this is in $|R^i_{mec}|$, where the MEC had the effect of decreasing the reflectance in the limited frequency region of 1.7 – 2.2 kHz. For frequencies between 6.4 – 9 kHz the effect of the MEC is to reduce the magnitude of the reflectance. Above about 9 kHz the MEC do not have an effect on the reflectance magnitude. However, differences in the phase of the reflectance are noted.

With the intact MEC, and the plugged foramen cavity, the phase of the reflectance is between -0.75π and 0.25π. With a bulla open cavity or when there is no middle ear cavity at all, the phase is between 0π and -2.25π. Thus having a closed cavity behind the eardrum results in an increase in the phase of the reflectance.

4.9 Summary

A middle ear model based on anatomical considerations has been formulated. To uniquely estimate the parameters of the proposed model, eardrum impedance measured with various "surgical modifications" to the cochlea and ossicles are modeled. In addition, a model based on the lengths and diameters of the middle ear cavities has been investigated.

The main consideration of the present work has been to estimate acoustic parameters for the cat anatomy. The model and the outlined methodology, for estimating the parameters of the model, is general enough that it can be used to model the anatomy of the human middle ear, as well as other animals, provided that eardrum impedance measurements with specific "surgical modifications" are available.

The middle ear model started with the most simple case of the "interrupted incus" first and proceeded to the most complicated case of the intact cochlea, ossicles, and middle ear cavities

termed the "comprehensive model." As we proceeded, the following conclusions were reached at each step:

- *Interrupted incus:* For stimulus frequencies between 100 Hz to 7 kHz at most 10% of the incident wave is dissipated by the eardrum and the ossicles; the rest is reflected back into the earcanal. For frequencies between 8-12 kHz, up to 75% of the incident wave is dissipated by the incudo-malleolar joint.

  Model fit to measured $|R_{ec}^{ii}|$ is excellent. Model phase of R_{ec}^{ii} is quite good for frequencies below 10 kHz. For frequencies between 10 kHz and 15 kHz the model phase of R_{ec}^{ii} is greater that the data by as much as $\pi/2$, indicating that at these frequencies a more accurate model for the uncoupled portion of the eardrum Z_{du} is needed. Due to the paucity of data at such high frequencies, a formulation of a more accurate eardrum model does not seem feasible at this time.

- *Drained cochlea:* For frequencies between 300 Hz and 7 kHz the incident wave absorbed by the annular ligament is at most approximately 10%.

- *Intact ossicles and cochlea:* For the "intact" case, the load to the stapes is the impedance of the cochlea. The cochlear input impedance has an important effect on the impedance measured at the eardrum. In the frequency region between 300 Hz and 8 kHz as much as 80% of the incident wave is absorbed by the cochlea; the maximum absorption occurred near 1.6 kHz. Some of the fine structure observed in the eardrum reflectance can be attributed to the fine structure observed in the magnitude as well as the phase of the cochlear input impedance. *Thus an accurate model of the cochlear input impedance is very important in order to be able to model the eardrum impedance and reflectance.*

In the past, researchers have modeled the eardrum impedance using an inaccurate representation for the cochlea. What those input impedance cochlear models lacked was compensated for by the parameters of their middle ear model. Thus when modeling the middle ear, an inaccurate representation of the cochlear input impedance will result in an inaccurate representation for the middle ear.

- *Middle ear cavities:* A model for the middle ear cavities based on lengths and diameters of the cavities has been developed. The parameters estimated are consistent with measured volumes for those cavities by other researchers. With the intact middle ear cavities there is a resonant frequency of about 4.5 kHz in the middle ear cavity impedance. When the bulla cavity is open the resonant frequency shifts to about 3.3 kHz. When the foramen is plugged then there is a zero in the driving point impedance at about 12 kHz. It is also shown that, for the intact case, there is a second bulla resonance in the 26 kHz frequency region that has not been previously measured.

  Non-planar wave propagation resulting from sudden changes in area due to the foramen were taken into account by using the Karal correction to the plane-wave theory. Acoustically the effect of the non-planar wave propagation is to increase the effective length of the cavities by as much as a factor of two in the frequency region between 500 Hz and 3.6 kHz, for a particular set of cavity dimensions.

- *Losses in the model:* Losses in the middle ear cavity model are due to visco-thermal boundary layer effects at the surface of the cavity walls. Future measurements of the middle ear cavity surface area would help to further constrain the parameters of the model.

- *The bony septum:* The effect of removing the cat bony septum is to shift the first bulla

resonance from about 4.5 kHz to approximately 10 kHz, while the second bulla resonance shifts from 26 kHz to approximately 20 kHz.

- *The comprehensive model:* The series model for combining the impedance of the eardrum, ossicles and cochlea with the impedance of the MEC has been reexamined. It has been determined that the errors made in making such an assumption are insignificant from an impedance measurement point of view. That the series model assumption may play a more significant role in transfer function calculations is debatable and needs further analysis.

  From the eardrum reflectance point of view, having a middle ear cavity behind the eardrum results in an increase in the reflectance magnitude. This indicates that the MEC could have a small but detrimental effect on the hearing ability of a given species. Clearly, this cannot be the complete story and one must look at other measures to get more insight about the effects of the MEC. Examples of these include the transfer function between the eardrum pressure and the stapes displacement, the transfer function between the eardrum pressure and the scala vestibule pressure, and the transfer function between the eardrum pressure and cochlear microphonic at the round window.

Chapter 5

Cylindrical cavities with area discontinuities: measurements and model

Introduction

In Chapter 4 a chain-matrix model for the middle ear cavities was used. It needs to be proven that such a model is an accurate representation for the middle ear cavities and for the ear canal. To prove that the middle ear cavity model used in Chapter 4 is tenable we make impedance measurements on several cavities. The resulting measurements are compared to model computations.

The goals of this chapter are two folds. First, a method of accurately measuring acoustic impedances is described. Briefly, the *Thevenin* equivalent parameters of the pressure transducer using a four-cavity calibration method of Allen (1986) for frequencies up to 15 kHz is obtained. * The calibrated transducer is then used to measure the unknown impedance. Second, a general method of modeling the measured impedances of cavities with a varying cross sectional area is

*This measurement technique is limited by the upper-frequency limit of the particular transducer used. The Sokolich transducer used in (Allen, 1986) had an upper- frequency break point of $\approx$ 20 kHz. Due to their readily commercial availability, we have used the ER-2 from Etymōtic Research to make the measurements reported in the present Chapter.

described (Puria and Allen, 1991a). The model is formulated so that the following effects are explicitly accounted for: (a) variations in cross sectional area, (b) non-planar wave propagation due a jump in cross sectional area, (c) viscous and thermal losses at the walls, as well as (d) finite wall impedances.

5.1 Acoustic Impedance Measurements

Regardless of the system being described, be it electrical, mechanical, acoustical, or biological, differential equations are commonly used to describe the dynamics of that system. We are interested in acoustic measurements. Since differential equations describing acoustic and electrical systems parallel each other, one can be described in terms of the other by use of dynamical analogies (Beranek, 1954; Olson, 1958; Pierce, 1989). Pressure and volume velocity in an acoustical system correspond to voltage and current in an electrical circuit. From these two analogies one can readily define the acoustic impedance given the pressure P and the volume velocity U

$$Z(\omega) = P(\omega)/U(\omega). \tag{5.1}$$

According to this definition one must measure both the pressure and the volume velocity of the particular system under consideration. In general, measuring the volume velocity, with existing techniques such as the two-microphone method, leads to erroneous results and sometimes intractable artifacts. It is desirable to formulate an alternative method where only pressure measurements are used.

Rabinowitz (1981), and Lynch (1981) formulated such a method for measuring admittances. They characterized their pressure transducer in terms of a Norton equivalent circuit. An equivalent approach is to describe the pressure transducer in terms of its Thevenin equivalent source pressure

P_o and source impedance Z_o (Allen, 1986).

In both cases, the source parameters are evaluated by making pressure measurements on several acoustic loads on the transducer. The impedances of the acoustic loads are either know or can be computed based on the dimensions of the cavity. The source parameters are obtained by doing a minimum mean squared error fit to the measured pressures. Since there are two complex quantities that must be evaluated, a minimum of two complex pressure measurements on two different impedance loads must be made. Rabinowitz (1981), and Lynch (1981) evaluated their source parameters based on the two-load method. In order to overdetermine the source parameters Allen (1986) used the four-load method. The four-load method has the advantage of reducing the minimum mean squared error in the presence of measurement noise.

Once the source parameters are estimated one needs only to measure the pressure response P_x of the system under consideration with a high-impedance probe-tube microphone. To compute the impedance one simply uses the pressure divider rule

$$Z_x(\omega) = \frac{P_x(\omega)}{P_o(\omega) - P_x(\omega)} Z_o(\omega). \tag{5.2}$$

In Eq. (5.2) Z_x is the impedance of the unknown tube normalized by the characteristic impedance of the calibration tubes.

In this study the four-load method will be used to measure all impedances. This method has been used in the past by Dear (1987) to measure the acoustic impedance of the chinchilla ear, and most recently it was used by Keefe and Ling (1989) to measure human ear canal impedances.

5.1.1 Thevenin equivalent source parameters

As previously mentioned, essential to the measurement of an unknown impedance is the computation of Thevenin equivalent source parameters $P_o(\omega)$ and $Z_o(\omega)$ of the transducer. The computation

of these parameters from pressure measurements made on four equi-diameter calibration-cavities will now be described in greater detail.

For a cavity, of known length and diameter, it is possible to compute the impedance by use of a model. This model must take the viscous and thermal losses into account, and in addition it should also be computationally efficient. The model (see Appendix D) of Keefe (1984) is to be used to make theoretical calculations of the impedance of the cavities.

Although the physical length of each of the four closed calibration-cavities can be approximately measured, the acoustic distance, from the measurement plane to the end of the cavity, is not known. In order to estimate the Thevenin equivalent source parameters it is important to accurately estimate the acoustic length of each cavity. To this end an iterative procedure is used to estimate the acoustic length of the four cavities.

The algorithm for iteratively computing the Thevenin equivalent parameters is initiated by assuming the physically measured length for each of the four cavities. From the four lengths one obtains the four model impedances Z_1, Z_2, Z_3, Z_4. Using Eq. (5.2), the relationship between the four impedances (Z_1, Z_2, Z_3, Z_4), the four known pressure measurements (P_1, P_2, P_3, P_4), and the Thevenin parameters, can be put matrix form:

$$\begin{bmatrix} Z_1 & -P_1 \\ Z_2 & -P_2 \\ Z_3 & -P_3 \\ Z_4 & -P_4 \end{bmatrix} \begin{bmatrix} P_o \\ Z_o \end{bmatrix} = \begin{bmatrix} P_1 Z_1 \\ P_2 Z_2 \\ P_3 Z_3 \\ P_4 Z_4 \end{bmatrix}. \tag{5.3}$$

Solving this over-specified system of equations by the least-squares-method we obtain

$$\begin{bmatrix} P_o \\ Z_o \end{bmatrix} = \frac{1}{\Delta} \begin{bmatrix} \sum |P_i|^2 & -\sum Z_i^* P_i \\ \sum P_i^* Z_i & -\sum |Z_i|^2 \end{bmatrix} \begin{bmatrix} \sum |Z_i|^2 P_i \\ \sum |P_i|^2 Z_i \end{bmatrix}, \tag{5.4a}$$

where

$$\Delta = \left(\sum |Z_i|^2\right)\left(\sum |P_i|^2\right) - \left(\sum P_i^* Z_i\right)\left(\sum Z_i^* P_i\right). \tag{5.4b}$$

The $(^*)$ denotes the conjugate.

With the estimated P_o and Z_o and the four Z_i's, one can compute the four resulting pressure responses $\tilde{P}_x$ by using Eq. (5.2) once again. The error norm in assuming this particular set of lengths is:

$$E = \|P_x(\omega) - \tilde{P}_x(\omega)\| \tag{5.5}$$

Next one does a gradient search, with respect to the four lengths, on Eq. (5.5) to find a new set of lengths. The procedure is repeated until the error norm in Eq. (5.5) reaches some desirable minimum.

The Thevenin equivalent source parameters $P_o(\omega)$ and $Z_o(\omega)$ are subsequently used in Eq. (5.2) to calculate any unknown impedance. The impedance obtained in this manner is an impedance that is normalized to the characteristic impedance (Z_{ot}) of the calibration cavities.

5.2 The chain-matrix formulation for cavities

One criterion for the formulation of the cavity model is that it must be general enough so as to be able to represent a cavity with an arbitrary cross-sectional area. The well known Webster-Horn equation is typically used to describe wave propagation in one dimension. However, for arbitrary area functions there are no analytical solutions to the Webster-Horn equation and thus one must

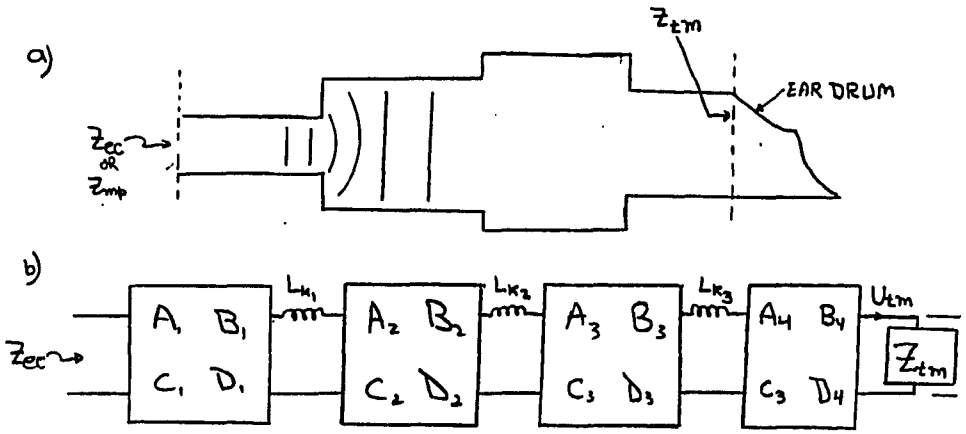

Figure 5.1: (a)Illustration of a cavity as a cascade of constant diameter cylindrical tubes. Z_{mp} is the impedance at the measurement-plane and Z_{rl} is the radiation load impedance of the cavity. In this example Z_{mp} is the impedance measured at the entrance of the earcanal and Z_{rl} is the eardrum impedance. (b) The chain-matrix representation of the geometry shown in (a). The elements of each of the matrices are formulated such that visco-thermal effects and finite wall impedance effects are included. Non-planar wave propagation due to the jump in area are incorporated in the model by L_{k_i}.

approximate the continuous area function by a series of stepped-areas.

Our model for the cavities, with an arbitrary cross-sectional area, can be best illustrated by way of an example. The sketch of a cavity is shown in Figure 5.1a. This simple cavity is approximated by four cylindrical tubes each of a different length and diameter. The impedance at the measurement-plane (mp) is $Z_{mp}(\omega)$. The load to the cavity is a radiation impedance termed $Z_{rl}(\omega)$. As an example, if Z_{mp} were the impedance measured at the entrance of the ear canal then Z_{rl} would be the impedance of the eardrum and the cylindrical tubes would approximately represent the earcanal.

For each cylindrical tube of length l_i and diameter d_i, one can write down the pressure and

volume-velocity input-output relationship, in terms of the two-port chain-matrices:

$$\begin{bmatrix} P(x) \\ U(x) \end{bmatrix} = \begin{bmatrix} A & B \\ C & D \end{bmatrix} \begin{bmatrix} P(x+l_i) \\ U(x+l_i) \end{bmatrix}, \tag{5.6a}$$

where the elements of the ABCD chain-matrix are

$$\begin{bmatrix} A & B \\ C & D \end{bmatrix} = \begin{bmatrix} cosh(\gamma_i l_i) & Z_{oi} sinh(\gamma_i l_i) \\ \frac{1}{Z_{oi}} sinh(\gamma_i l_i) & cosh(\gamma_i l_i) \end{bmatrix}. \tag{5.6b}$$

The propagation constant γ_i and the characteristic impedance Z_{oi} in Eq. (5.6b) include viscous and thermal losses (see Appendix D). Discussion regarding the Karal correction between each section represented by the inductances L_{k_i} in Fig. 5.1 is deferred for the moment.

The chain-matrix is started at the radiation load end ($x = x_{rl}$) of the cavity. The assumption that $U(x_{rl}) = 1$ gives rise to a pressure drop $P(x_{rl}) = Z_{rl}(\omega)$. Equation (5.6) is then recursively calculated with the space index starting at $x = x_{rl}$ and "marching" towards the measurement-plane ($x = x_{mp}$). The ratio of $P(x_{mp})$ and $U(x_{mp})$ is the desired impedance $Z_{mp}(\omega)$ at the measurement-plane. This model is exactly analogous to that described for the cochlear model in Chapter 2.

5.2.1 Higher order modes due to a discontinuity

The chain-matrix formulation, based on the assumption of plane wave propagation, described above is general enough so as to be able to model cavities with sudden changes in cross-sectional areas. However, sudden changes in cross-sectional area result in sudden changes in pressure. These changes in pressure, at the area discontinuities, result in non-planar wave propagation. If the chain-matrix formulation is to be used for cavities with varying cross-sectional areas then these two-dimensional effects must be taken into consideration.

The problem of changes in propagation of sound due to a sudden change in cross-sectional area in both cylindrical tubes and rectangular ducts was first studied by Miles (1944; 1946a; 1946b) . He in essence formulated the basic equations that dictates propagation of sound near an area discontinuity. However, Miles did not provide any numerical results or a simplified intuitive feel for the effects due to a jump in area. The problem was studied again for the cylindrical tubes case by Karal (1953). Karal concluded that effects due to an abrupt change in area A_1 (radius r_1) to an area A_2 (radius r_2) of cylindrical tubes introduces an additional impedance. This impedance arises due to higher-order modes present in the neighborhood of the area discontinuity. This impedance is shown to be an inductance L_k, located at the jump in area, and is a function of the ratio of the tube radii $\alpha = r_1/r_2$:

$$L_k(\alpha) = \frac{8\rho_a}{3\pi^2 r_1} H(\alpha). \tag{5.7}$$

This inductance will be reffered to as the Karal correction. The function $H(\alpha)$ is in terms of an infinite sum of Bessel functions. By approximating $H(\alpha)$ by the straight line $(1 - \alpha)$ Sondhi (1983) found a simple closed form formula for the Karal correction. Sondhi's approximation to the Karal correction is:

$$L_k = \frac{8\rho_a}{3\pi^{\frac{3}{2}}} \left| \frac{1}{\sqrt{A_1}} - \frac{1}{\sqrt{A_2}} \right|. \tag{5.8}$$

Since measurements in the present work are in cylindrical tubes Sondhi's approximation will be used. It is noted that similar lumped parameter approximations for the rectangular duct case can be found in (Morse and Ingard, 1968, pp 483-490), (Morse and Feschbach, 1953, pp 1443-1447). The added inductance L_k increases the total acoustic inductance of the tube and can thus be interpreted as an increase in the equivalent length of the tube.

A short-coming of Karal's formulation is that it is for the inviscid case. If the viscous boundary

layer thickness is sufficiently close to the tube radius then one can anticipate that there will a resistive component in series with the inductive component. Hudde and Letens (1985) have analyzed the jump in area in cylindrical tubes with yielding walls at the discontinuity, but also under the inviscid fluid flow assumption. For the hard wall case Hudde and Letens's results reduce to those of Karal. Since the tubes we shall measure have hard walls we will not presently consider the formulation developed by Hudde and Letens. We shall attempt to experimentally measure the viscous effects due to an area discontinuity on the driving point impedance of the cavity. These experimental results have the potential for indicating whether further theoretical results need to carried out for the viscous case.

5.2.2 Non-planar wave propagation

The chain-matrix formulation with the Karal correction only takes into account non-planar wave propagation near the junction where there is a sudden jump in area. If there are higher-order modes propagating in the constant diameter portion of the cylindrical tube then Eq. (5.6) must be modified to include those higher-order modes. Equation (5.6) is formulated for a two-port network. That this corresponds to wave propagation in a single transmission line is obvious. In keeping with the transmission line analogy each higher-order mode can be thought to propagate in its own transmission line. One way to incorporate calculations of the higher-order modes is to accordingly increase the number of ports in Eq. (5.6). This has been done for the scattering matrix formulation by Hudde and Letens (1985). For the range of frequencies considered in the present experiments, higher-order modes are believed to be evanescent and thus we will only consider plane wave propagation.

5.3 Impedance measurements and model results

In this section we show impedance measurements on several cylindrical cavities. The cavities were designed so that there is an area discontinuity in the acoustic path. The area discontinuity in each cavity is made by adjoining two cylindrical tubes of different diameters together. In all three cases studied, the first cylindrical tube has an i.d. equal to that of the calibration cavity. The length of the first cavity (l_1) depends on the location of the tip of the probe tube microphone. Thus this length varies from one experiment to the next. A second cavity is joined to the first cavity by a brass coupler. Regardless of the diameter of the second cavity, the same coupler is always used. The coupler has the same i.d. as the calibration cavity. A good seal is ensured, to prevent low frequency leaks, by using vacuum grease between the coupler and the second cavity that sits on top of the coupler. In the last example, a constriction is introduced in the acoustic path. This is done by inserting a disk having an o.d. identical to the i.d. of the second cavity. The disk has a circular opening of the desired diameter in the center. This disk is centered on top of the coupler.

Since there is a hard wall at the end of the second tube, the radiation load impedance Z_{rl} for the experiments reported in this chapter is assumed to be infinite. All cylindrical tubes used for this study are made of acrylic material. The physical lengths and diameters of the cavities and the disk to be placed on top of the coupler were measured with a caliper. These dimensions are listed in Table 5.1.

The acoustic measurements were made on an AT&T 6386 WGS personal computer. The PC was equipped with an acoustic measurement system called DSP-16+ made by the Ariel Corporation. One of the two D/A's of the DSP-16+ was connected to an ER-2 pressure transducer. An ER-7C probe-mic system was connected to a 20 dB "low-noise" amplifier (built "in house"). the output of which was connected to one of the two A/D's of the DSP-16+ board. Pressure

measurements were made by a software package known as SYSid. The stimulus generated by SYSid was a wide-band chirp.

The measurements were made with a maximum frequency of 15,152 Hz, sampled at 256 frequency points. The transducer roll-off frequency is approximately 12 kHz and thus one can expect the data to be noisy above that frequency. For this reason we make comparisons between the measured data and model results for frequencies up to 12 kHz.

5.3.1 Decrease in diameter

Figure 5.2 shows model calculations and measured impedance in a cavity with a decrease in diameter from 0.74 cm to a diameter of 0.2 cm. The length of each cavity is 0.63 cm and 0.96 cm. Recall that higher-order mode effects due to an area discontinuity can be accounted for by the Karal correction. To illustrate the relative effect of the Karal correction on the driving point impedance at the entrance to the cavity, the chain-matrix was computed both with the Karal (WK) correction and without the Karal (NK) correction. Both of these model computations are shown in Fig. 5.2 and all subsequent figures in this chapter. There are three different panels shown in Fig. 5.2 . The top panel shows the magnitude of the impedance for four orders of magnitude. The lower left panel shows the real part of the impedance and the lower right panel shows the phase of the impedance. All subsequent impedance figures in this chapter will follow this presentation format.

For frequencies below 7 kHz, magnitude and phase of both model computations and the measured impedance are virtually identical. In the model, the Karal correction does not affect the real part of the impedance at frequencies below 7 kHz. For frequencies between approximately 220 Hz and 7 kHz the real part of the model computation is within the measured data by a factor of approximately 2.5 (8 dB). Figure 5.2 shows that below 220 Hz the real part of the measured data is

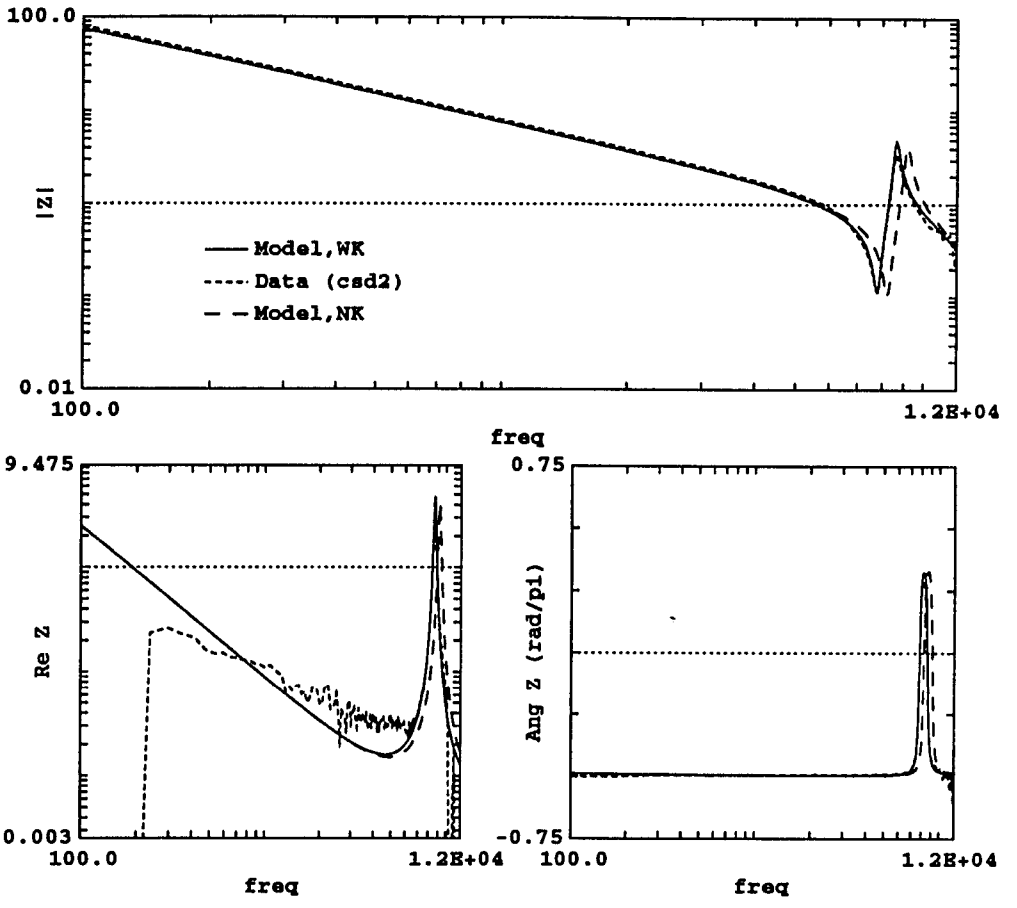

Figure 5.2: Impedance of cavity with decrease in diameter: dimensions (in cm) used for the model are $l_1 = 0.63, d_1 = 0.74$, and $l_2 = 0.96, d_2 = 0.2$. The upper panel shows the magnitude of the normalized impedance from 100 Hz to 12 kHz. The lower left panel shows the real part of the impedance and the lower right panel shows the phase of the impedance. Two model computations are shown: model with Karal correction (WK), and the model without Karal correction (NK). All subsequent figures in this chapter showing impedances will follow this format. There is good agreement between model result and measured data when the Karal correction is included in the model. The real part of the impedance becomes negative for frequencies below about 200 kHz due to calibration errors.

Table 5.1: Measured lengths (l) and diameters (d) of the cavities and disk used to illustrate the acoustic impedance measurements.

Cavity	Description	$l\,(cm)$	$d\,(cm)$
ld1	large diameter 1	1.06	1.91
sd2	small diameter 2	0.96	0.2
con	constriction	0.24	0.21

negative. There are two reasons why the real part of the measured impedance becomes negative. The first is due to due to errors in the calibration procedure and the second is due measurement noise.

Figure 5.2 shows that the most apparent effect of the Karal correction, for this particular cavity, is in the approximate frequency region above 7 kHz and below 12 kHz. In this frequency region, the magnitude, real part, and the phase of the measured data as well as model calculations with the Karal correction are in good agreement. The main observable effect of the Karal correction, in the impedance domain, is to shift the pole and the zero of the impedance to a lower frequency.

As mentioned previously, transformation of impedances to the reflectance domain gives important insight regarding the system under consideration. We shall likewise presently analyze properties of cavities in the reflectance domain.

Figure 5.3 shows the impedance of Fig. 5.2 transformed to the reflectance domain using Eq. (4.1). Recall that model impedances have already been normalized by the characteristic impedance of the first cavity, and measured data has been normalized by the characteristic impedance of the calibration cavities (unless otherwise specified, both characteristic impedances will be the same when referring to normalized impedances). In Fig. 5.3 , and subsequent reflectance domain plots, the magnitude of the reflectance is shown in the upper panel and the group delay in

milli seconds) of the reflectance [see Eq. (4.7)] is shown in the lower panel. The ordinate scale in each case has been chosen to show the full range of measured data.

For frequencies below 7 kHz, the measured and model reflectance magnitude are approximately 0.97. For frequencies below 6 kHz, The group delay in *both* model cases is approximately 0.042 ms. Using Eq. (4.10) we obtain an acoustic length of approximately 0.729 cm. The measured group delay is 0.0419 ms corresponding to an acoustic length of 0.724 cm. The group delay in this frequency region is due to reflections from the first discontinuity. The physical distance to the first area discontinuity was approximated to be 0.63 cm. The average of the measured and model acoustic lengths is longer than the physical length by 0.0965 cm.

For frequencies between 7 kHz and 12 kHz the magnitude of the reflectance at first decreases reaching a minimum of approximately 0.43 for the data and 0.54 for the model at approximately 8.2 kHz. After reaching a minimum it increases again towards unity. In the same frequency region the group delay starts to increase reaching a maximum at about 8.2 kHz at which point it decreases. The bottom panel of Fig. 5.3 shows that at its maximum, the group delay is greater than 0.8 ms corresponding to an acoustic length greater than 27.8 cm. This acoustic length is more than an order of magnitude bigger than the entire length of the cavity. The model calculation without the Karal correction also has a comparable acoustic length, but at a higher frequency, indicating that the large acoustic length in the narrow frequency range arises independent of the Karal correction.

The natural question to ask is how does one account for the large group delay in the limited frequency region near 8.2 kHz? The answer to this question is gotten by going back to the impedance domain shown in Fig. 5.2 . In the 7 kHz to 12 kHz frequency region, the magnitude of the impedance goes from a local minimum of about 0.12 to a local maximum of about 5. At approximately 8.2 kHz, the magnitude is unity; and also near 8.2 kHz the impedance makes a

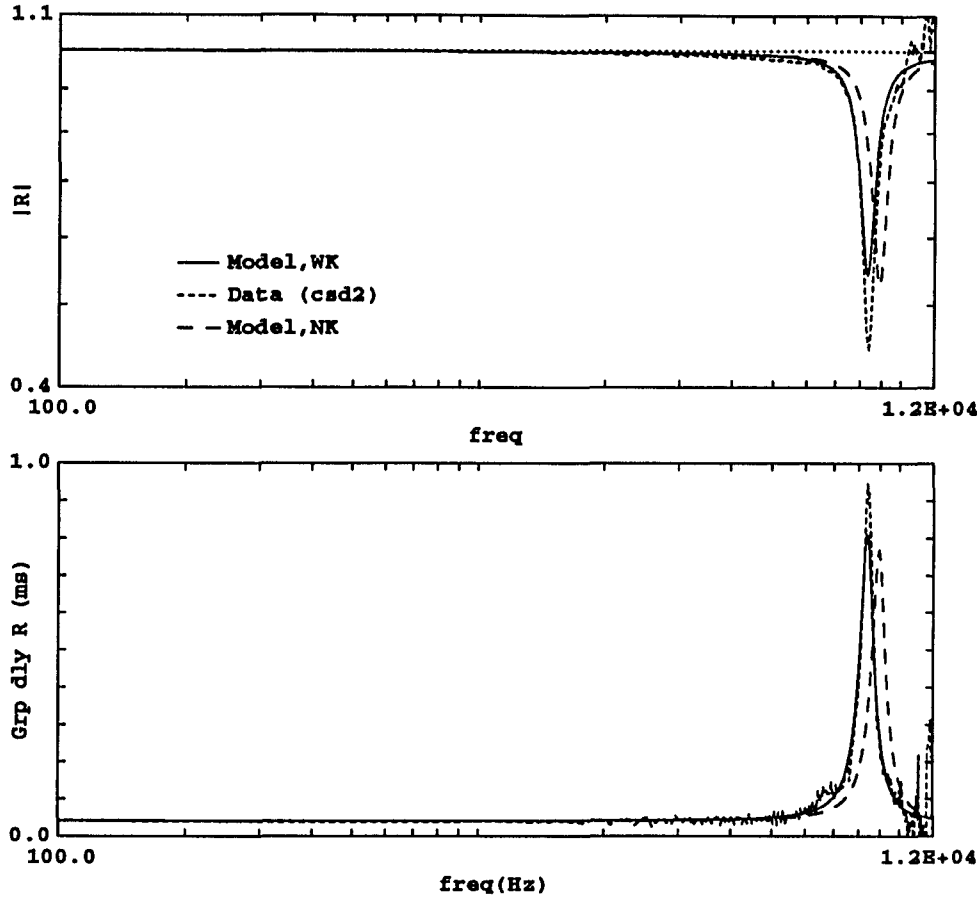

Figure 5.3: Reflectance and group delay of cavity with decrease in diameter: The upper panel shows the magnitude of the group delay and the lower panel shows the group delay in milli seconds (ms). Two model computations are shown. Model with Karal correction (WK), and the model without Karal correction (NK). All subsequent figures in this chapter showing reflectance will follow this format. The magnitude of the reflectance shows that there are more losses in the data than in the model. Other than this there is good agreement between the model with the Karal correction and measured data.

transition through zero phase. Recall that the driving point impedance of the two cavities was normalized by the characteristic impedance of the first cavity. This means that near 8.2 kHz the impedance of the second tube is exactly matched to the characteristic impedance of the first tube. When a tube (or for that matter any transmission line) is terminated in its characteristic impedance, it appears infinitely long when viewed from it's driving point impedance. In other words near 8.2 kHz there is no reflected wave and thus the large group delay. More will be said regarding the group delay as we analyze other examples.

5.3.2 Increase in diameter

Figure 5.4 shows model calculations and measured impedance in a cavity with an increase in diameter from 0.74 cm to a diameter of 1.91 cm. The respective lengths are 0.63 cm and 1.1 cm. As in the previous case (decrease in diameter) the effect, in the impedance domain, of including the Karal correction is to shift the pole and the zero to the lower frequencies.

For frequencies below 12 kHz, there is good agreement between the impedance magnitude of the data and the model with the Karal correction. With the exception of limited frequency regions between 2 kHz to 5 kHz, and 8 kHz to 11 kHz, the real part of the measured impedance appears quite noisy. This is most likely due to errors in the calibration procedure. Consequently the phase is in error in the same frequency region.

Impedance converted to reflectance is shown in Fig. 5.5 . For frequencies below about 1.5 kHz, the magnitude of the reflectance is greater than unity for the measured data. This is due to the real part of the impedance being negative in that frequency region.

The group delay show in the lower panel of Fig. 5.5 is frequency dependent. Near 100 Hz, the group delay for the data is about 0.46 ms, and for both model cases it is about 0.47 ms. From this maximum value the group delay starts to decrease reaching a minimum, near 8 kHz, of about 0.06

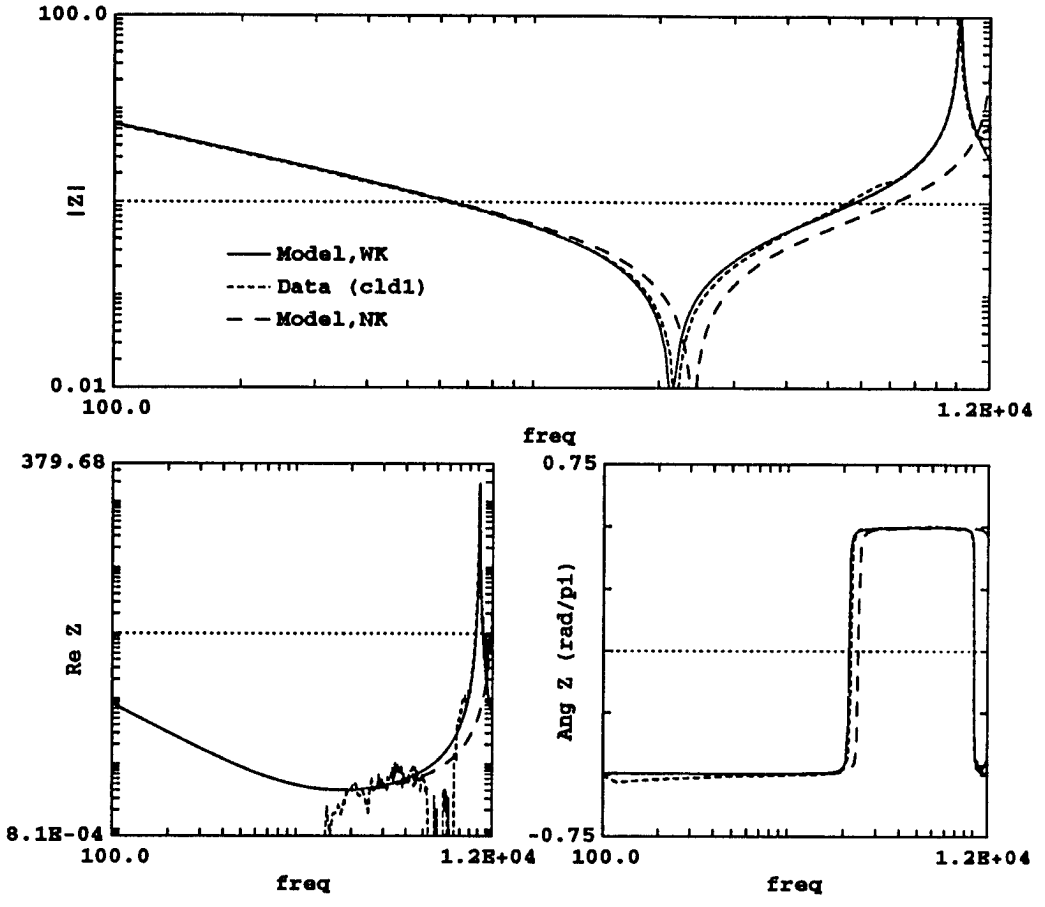

Figure 5.4: Impedance of cavity with increase in diameter: dimensions used for the model are $l_1 = 0.63, d_1 = 0.74$, and $l_2 = 1.1, d_2 = 1.91$. There is good impedance magnitude agreement between the model with Karal correction and measured data. The real part and phase are noisy for frequencies below about 2 kHz due calibration errors and measurement noise.

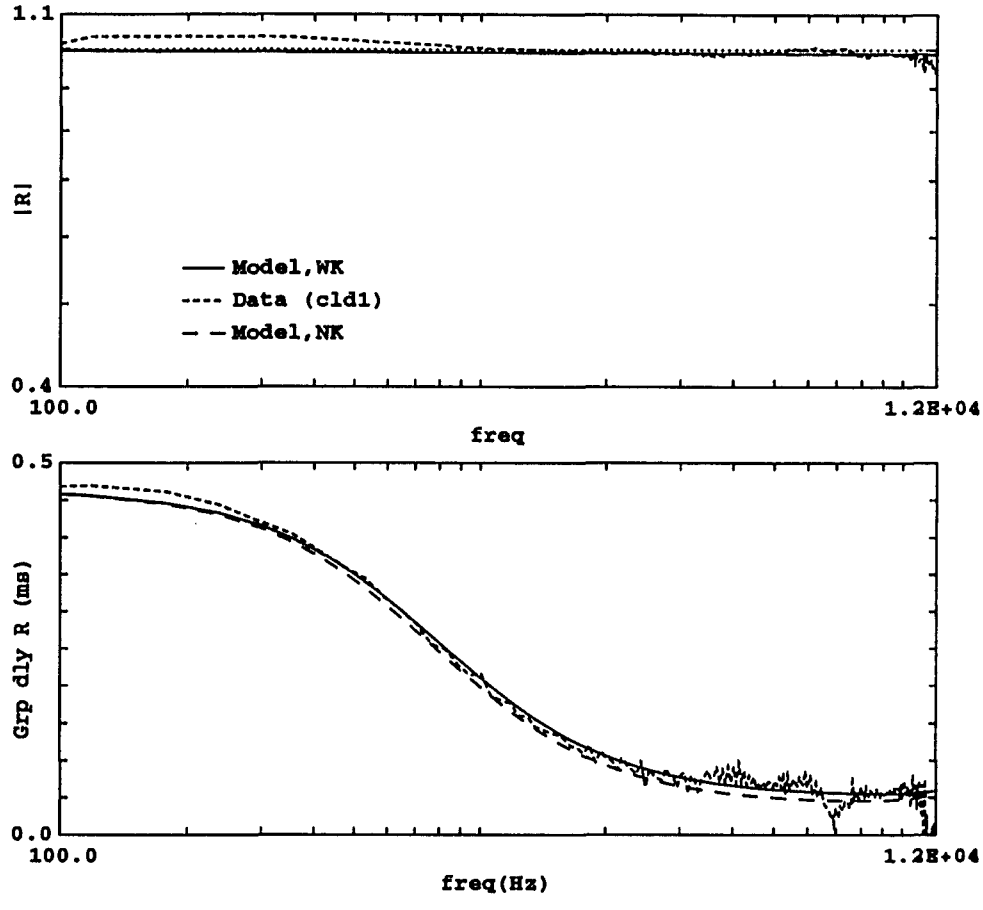

Figure 5.5: Reflectance and group delay of cavity with increase in diameter: The magnitude of the reflectance is greater than one for frequencies where the real part of the impedance is negative. For this case, the group delay for both model cases differ from the data by at most 0.01 ms.

ms for the data, 0.058 ms for the model with the Karal correction, and 0.048 ms for the model without the Karal correction. Above 8 kHz the group delay starts to increase. In fact if the model calculations were carried out to much higher frequencies, then one would see that the group delay is periodic in frequency. For the NK correction case the period Δ_f can be shown to be related to the round trip travel time in the second cavity, i.e.

$$\Delta_f = \frac{c_a}{2l_2}. \tag{5.9}$$

Where l_2 is the length of the second cavity and c_a is the speed of sound in air. This gives us Hz as the units for Δ_f. For the model calculations with the Karal correction the round trip travel time is slightly longer due to the effect of the inductor L_{k_i}. Consequently, one can expect Δ_f to be slightly less in model calculations with the Karal correction.

5.3.3 Constriction in area

The previous two examples consisted of two cylindrical cavities with either a decrease in diameter or an increase in diameter. In the next example a constriction of length l_c and diameter d_c is placed in the acoustic path.

We have used the Karal correction to account for the effect of higher-order modes due to a sudden jump in diameter. Since we are now placing a constriction in its acoustic path, the question of how to model a constriction needs to be examined. One solution to this is to model the constriction simply as a cylindrical tube. This results in two area discontinuities and thus two Karal correction inductors on each side of the constriction are needed. This is a valid solution provided that the higher order modes due to each jump in diameter have sufficiently dissipated by the time they arrive at the other discontinuity. This occurs under the condition of $l_c/d_c >> 0.5$ (Karal, 1953). If this condition is not satisfied then the solution given by Eq. (5.7) cannot be used

and more exact solutions must be computed (Karal, 1953). For this reason we have chosen the ratio of the tube length to the tube diameter (l_c/d_c) of the constriction to be greater than one.

Thus, for this case the wave propagates down the first tube a distance l_1 of 0.63 cm, the diameter d_1 of the tube then decreases from 0.74 cm to a diameter of 0.215 cm. The wave then propagates in this constricted region for a distance l_c of 0.24 cm. It then encounters an increase in diameter of 1.91 cm. The wave then propagates down the second tube for a distance l_2 of 0.85 cm. At that point the wave is reflected by the hard-wall at the end of the second cavity. Once the wave is reflected, it propagates back towards the source.

To look at the possible effect of the dimensions of the middle ear cavities on its driving point impedance, we have attempted to choose the cavity dimensions as close to those listed in Table 4.2. However, we were limited by the availability of cylindrical tubes and thus the chosen cavities.

Figure 5.6 shows the model calculations and measured impedance for a cavity with two cylindrical tubes and a constriction as described above. As in the previous examples, not including the Karal correction in the model results in an error in the pole/zero frequencies of the impedance. Without the Karal correction the poles and the zeros are shifted to a higher frequency by almost 1/3 of an octave. The magnitudes of the model with Karal correction and the measured data are in good agreement for frequencies below about 12 kHz. The exception to this being near the pole and the zero frequencies where the model magnitude at the pole is greater than the measured data, and at zero the model magnitude is less than the measured data.

In the frequency region below about 500 Hz and above 10 kHz the real part of the impedance, and thus the phase, are noisy. When the real part of the measured impedance is not noisy it is greater than that of the model by as much as a factor of 2.7 (8.6 dB).

Impedance of Fig. 5.6 converted to the reflectance domain is shown in Fig. 5.7 . The

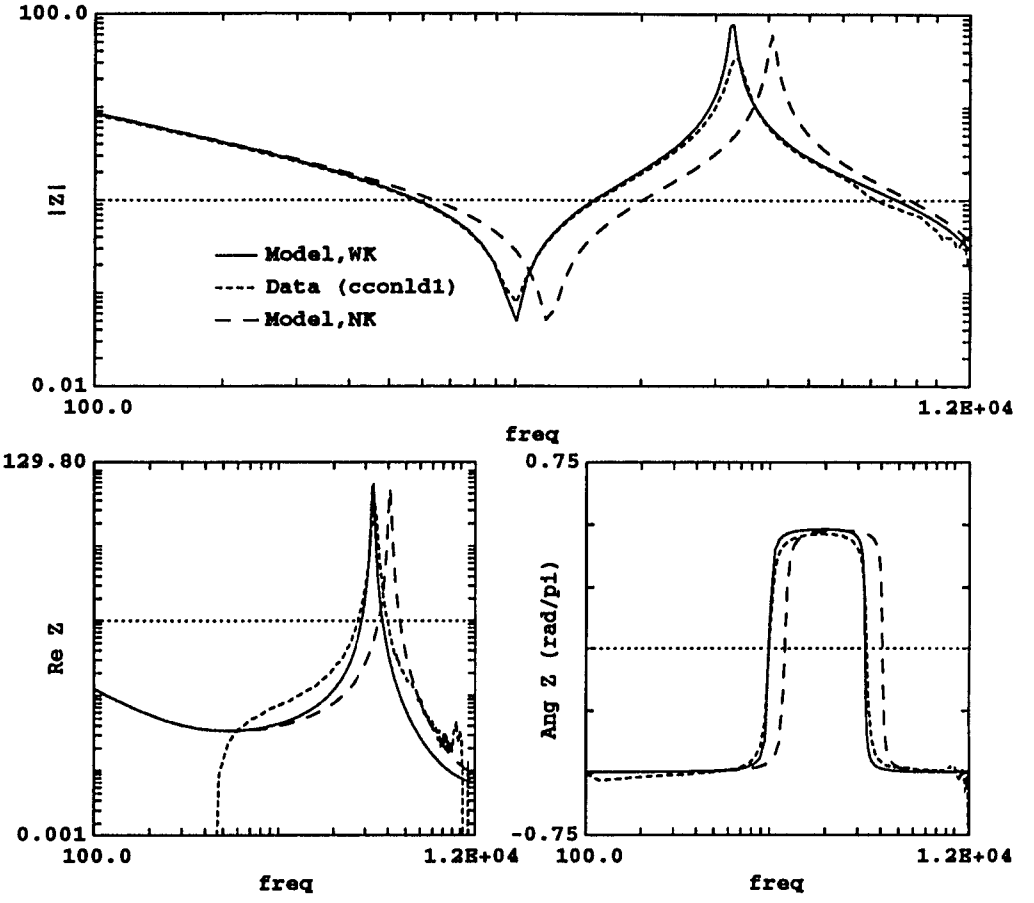

Figure 5.6: Impedance of cavity with a constriction in diameter: dimensions used for the model are $l_1 = 0.63, d_1 = 0.74, l_c = 0.24, d_c = 0.215$, and $l_2 = 0.85, d_2 = 1.91$. The impedance magnitude for the model with the Karal correction and the experimental data are in good agreement. This indicates that a constriction in a cavity can be represented by a cylindrical tube. For frequencies above about 500 Hz, the real part of the measured data is higher than the real part of the model by a factor of as much as 2.7 (8.6 dB). This suggests that there is a real part to Karal correction that has not been taken into account.

magnitude of the reflectance is greater than unity in the frequency region below 500 Hz and above 10 kHz. This is due to the real part of the impedance being negative in that frequency region. Between 700 Hz and 10 kHz, the magnitude of both model reflectance calculations are greater than the data by a factor of about 1.08 (0.69 dB).

The corresponding group delay is shown in the lower panel of Fig. 5.7 . The measured group delay starts to increase from a value of about 0.38 ms at 100 Hz reaching a maximum of about 0.64 ms near 900 Hz. It then starts to decrease. Above about 6-7 kHz the group delay starts to become a bit noisy but its average value was estimated to be close to 0.04 ms at 12 kHz. Figure 5.7 also shows the group delay for the corresponding model calculations. Clearly there is remarkably good agreement between the model with the Karal correction and the measured data for all frequencies below 12 kHz.

The group delay calculations with Karal correction is seen to be greater than the calculations without the Karal correction at most by 51% in the frequency region between 100 Hz and about 1.4 kHz. *Thus, for this particular cavity, the effect of the higher order modes is to increase the acoustic length of the cavity in the limited frequency region between 100 Hz and 1.4 kHz by as much 51%.* For frequencies above 1.4 kHz the group delay for the model with the Karal correction appears below the case without the Karal correction.

5.4 Discussion and conclusions

In the present chapter a model for representing a cylindrical cavity whose cross-sectional area varies along the axis of wave propagation is presented. In the model, the varying cross-sectional area is approximated as a series of stepped area cylindrical tubes. A chain-matrix is used to represent each cylindrical tube of constant cross-sectional area. The chain-matrix is formulated so

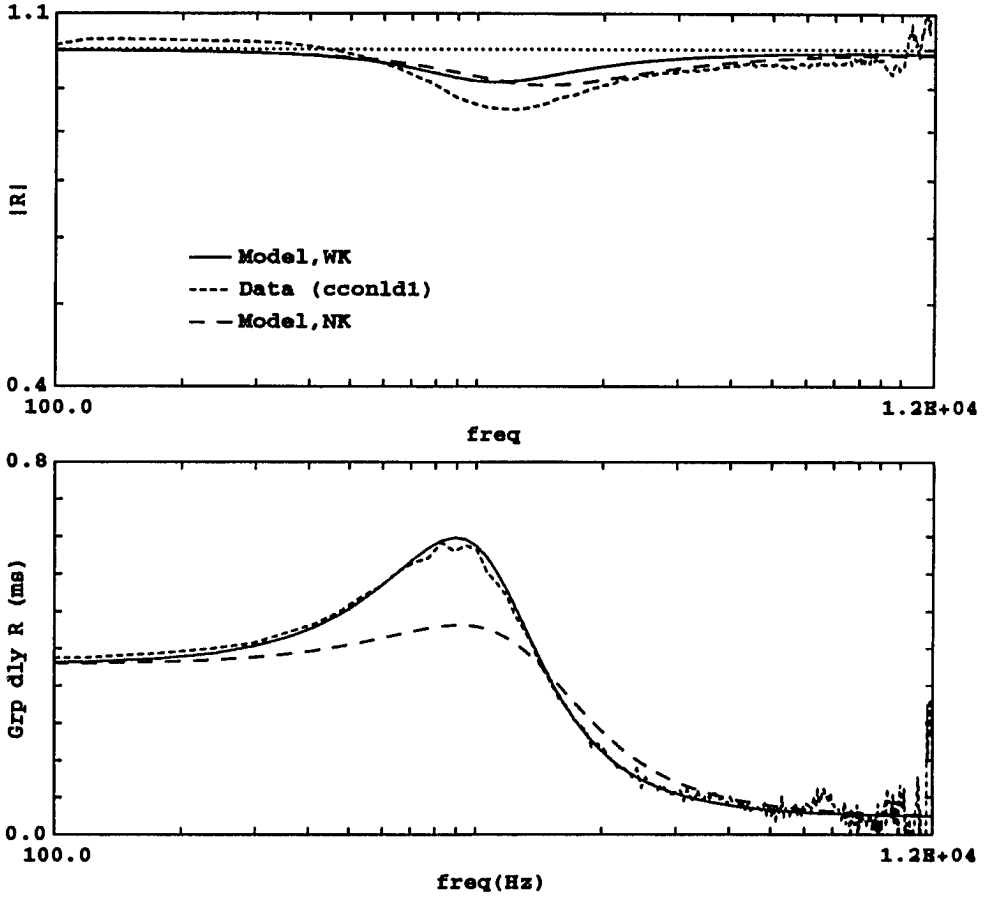

Figure 5.7: Reflectance of cavity with a constriction in diameter: Agreement between the measured group delay and the model with the Karal correction is excellent. With the Karal correction in the model, the group delay in the frequency below 1.4 kHz is greater than the model without the Karal correction by a factor of about 51%. This indicates that the effect of the higher order modes is to increase the acoustic length of the cavity by about 51% in the frequency region below 1.4 kHz. The discrepancies in the measured reflectance magnitude and model calculations are due to discrepancies in the real part of the impedance.

as to explicitly take into account the visco-thermal losses at the tube walls.

The problem of particular interest is one with sudden changes in cross-sectional area. In such cases, higher-order modes exited by an area discontinuity are modeled as the Karal correction to the plane wave theory. The Karal correction is an inductor that appears in series with two chain-matrices.

5.4.1 The model

The parameters for the cavity model are the dimensions of the cavity in terms of stepped areas. As a result, it is a completely physical model for the cavities. This model is verified by making impedance measurements on three cavities with area discontinuities. In the first example there is a sudden decrease in diameter, in the second example there is a sudden increase in diameter, and in the final example there is a constriction in the area function.

Each of the three cavities for the impedance measurements consisted of two cylindrical tubes. The dimensions of the first tube were always the same in all three examples. The physically measured dimensions are listed in Table 5.1 and the dimensions used in the model are shown in captions to Figs. 5.2, 5.4, and 5.6. In comparison, the length l_2 of the second tube used in the model is longer than the physically measured length by about 0.04 cm. Recall that to reduce low frequency leaks, a layer of vacuum grease was applied between the cylindrical cavities; the thickness of this layer is the most likely explanation for the increase in the length of the second cavity.

5.4.2 Losses in the model

Losses in the chain-matrix model arise due to visco-thermal losses at the inner surface of the cavity walls. In that sense losses in the present model arise in a natural manner. However, measurements

indicate that there are more losses in the data than in model calculations. This was particularly true for the case when there is constriction in the area. Recall that the Karal correction was formulated for the inviscid case. The inability of the model to not be able match the real part of the impedance, or equivalently the magnitude of the reflectance, indicates that the visco-thermal losses in the model are inadequate. This indicated that either the Karal correction is inadequate or that losses in the chain-matrix are inadequate. However, the real part of the measured data and real part of model calculations for the calibration cavities indicate that the losses due wave propagation are sufficiently accurate. This points the way towards further theoretical analysis of the Karal correction for the inviscid case. But first, more measurements on more cavities with different types of constrictions need to be made to strengthen this argument.

5.4.3 The effect of a constriction

In all three examples it is clear that including the Karal correction in model calculations is important in order to model the measured driving point impedance data with physically measured dimensions of the cavity.

Let us now consider what effect a constriction has on the driving point impedance of a cavity. To do this, comparison of Fig. 5.4 and Fig. 5.6 is in order (from now on we only consider the model calculations with the Karal correction). For the jump in area case (Fig. 5.4) there is a pole in the impedance near 10.2 kHz whereas for the area constriction case (Fig. 5.6) there is a pole in the impedance near 3.2 kHz. Similarly the zero has shifted from about 2.2 kHz to about 1 kHz. *Thus, for this particular set of cavity dimensions, the presence of the constriction in it's acoustic path has resulted in the pole frequency to shift down to a lower frequency by almost a factor of 3, and zero frequency by a factor of about 2.2.* A physical interpretation of this is that an area constriction has the effect of increasing the effective acoustic length of the cavity in a limited frequency region.

This interpretation was obtained by analyzing the group delay in each case (Figs. 5.5 and 5.7).

Recall that the same second cavity was used for the two cases. Thus the difference between the two cavities is that there is disk of length $l_c = 0.24$ cm placed in the second cavity for the constriction in diameter case. Thus the length of the second cavity for the area constriction example is 0.82 cm whereas the length of the second cavity for the jump in area example is 1.06 cm. If model computations were made with a jump in area with a second cavity of length 0.82 cm rather than 1.06 cm then the pole would have been at about 10.5 kHz rather than 10.2 kHz.

The conclusions stated above are important when one considers the possible role the bony septum, located between bulla cavity and the tympanic cavity of the cat middle ear cavity, has on the signal processing performed by the middle ear cavities. More is said regarding the application of this model in Sec. 4.7.3 of Chapter 4.

For future measurements, in it is recommended that measurements and calculations be made to much higher frequencies. The reason to do this is to test the adequacy of the model at much higher frequencies than has been considered in the present study.

Chapter 6

Summary and Conclusions

The inner ear and the middle ear of the auditory periphery have been studied in this thesis. And a model for the earcanal is proposed. The main consideration has been to analyze each subsystem from an acoustic impedance point of view. Impedance of each subsystem was considered for modeling purposes mainly due to the availability of accurate impedance measurements for each anatomical entity in the published literature.

A new model based on the chain-matrix formulation is developed for the cochlea. This model is used to analyze effects due to variations in the scalae cross-sectional area, perilymph viscosity, cochlear map, and the helicotrema on the cochlear input impedance.

Similarly, a chain-matrix model is developed to analyze cavities with variations in cross-sectional areas. This model includes two-dimensional effects due to cross-sectional area discontinuities, visco-thermal effects at the surface of the cavity walls, and effects due to finite wall impedances. This formulation is used to model the middle ear cavities and the earcanal. These model effects are experimentally verified by making impedance measurements on cylindrical cavities with cross-sectional area discontinuities.

A network topology for the ossicular path of the middle ear presented. A method for

constraining the parameters of the middle ear model based on "surgically modified" impedance measurements near the eardrum is used to estimate the parameters of the middle ear model. The inner ear model, the middle ear model, the middle ear cavity model, and the model for the earcanal are combined to obtain a comprehensive model for the cat eardrum impedance.

From these modeling considerations the following conclusions regarding the importance of various anatomical entities of the auditory periphery have been reached:

- It well known that, in most mammals, the cross-sectional area is tapered from the base of the cochlea to the apex of the cochlea. Until now scalae cross-sectional area variations of the cochlea were not considered to be important. This deficiency of previous cochlear models is shown to result in a deviation of as much as 20 dB of the measured cochlear input impedance data. It is further shown that the measured cochlear input impedance data can now be modeled accurately provided that the scalae cross-sectional area is represented accurately.

  With this model for the cochlear input impedance it is shown that some of the fine structure of the measured eardrum impedance/reflectance is due, in part, to the fine structure of the cochlear input impedance.

- The effect of perilymph viscosity is shown to be important when the tube radius becomes comparable to the viscous boundary layer. For the cat, chinchilla, and guinea pig the viscous boundary layer is shown to be important for frequencies below approximately 150 Hz.

- When the cochlea is modeled with a realistic scalae geometry, then the effect of the helicotrema on the cochlear input impedance is shown to be insignificant.

- Standing waves exist in model cochleae when there are reflections at both the stapes end

and the apical end of the cochlea. Apical reflections, and thus standing waves, can be eliminated by taking into account the scalae area variations and perilymph viscosity. In such a model, reflections are dissipated by the viscous boundary layer when it is comparable to the scalae radius. Alternatively, apical reflections, due to the end of the cochlear map, can be eliminated by using a cochlear map of the form: $f_{CF}(x) = A[10^{-\frac{\alpha}{x_L}(x-x_L)} - 1]$. Eliminating apical reflections eliminates the need for an "infinite length" cochlear model.

- Parameters for the ossicular path of the middle ear were obtained by modeling previously published eardrum impedance data in the following order: (1) "interrupted incus," (2) "drained cochlea," and (3) "intact" ossicles and cochlea. The first two of the eardrum measurements are for the "surgically modified" middle ear and cochlea. This method of evaluating the parameters for the middle ear is useful in constraining those parameters. It is also useful in helping to gain an understanding the role the various middle ear components play in the transduction process.

- By modeling the "interrupted incus" case we conclude that at most 10% of the incident wave is dissipated by the eardrum and the ossicles for frequencies between 100 Hz and 7 kHz. For frequencies between 8-12 kHz, up to 75% of the incident wave is dissipated by the incudo-malleolar joint.

  Above approximately 10 kHz, the middle ear model is not able to approximate the measured eardrum impedance and reflectance data. A future experiment, that would help towards understanding high frequency eardrum transduction properties, would be to measure the eardrum impedance for the "blocked malleus" case for frequencies much greater than 10 kHz.

- Between 300 Hz and 7 kHz, at most 10% of the incident wave is absorbed by the annular ligament.

- The cochlear load has a profound influence on the impedance and reflectance measured at the eardrum. As much as 80% of the incident wave is absorbed by the cochlea near the 1.6 kHz frequency region.

- The chain-matrix model for cavities is used to compute the impedance of the middle ear cavities. This model represents the middle ear cavities in terms of its length and diameters. Various "surgical modifications" are simulated using the middle ear cavity model and are shown to be in good agreement with animal data. We know from previous measurements that there is a resonance in the cat middle ear cavity impedance near 4.5 kHz. Based on the chain-matrix model for the middle ear cavities it is conjecture that there is a second bulla resonance near the 26 kHz frequency region.

- Model computations for the case when the bony septum of the cat middle ear cavity is removed are reported. Without the bony septum, the first bulla resonance frequency is at about 10 kHz while the second bulla resonance frequency is at about 20 kHz. Thus, the cat middle ear cavity appears to have a much larger acoustic length than its physical length due to the foreman of the septum.

- It is shown that the model for the middle ear ossicles and the model for the middle ear cavities can be combined to obtain a comprehensive model, for the cat eardrum, using the series model assumption.

- Experimental observations on several species has previously shown that the magnitude of the ear canal pressure to the stapes transfer function increases when the middle ear cavities are

vented to the atmosphere. It is shown that this experimental observation is consistent with our observation, on the comprehensive model of cat auditory periphery, that, in general, the reflectance at the eardrum decreases when middle ear cavities are vented to the atmosphere.

- The chain-matrix model used to represent a cavity with varying cross-sectional area is experimentally verified by making impedance measurements on several cavities with cross-sectional area discontinuities. The cavities were constructed to illustrate the effect of sudden changes in the cross-sectional area of a cat middle ear cavity. It is shown that higher-order modes due an area discontinuity can be approximated by the so called Karal correction to the plane wave propagation. The effect of a constriction, such as the foramen, is shown to result in an increase in the effective length of the cavity for a limited frequency region.

Appendix A

List of Symbols

Many of the important symbols used in each chapter are summarized here. If a symbol is used in several chapters then it only appears here under the chapter where it first appeared. If there are no units specified then the units for the symbol are assumed to be either dimensionless or the symbol is descriptive and thus it does not have units.

Chapters 2 and 3

A, B, C, D	elements of the 2×2 two-port chain matrix
A_{fp}	area of footplate (cm^2)
$\beta(x)$	BM width $[\beta_o exp(\beta_1 x)]$ (cm)
β_o	BM width at the base (cm)
β_1	rate of change parameter of the BM width (cm^{-1})
c	velocity of sound in water (cm/s)
$C(x)$	capacitive component of Y
δ	viscous boundary layer thickness (cm)
Δ	space discretization length (cm)
f	frequency (Hz)
$f_{CF}(x)$	cochlear map (Hz)
F_v, F_t	complex functions

γ	ratio of specific heats
$G(x)$	conductive component of Y
$\Gamma(x)$	propagation constant (cm^{-1})
$\jmath$	$\sqrt{-1}$
J_n	complex Bessel functions of order n
$K_b(x), K_b'(x)$	BM specific stiffness (dyn/cm^3)
K_{rw}	round window stiffness (dyn/cm^5)
$L(x)$	inductive component $[L_0 + L_v]$ of Z
$L_0(x)$	component of L due to fluid inertia
$L_v(x)$	component of L due to fluid viscosity
$M\Omega$	$10^6\ dyn - s/cm^5$
η	coefficient of viscosity $(g\ cm^{-1}\ s^{-1}$ $(g \cdot cm^{-1} \cdot s^{-1})$
n_p	number of sections along x_L
ρ	mass density of perilymph (g/cm^3)
$P(x)$	pressure difference across BM partition (dyn/cm^2)
$R_v(x)$	resistive component of Z
$r_0(x)$	tube radius (cm)
r_v	ratio of the tube radius to viscous boundary layer thickness
r_t	ratio of the tube radius to thermal boundary layer thickness
s	$\jmath\omega$
$S(x)$	scala area (cm^2)
$S_V(x)$	scala vestibule area (cm^2)
$S_T(x)$	scala tympani area (cm^2)
S_0	scala area at the base (cm^2)
s_1	rate of change parameter for scala area (cm^{-1})
$U(x)$	volume-velocity through scalae (cm^3/s)
u_{st}	particle-velocity of stapes (cm/s)
$V_{BM}(x)$	BM volume-velocity (cm^3/s)

ω angular frequency ($2\pi f$)
x distance from stapes (cm)
x_L length of cochlea (cm)
$Y(x)$ shunt acoustic admittance per unit length ($cm^4 \cdot dyn^{-1} \cdot s^{-1}$)

$Y'(x)$ BM acoustic admittance per unit length ($cm^4 \cdot dyn^{-1} \cdot s^{-1}$)
$Z(x)$ per unit length series acoustic impedance $[R_v + sL]$ ($dyn - s/cm^6$)
$Z'(x)$ equivalent impedance per unit length for the two chambers [Eq. (2.1)]
$Z_{BM}(x)$ BM trans-membrane specific impedance, [Eq. (C.1)] ($dyn - s/cm^3$)

$Z_c(\omega)$ complex cochlear input impedance [Eq. (2.10)] ($dyn - s/cm^5$)
$Z_{crw}(\omega)$ Z_c with the round window impedance added in series [Eq. (3.5)]
$|Z_c|$, $|Z_{crw}|$ magnitude of Z_c and Z_{crw}
$\angle Z_c$, $\angle Z_{crw}$ phase of Z_c and Z_{crw}

$Z_a(x)$, $Z_b(x)$ elements of the T network [Eq. (2.7a)] ($dyn - s/cm^5$)
Z_h acoustic impedance of helicotrema [Eq. (2.11)] ($dyn - s/cm^5$)
$Z_o(x)$ characteristic impedance of tube ($dyn - s/cm^5$)

Chapter 4

d_{tc} diameter of the tympanic cavity (cm)
d_f diameter of the foramen cavity (cm)
d_{bc} diameter of the bulla cavity (cm)
$\Im m[Z]$ imaginary component of [Z]

$k\Omega$ 10^3 $dyn - s/cm^5$
l_{tc} length of the tympanic cavity (cm)
l_f length of the foramen (cm)
l_{bc} length of the bulla cavity (cm)

P_{ec} earcanal pressure (dyn/cm^2)
P_{bc} pressure in the bulla cavity (dyn/cm^2)
P_{tc} pressure in the tympanic cavity (dyn/cm^2)
R^{i}_{ec} ear canal reflectance for the intact ossicles and cochlea case

R^{dc}_{ec} ear canal reflectance for the drained cochlea case
R^{ii}_{ec} ear canal reflectance for the incus interrupted case
$\Re e[Z]$ real component of [Z]
T_r transformer ratio

τ_{gd} group delay (s)
U_{ec} earcanal volume velocity (cm^3/s)
Z_{ec} earcanal impedance ($dyn - s/cm^5$)
Z_{du} uncoupled portion of the eardrum impedance ($dyn - s/cm^5$)

Z_{dc} coupled portion of the eardrum impedance ($dyn - s/cm^3$)
Z_{jim} impedance due to the incudo-malleolar joint ($dyn - s/cm^3$)
Z_{jis} impedance due to the incudo-stapedial joint ($dyn - s/cm^3$)
Z_{al} annular ligament impedance ($dyn - s/cm^5$)

Z_i impedance due to the incus ($dyn - s/cm^3$)
Z_m impedance due to the malleus ($dyn - s/cm^3$)
Z_{rl} radiation load impedance ($dyn - s/cm^5$)
Z_s stapes impedance ($dyn - s/cm^5$)

Z_{doc} impedance at the eardrum with open middle ear and earcanal cavities ($dyn - s/cm^5$)
Z_{ot} characteristic impedance of transducer tube ($dyn - s/cm^5$)
Z_{mec} intact middle ear cavity impedance
Z_{bo} bulla open middle ear cavity impedance

Z_{pf} plugged foramen middle ear cavity impedance
Z_{ec}^{i} ear canal impedance for the intact ossicles and cochlea case
Z_{ec}^{dc} ear canal impedance for the drained cochlea case
Z_{ec}^{ii} ear canal impedance for the incus interrupted case

Chapter 5

A_i area of i^{th} cylindrical tube (cm^2)
γ_i complex propagation constant for the i^{th} tube (cm^{-1})
l_i length of the i^{th} cylindrical tube (cm)
L_k Karal correction ($dyn - s^2/cm^5$)

P_o normalized Thevenin equivalent source pressure
Z_o normalized Thevenin equivalent source impedance
Z_{oi} characteristic impedance of the i^{th} tube ($dyn - s/cm^5$)

Appendix B

Lossy cylindrical tube theory

Lossy transmission-line theory describes the acoustical properties of a tube, having section length Δ and area S, in terms of the per unit length series acoustic impedance $Z(\omega)$ and the per unit length shunt acoustic admittance $Y(\omega)$. This theory, originally formulated by Kirchhoff (1868), is a linear acoustic theory which includes viscous and thermal boundary layers to account for the propagation of losses. To calculate Z and Y, one needs to know the scalae radius $r_0(x) = \sqrt{S(x)/\pi}$, and the viscous and thermal boundary layer thickness (see below), which are proportional to $\omega^{-1/2}$. Given Z and Y, one may calculate the propagation "constant" (which is not a constant), and the characteristic impedance using standard transmission line formulas.

Lossy series impedance: The per unit length series acoustic impedance Z is given by (Benade, 1968; Flanagan, 1983; Keefe, 1984):

$$\begin{aligned} Z(x,\omega) &= R_v(x,\omega) + sL(x,\omega) \\ &= \frac{s\rho/S(x)}{1-F_v}, \end{aligned} \tag{B.1}$$

where the functions R_v and L are defined as the resistive and inductive parts of Z. The viscous factor F_v is given by

$$F_v = \frac{2J_1(r_v\sqrt{-j})}{r_v\sqrt{-j}J_0(r_v\sqrt{-j})}. \tag{B.2}$$

In the preceding equation

$$r_v = r_0/\delta \tag{B.3}$$

is the ratio of the tube radius $r_0 = \sqrt{S/\pi}$, and the viscous boundary layer thickness

$$\delta = \sqrt{\frac{\eta}{\rho\omega}}. \tag{B.4}$$

Lossy shunt admittance: The per unit length shunt acoustic admittance Y is defined as (Benade, 1968; Flanagan, 1983; Keefe, 1984):

$$\begin{aligned} Y(x,\omega) &= G(x,\omega) + sC(x,\omega) \\ &= (sS(x)/\rho c^2)[1 + (\gamma - 1)F_t] \end{aligned} \tag{B.5}$$

where the thermal factor F_t is given by

$$\begin{aligned} r_t(x) &= r_v\sqrt{N_p} \\ F_t &= \frac{2J_1(r_t\sqrt{-j})}{r_t\sqrt{-j}J_0(r_t\sqrt{-j})}. \end{aligned} \tag{B.6}$$

The tube radius, normalized by the thermal boundary layer thickness, is r_t and is related to r_v by the Prandtl number $N_p = \eta c_p/\kappa$. The functions G and C are defined as the conductive and compliant parts of Y.

The thermodynamic constants used in the foregoing equations are listed in Table B. The Bessel functions J_0 and J_1 are must be evaluated at a $-\pi/4$ angle in the complex plane since r_t

Table B.1: Thermodynamic constants for perilymph

Name	Parameter	value	units
Density	ρ	1	g/cm^3
Viscosity	η	0.02	$g \cdot cm^{-1} \cdot sec^{-1}$
Sound speed	c	1.5×10^5	cm/sec
Prandtl number	N_p	7.02	*dimensionless*
Ratio of specific heats	γ	1	*dimensionless*

and r_t are real and $\arg(\sqrt{-j}) = -\frac{\pi}{4}$. Benade (1968), Keefe (1984) and others have given results leading to small and large tube radius approximations for F_v and F_t. In the interest of preserving the accuracy of Eqs. (B.1) and (B.5), since any error might propagate in the recursive solutions, we calculate the Bessel functions of complex arguments with double precision accuracy.

The real and imaginary parts of $Y(x,\omega)$ are defined as $G(x,\omega)$ and $\omega C(x,\omega)$. The real and imaginary parts of $Z(x,\omega)$ are defined as $R_v(x,\omega)$ and $\omega L(x,\omega)$. We further break down the definition of L into two components, L_0 and L_v. The fluid inertia term L_0 increases from the base to the apex. Since F_v is complex, it is evident from Eqs. (B.1) and (B.2) that the presence of viscosity gives rise to a real part and a reactive part. By definition, $R_v(x,\omega)$ is the increased resistance, and $L_v(x,\omega)$ is the added mass due to viscosity. For the inviscid case, $(\eta \to 0)$, $r_v \to \infty$, and from the large argument approximation to the Bessel functions (Morse and Feschbach, 1953, p. 1321), $F_v \to 0$. As a result, $R_v \to 0$ and $L \to L_0 = \frac{\rho}{S(x)}$. In using the above results, we assume that S is constant over a section length Δ.

Appendix C

Derivation of basilar membrane impedance

The equations describing the parameters corresponding to a BM with fourth order partition dynamics are summarized here (Allen, 1980). The BM specific-impedance is

$$Z_{BM}(x,s) = s(m_T + m_{oc}) + K_b(x)/s + G^2(x) \times H_T(x,s), \tag{C.1}$$

where K_b is the BM stiffness, m_{oc} is the organ of Corti (OC) mass, m_T is the mass of the tectorial membrane, and $G(x)$ is the shear gain. The transduction filter $H_T(x,s)$ is defined as:

$$H_T(x,s) = \frac{(r_c + k_c/s)(k_T/s + r_T + sm_T)}{(k_c + k_T)/s + (r_c + r_T) + sm_T}, \tag{C.2}$$

where k_c and r_c are the stereocilia stiffness and damping, and similarly k_T and r_T are the tectorial membrane stiffness and damping. Equation (C.2) can be rendered dimensionless by redefining $k_c(x)$, $k_T(x)$, $r_c(x)$, $r_T(x)$ in terms of $\omega_z(x)$, $\omega_p(x)$, $\zeta_z(x)$, $\zeta_p(x)$ (Allen, 1980). Where ω_p, ω_z are the pole, zero frequencies of the transduction filter and ζ_p, ζ_z are the damping factors associated

with the pole and the zero. Equation (C.2) then becomes

$$H_T(x,s) = \frac{G(x)}{\Lambda^2}\left(\frac{(s/\omega_z)^2 + 2\zeta_z(s/\omega_z) + 1}{(s/\omega_p)^2 + \zeta_p(s/\omega_p) + 1}\right), \tag{C.3}$$

where

$$\Lambda = \frac{\omega_p}{\omega_z}. \tag{C.4}$$

In this form, one needs to only to specify $\omega_z(x)$, $\omega_p(x)$, $\zeta_z(x)$, $\zeta_p(x)$ and the gain $G(x)$ to calculate Eq. (C.2). To estimate the parameters we have assumed the following:

$$\omega_p(x) = 1.3 \cdot \omega_{CF}(x) \tag{C.5}$$

$$\omega_z(x) = 0.65 \cdot \omega_{CF}(x) \tag{C.6}$$

$$\zeta_p(x) = 0.3 \tag{C.7}$$

$$\zeta_z(x) = 0.5 \tag{C.8}$$

$$G(x) = 0.5 \cdot \exp\{(x - x_L)/x_L\} \tag{C.9}$$

and

$$\omega_{CF}(x) = 2\pi f_{CF}(x), \tag{C.10}$$

where $f_{CF}(x)$ is the cochlear map. It is assumed in Eqs. (C.5) and (C.6) that the pole and the zero lie above and below $f_{CF}(x)$. K_b in Eq. (C.1) is evaluated according to:

$$K_b(x) = (m_T + m_{oc})\omega_{CF}^2 - m_T\omega_p^2(1 + (\omega_z/\omega_p)^2)G(x) \times \left[\frac{(\omega_z/\omega_{CF})^2 - 1}{(\omega_p/\omega_{CF})^2 - 1}\right]. \tag{C.11}$$

The specific-mass of the organ of Corti is

$$m_{oc} = \rho_{oc} \cdot h_{oc}(x), \tag{C.12}$$

and the specific-mass of the tectorial membrane (TM) is

$$m_T = \rho_T \cdot h_T(x), \tag{C.13}$$

where ρ_{oc} and ρ_T are densities of the OC and the TM, $h_{oc}(x)$ is the height of the OC, and $h_T(x)$ is height (thickness) of the TM. We assume that $\rho_{oc} = \rho_T = \rho$ the density of water. With these assumptions, $m_{oc} + m_T$ is 0.04 g/cm^2. The cochlear map from the model was generated by plotting the peak location of the BM velocity as a function of the input frequency. Using Eq. (C.11), the resulting calculated cochlear map fell below (in frequency) the actual cochlear map [either Eq.3.1,3.2,3.3)] by $\approx 1/\sqrt{3}$. This deficiency in the model of the basilar membrane stiffness $K_b(x)$ [Equation (C.11)] was accounted for by multiplying $K_b(x)$ by a constant (≈ 3) so as to make the model cochlear map and desired cochlear map coincide.

The total stiffness in Z_{BM} [Eq. (C.1)] is

$$K(x) = K_b(x) + G^2(x)\frac{k_c(x)k_T(x)}{k_c(x) + k_T(x)}. \tag{C.14}$$

For the parameters chosen $G^2(x) << 1$, and the parallel combination of k_c and k_T is typically less than 0.1 of $K_b(x)$. Thus the second term of Eq. (C.14) has a negligible effect [i.e. $K(x) \approx K_b(x)$]. Throughout the paper we will refer to the BM stiffness as $K(x)$.

As yet, $f_{CF}(x)$ is the only unspecified function needed to completely evaluate Z_{BM}; the effect of this function on Z_c is one of the concerns of the study in Chapter 3.

Appendix D

Acoustical wave propagation in lossy cylindrical tubes: Approximations to the transmission line parameters

In appendix B, exact solutions for a lossy cylindrical tubes were given in terms of the per unit length series acoustic impedance, and per unit length shunt acoustic admittance. Those solutions were in terms of complex Bessel functions. Evaluations of Bessel functions are computationally expensive. The iteration procedure outlined in Sec. 5.2 requires model impedance computations for the four calibration cavities many times over. To reduce the amount of time it takes for the length estimation procedure, it was desirable that an approximate solution to equations (B.1) and (B.5) be used rather than the exact solutions.

This appendix summarizes Keefe's (1984, Eq. 13) approximations ($r_v > 2$) for the lossy characteristic impedance and lossy propagation constant used in Chapter 5 of this work. The subscript a indicated in many of the parameters defined below stands for air.

The boundary layer thickness is defined as

$$\delta_a = \sqrt{\frac{\eta_a}{\rho_a \omega}}, \tag{D.1}$$

where $\omega = 2\pi f$. The radius of a tube given its area is $r = \sqrt{\frac{A}{\pi}}$. We define r_{v_a} the tube radius normalized by viscous boundary layer thickness as

$$r_{v_a} = r/\delta_a. \tag{D.2}$$

The characteristic impedance is defined as,

$$Z_o = zc_r + jzc_i \tag{D.3}$$

where the real part of the characteristic impedance is

$$zc_r = r_o(1 + 0.369/r_v), \tag{D.4}$$

and the imaginary part is

$$zc_i = -r_o(0.369/r_v + 1.149/r_v^2 + 0.303/r_v^3). \tag{D.5}$$

The above parameters are defined in terms of

$$r_o = \frac{\rho_a c_a}{A}. \tag{D.6}$$

The propagation constant is defined as,

$$\gamma_a = \alpha_a + j\beta_a, \tag{D.7}$$

where the real part of the propagation constant is

$$\alpha_a = \frac{\omega}{c_a}(1.045/r_v + 1.08/r_v^2 + 0.75/r_v^3) \tag{D.8}$$

and the imaginary part is

$$\beta_a = \omega / v_p, \tag{D.9}$$

with

$$v_p = \frac{c_a}{1 + 1.045/r_v}. \tag{D.10}$$

The thermodynamic constants listed below (Benade, 1968) are valid for $26.85 \pm 10\ ^\circ C$.

$$\rho_a = 1.1769 \times 10^{-3}(1 - 0.00335T)\ \ g \cdot cm^{-3} \tag{D.11}$$

$$\eta_a = 1.846 \times 10^{-4}(1 + 0.0025T)\ \ g \cdot sec^{-1} \cdot cm^{-1} \tag{D.12}$$

$$c_a = 3.4723 \times 10^{4}(1 + 0.00166T)\ \ cm \cdot sec^{-1} \tag{D.13}$$

The temperature difference T is $(t - 26.85)$, where t is in degrees celcius; for room temperature $T = 0$.

Note that for the lossless case ($\eta_a \rightarrow 0$) the characteristic impedance $Z_o = \rho_a c_a / A$ and the propagation constant $\gamma = \omega / c_a$, as is to be expected.

Equations (D.3) – (D.10) may be alternatively written in terms of the series impedance $Z(\omega)$ and the shunt admittance $Y(\omega)$ representations of the transmission line formalism (Keefe, 1984, Eq. (12)). Effects of finite wall admittance $Y_w(\omega)$ are included in the chain-matrix formulation by adding to the transmission line shunt admittance (Flanagan, 1983), i.e.

$$Y'(\omega) = Y(\omega) + Y_w(\omega). \tag{D.14}$$

A further analysis of the effects of finite wall admittance on wave propagation can be found in Morse and Ingard (1968, pp. 475-479).

Bibliography

Allen, J. B. (**1977**). "Cochlear micromechanics-a mechanism for transforming mechanical to neural tuning within the cochlea," *J. Acoust. Soc. Am.*, **62**, 930-939.

Allen, J. B. (**1979**). "Cochlear models - 1978." In *Models of the Auditory Systems and Related Signal Processing Techniques*, edited by M. Hoke and E. de Boer, *Scand. Audiol. Suppl.* **9**, 1-16.

Allen, J. B. (**1980**). "Cochlear micromechanics - A physical model of transduction," *J. Acoust. Soc. Am.*, **68**, 1660-1670.

Allen, J. B. (**1986**). "Measurement of eardrum acoustic impedance." In *Peripheral Auditory Mechanisms*, edited by J. B. Allen, J. L. Hall, A. Hubbard, S. T. Neely, and A. Tubis. (Springer-Verlag), pp. 44-51.

Allen, J. B. (**1990**). Personal communication.

Aritomo, H., and Goode, R. L. (**1987**). "Cochlear input impedance in fresh human temporal bones," *American Academy of Otolaryngology abstract.*

Benade, A. H. (**1968**). "On the propagation of sound waves in a cylindrical conduit," *J. Acoust. Soc. Am.*, **44**, 616-623.

Beranek, L. L. (**1954**). *Acoustics.* (McGraw-Hill, New York).

Cabezudo, L. M. (**1978**). "The ultrastructure of the basilar membrane in the cat." *Acta Otolaryngol*, **86**, 160-175.

Carlin, H. J., and Giordano, A. B. (**1964**). *Network Theory - An Introduction to Reciprocal and Nonreciprocal Circuits.* (Prentice-Hall, New Jersey).

Dallos, P. (1970). "Low-frequency auditory characteristics: Species dependence," *J. Acoust. Soc. Am.*, **48**, 489-499.

Dallos, P. (1973). *The auditory periphery-biophysics and physiology.* (Academic Press, New York).

Dancer, A., and Franke, R. (1980). "Intracochlear sound pressure measurements in guinea pigs," *Hearing Research*, **2**, 191-205.

Dear, S. P. (1987). *"Impedance and sound transmission in the auditory periphery of the chinchilla.* PhD thesis, U of Pennsylvania.

Diependaal, R. (1988). "Nonlinear and active cochlear models: analysis and solution methods." PhD thesis, Delft University.

Eldredge, D. H., Miller, J. D., and Bohne, B. A. (1981). "A frequency-position map for the chinchilla cochlea," *J. Acoust. Soc. Am.*, **69**, 1091-1095.

Fahey, P. F., and Allen, J. B. (1985). "Nonlinear phenomena as observed in the ear canal and at the auditory nerve," *J. Acoust. Soc. Am.*, **77**, 599-612.

Fernández, C. (1952). "Dimensions of the cochlea (guinea pig)," *J. Acoust. Soc. Am.*, **24**, 519-523.

Flanagan, J. L. (1962). "Computational model for basilar-membrane displacement," *J. Acoust. Soc. Am.*, **34**, 1370-1376.

Flanagan, J. L. (1983). *Speech Analysis Synthesis and Perception.* (Springer-Verlag), 2 edition.

Greenwood, D. D. (1961). "Critical bandwidth and the frequency coordinates of the basilar membrane," *J. Acoust. Soc. Am.*, **33**, 1344-1356.

Greenwood, D. D. (1990). "A cochlear frequency-position function for several species - 29 years later," *J. Acoust. Soc. Am.*, **87** , 2592-2605.

Guinan, J. J., and Peake, W. T. (1967). "Middle-ear characteristics of anesthetized cats," *J. Acoust. Soc. Am.*, **41**, 1237-1261.

Gyo, K., Aritomo, H., and Goode, R. L. (1987). "Measurement of the ossicular vibration ratio in human temporal bones by use of a video measuring system," *Acta Otolaryngol (Stokh)*, **103**, 87-95.

Hall, J. L. (1974). "Two-tone distortion products in a nonlinear model of the basilar membrane," *J. Acoust. Soc. Am.*, **56**, 1818-1828.

Helmholtz, H. L.F. (1885). *On the sensations of tone*, 2nd edition.

Hubbard, A. E., and Geisler, C. D. (1972). "A hybrid-computer model of the cochlear partition," *J. Acoust. Soc. Am.*, **51**, 1895-1903.

Hudde, H., and Letens, U. (1985). "Scattering matrix of a discontinuity with a nonrigid wall in a lossless circular duct," *J. Acoust. Soc. Am.*, **78**, 1826-1837.

Karal, F. C. (1953). "The analogous acoustical impedance for discontinuities and constrictions of circular cross section," *J. Acoust. Soc. Am.*, **25**, 327-334.

Keefe, D. H., and Ling, R. (1989). "On ear canal measurement techniques applied to hearing development," *J. Acoust. Soc. Am. Suppl.*, **1**, 85.

Keefe, D. H. (1984). "Acoustical wave propagation in cylindrical ducts: Transmission line parameter approximations for isothermal and nonisothermal boundary conditions, *J. Acoust. Soc. Am.*, **75**, 58-62.

Kemp, D. T. (1978). "Stimulated acoustic emissions from within the human auditory system," *J. Acoust. Soc. Am.*, **64**, 1386-1391.

Kemp, D. T. (1979). "Evidence of mechanical nonlinearity and frequency selective wave amplification in the cochlea," *Arch. Otorhinolaryngol*, **224**, 37-45.

Kemp, D. T., "Towards a model for the origin of cochlear echoes," *Hearing Research*, **2**, 533-548.

Khanna, S. M., and Tonndorf, J. (1969). "Middle ear power transfer," *Arch. Klin. exp. Ohr.-. Nas. -u Kehlk. Heilk*, **193**, 78-88.

Khanna, S. M., and Tonndorf, J. (**1972**). "Tympanic membrane vibrations in cats studied by time-averaged holography," *J. Acoust. Soc. Am.*, **51**, 1904-1920.

Kim, D. O., Molnar, C. E., and Matthews, J. W. (**1980**). "Cochlear mechanics: Nonlinear behavior in two-tone responses as reflected in cochlear-nerve responses and in ear-canal sound pressure," *J. Acoust. Soc. Am.*, **67**, 1704-1721.

Kirchhoff, G., (**1868**). "On the influence of heat conduction in a gas on sound propagation," *Ann. Phys. Chem.*, **134**, 177-193.

Koshigoe, S., Kwok, W.-K., and Tubis, A. (**1983**). "Effects of perilymph viscosity on low-frequency intracochlear pressures and the cochlear input impedance of the cat," *J. Acoust. Soc. Am.*, **74**, 486-492.

Kringlebotn, M. (**1988**). "Network model for the human middle ear," *Scand. Audiol.*, **17**, 75-85.

Lesser, M. B., and Berkley, D. A. (**1972**). "Fluid mechanics of the cochlea, Part 1," *J. Fluid Mech.*, **51**, 497-512.

Liberman, M. C. (**1982**). "The cochlear frequency map for the cat: Labeling auditory-nerve fibers of known characteristic frequency," *J. Acoust. Soc. Am.*, **72**, 1441-1449.

Lynch, T. J., III, Nedzelnitsky, V., and Peake, W. T. (**1982**). "Input impedance of the cochlea in cat," *J. Acoust. Soc. Am.*, **72**, 108-130.

Lynch, T. J. (**1981**). "Signal processing by the cat middle ear: Admittance and transmission, measurements and models," PhD thesis, MIT.

Matthews, J. W. (**1980**). "Mechanical modeling of nonlinear phenomena observed in the peripheral auditory system." PhD thesis, Washington University, MO.

Matthews, J. W. (**1983**). In *Mechanics of Hearing*, edited by E. de Boer and M.A. Viergever, "The human external and middle ear: Models and concepts," (Delft University Press), 11-18.

Miles, J. (**1944**). "The reflection of sound due to a change in cross section of a circular tube."

J. Acoust. Soc. Am., **16**, 14-19.

Miles, J. (**1946**). "The analysis of plane discontinuities in cylindrical tubes. Part I," *J. Acoust. Soc. Am.*, **17**, 259-271.

Miles, J. (**1946**). "The analysis of plane discontinuities in cylindrical tubes. Part II," *J. Acoust. Soc. Am.*, **17**, 272-284.

Moller, A. R. (**1961**). "Network model of the middle ear," *J. Acoust. Soc. Am.*, **33**, 168-176.

Moller, A. R. (**1965**). "An experimental study of the acoustic impedance of the middle ear and its transmission properties," *Acta Otolaryng.*, **60**, 129-149.

Moller, A. R. (**1983**). *Auditory Physiology*, (Academic Press, New York).

Morse, P. M., and Feschbach, H. (**1953**). *Methods of Theoretical Physics*, Volume II. (McGraw-Hill, New York), p. 1321.

Morse, P. M., and Ingard, K. U. (**1968**). *Theoretical Acoustics*, (McGraw-Hill, New York).

Nedzelnitsky, V. (**1980**). "Sound pressures in the basal turn of the cat cochlea," *J. Acoust. Soc. Am.*, **68**, 1676-1689.

Neely, S. T., and Kim, D. O. (**1986**). "A model for active elements in cochlear biomechanics," *J. Acoust. Soc. Am.*, **79**, 1472-1480.

Olson, H. F. (**1958**). *Dynamical Analogies*, (Van Nostrand, New York).

Onchi, Y. (**1949**). "A study of the mechanism of the middle ear," *J. Acoust. Soc. Am.*, **21** 404-410.

Onchi, Y. (**1961**). "Mechanism of the middle ear," *J. Acoust. Soc. Am.*, **33**, 794-805.

Papoulis, A. (**1962**). *The fourier integral and its applications*, (McGraw-Hill, New York).

Peake, W. T., and Guinan, J. J. (**1967**). "Circuit model for the cat's middle ear," *MIT Research Laboratory of Electronics, Quarterly Prog. Rep.*, **84**, 320-326.

Peake, W. T., Rosowski, J. J., and Lynch, T. J., III (1991). "Acoustic coupling to cochlear windows." *To be submitted to Hearing Research.*

Peterson, L. C., and Bogert, B. P., (1950). "A dynamical theory of the cochlea," *J. Acoust. Soc. Am.*, **22**, 369-381.

Pickles, J. O. (1988). *An Introduction to the Physiology of Hearing*, (Academic Press), 2nd edition.

Pierce, A. D. (1989). *Acoustics*, (Acoust. Soc. Am., New York), Chap. 7.

Puria, S., and Allen, J. B. (1989). "Impedance measurements in the ear canal," *J. Acoust. Soc. Am. Suppl. 1*, **86**, S44.

Puria, S., and Allen, J. B. (1991). "A parametric study of cochlear input impedance," *J. Acoust. Soc. Am.*, **89**, 287-309.

Rabbitt, R. D., and Holmes, M. H. (1988). "Three-dimensional acoustic waves in the ear canal and their interaction with the tympanic membrane," *J. Acoust. Soc. Am.*, **83**, 1064-1080.

Rabbitt, R. D. (1990). "A hierarchy of examples illustrating the acoustic coupling of the eardrum," *J. Acoust. Soc. Am.*, **87**, 2566-2582.

Rabinowitz, W. M. (1981). "Measurement of the acoustic input immittance of the human ear," *J. Acoust. Soc. Am.*, **70**, 1025-1035.

Rhode, W. S. (1971). "Observations of the vibration of the basilar membrane in squirrel monkeys using the mossbauer technique," *J. Acoust. Soc. Am.*, **49**, 1218-1231.

Robert, W., Funnell, J., and Laszlo, C. A., (1982). "A critical review of experimental observations on ear-drum structure and function," *J. for Oto-Rhino-Laryngology and its related specialities*, **44**, 181-205.

Rosowski, J. J., Peake, W. T., and Lynch, T. J., III (1984). "Acoustic input-admittance of the alligator-lizard ear: Nonlinear features," *Hearing Research*, **16**, 205-223.

Rosowski, J. J., Carney, L. H., Lynch, T. J., III, and Peake, W. T. (1986). "The effectiveness of external and middle ears in coupling acoustic power into the cochlea." In *Peripheral*

Auditory Mechanisms, edited by J. B. Allen, J. L. Hall, A. Hubbard, S. T. Neely, and A. Tubis, (Springer-Verlag), pp. 3-12.

Ruggero, M. A., Rich, N. C., Robles, L., and Shivapuja, B. G. (**1990**). "Middle-ear response in the chinchilla and its relationship to mechanics at the base of the cochlea," *J. Acoust. Soc. Am.*, **87**, 1612-1629.

Shaw, E. A. G., and Stinson, M. R. (**1981**). "Network concepts and energy flow in the human middle ear," *J. Acoust. Soc. Am. Suppl. 1*, **69**, S44.

Shaw, E. A. G., and Stinson, M. R. (**1983**). In *Mechanics of Hearing*, edited by E. de Boer and M. A. Viergever, "The human external and middle ear: Models and concepts", (Delft University Press), 3-10.

Shera, C. A., and Zweig, G. (**1989**). "Transfer matrices of the human middle ear." *Unpublished manuscript*

Shera, C. A., and Zweig, G. (**1991a**). "Phenomenological characterization of eardrum transduction." *Accepted for Publication in J. Acoust. Soc. Am.*

Shera, C. A., and Zweig, G. (**1991b**). "A symmetry suppresses the cochlear catastrophe." *J. Acoust. Soc. Am.*, **89**(3).

Smith, P. H. (**1944**). "An improved transmission-line calculator," *Electronics*, January.

Sondhi, M. M. (**1978**). "Method for computing motion in a two-dimensional cochlear model," *J. Acoust. Soc. Am.*, **63**, 1468-1477.

Sondhi, M. M. (**1981**). "Acoustical inverse problem for the cochlea," *J. Acoust. Soc. Am.*, **69**, 500-504.

Sondhi, M. M. (**1983**). "An improved vocal tract model," *Int. Conf. on Acoust.*, **11**, 167-170.

Sondhi, M. M. (**1988**). Personal communication.

Tonndorf, J., and Khanna, S. M. (**1967**). "Some properties of sound transmission in the middle and outer ears of cats," *J. Acoust. Soc. Am.*, **41**, 513-521.

Tonndorf, J., and Pastaci, H. (**1986**). "Middle ear sound transmission: A field of early interest to Merle Lawrence," *Am. J. Otolaryngol*, **7**, 120-129.

Tonndorf, J., Khanna, S. M., and Fingerhood, B. J. (**1966**). "The input impedance of the inner ear in cats," *J. Acoust. Soc. Am.*, **75**, 752-763.

VanValkenburg, M. E. (**1964**). *Introduction to modern network synthesis*, (John Wiley & Sons, New York), third edition.

Viergever, M. A. (**1978**). "Basilar membrane motion in a spiral-shaped cochlea," *J. Acoust. Soc. Am.*, **64**, 1048-1053.

Viergever, M. A. (**1980**). "Mechanics of the inner ear." PhD thesis, (Delft U.P., Delft, The Netherlands), p. 69.

Viergever, M. A. (**1988**). "Asymmetry in reflection of cochlear waves." In *Auditory Frequency Selectivity*, edited by Brian C. J. Moore and Roy D. Patterson, A NATO Advanced Research Workshop.

von Békésy, G. (**1960**). *Experiments in hearing*. (McGraw-Hill, New York).

Weinberg, L. (**1962**). *Network analysis and synthesis*. (McGraw-Hill, New York), Chap. 7.

Wever, E. G., and Lawrence, M. (**1954**). *Physiological Acoustics*, (Princeton University Press).

Wever, E. G. (**1949**). *Theory of Hearing*. (John Wiley & Sons).

Wiener, F. M., Pfeiffer, R. R., and Backus, A. S. N. (**1966**). "On the pressure transformation by the head and auditory meatus of the cat," *Acta Otolaryng.*, **61**, 255-269.

Wilson, J. P. (**1980**). "The combination tone, $2f_1 - f_2$, in pshychophysics and ear canal recording." In *Psychophysical physiological and behavioral studies in hearing*, edited by G. Van den Brink and F. A. Wilson, (Delft University Press, Delft, The Netherlands), pp. 43-50.

Zurek, P. M. (**1981**). "Spontaneous narrowband acoustic signals emitted by human ears," *J. Acoust. Soc. Am.*, **69**, 514-523.

Zwislocki, J. (1950). "Theory of the acoustical action of the cochlea," *J. Acoust. Soc. Am.*, **22**, 778-784.

Zwislocki, J. (1957). "Some impedance measurements on normal and pathological ears," *J. Acoust. Soc. Am.*, **29**, 1312-1317.

Zwislocki, J. (1962). "Analysis of the middle-ear function, Part I: Input impedance," *J. Acoust. Soc. Am.*, **34**, 1514-1523.

Zwislocki, J. (1963). "Analysis of the middle-ear function, Part II: Guinea-pig ear," *J. Acoust. Soc. Am.*, **35**, 1034-1040.

Zwislocki, J. (1965). "Analysis of some auditory characteristics." In *Handbook of Mathematical Psychology*, edited by R. Duncan Luce, Robert R. Bush, and Eugene Galanter, (John Wiley & Sons, New York) Vol. 3, Chap. 1, p. 37.